International Journal of Precision Engineering and Manufacturing-Green Technology (2021) 8:703–742
https://doi.org/10.1007/s40684-020-00302-7

Online ISSN 2198-0810
Print ISSN 2288-6206

INVITED REVIEW PAPER

Directed Energy Deposition (DED) Process: State of the Art

Dong-Gyu Ahn[1]

Received: 14 October 2020 / Revised: 2 December 2020 / Accepted: 9 December 2020 / Published online: 15 February 2021
© The Author(s) 2021

Abstract
Metal additive manufacturing technologies, such as powder bed fusion process, directed energy deposition (DED) process, sheet lamination process, etc., are one of promising flexible manufacturing technologies due to direct fabrication characteristics of a metallic freeform with a three-dimensional shape from computer aided design data. DED processes can create an arbitrary shape on even and uneven substrates through line-by-line deposition of a metallic material. Theses DED processes can easily fabricate a heterogeneous material with desired properties and characteristics via successive and simultaneous depositions of different materials. In addition, a hybrid process combining DED with different manufacturing processes can be conveniently developed. Hence, researches on the DED processes have been steadily increased in recent years. This paper reviewed recent research trends of DED processes and their applications. Principles, key technologies and the state-of-the art related to the development of process and system, the optimization of deposition conditions and the application of DED process were discussed. Finally, future research issues and opportunities of the DED process were identified.

Keywords Additive manufacturing process · Directed energy deposition · State-of-the art · Research issues

List of Symbols

P	Power of laser
v	Travel speed
m_p	Feed rate of powders
α	Dilution ratio
δ	Depth of the molten pool
β	Height of the deposited bead
ω	Global energy density
d_l	Beam diameter of laser
Ω	Transverse traverse index
ξ	Distance between two subsequent tracks
ϖ	Track width
R_a	Arithmetical mean surface roughness

1 Introduction

Additive manufacturing (AM) technologies produce three-dimensional (3D) physical objects from digital information through layer-by-layer, line-by-line, piece-by-piece, or surface-by-surface depositions of materials on the substrate and the previous layer [1–5]. The AM is defined to be "a process of joining materials to make parts from 3D model data, usually layer upon layer, as opposed to subtractive manufacturing and formative manufacturing methodologies" by ASTM and ISO standards [1, 6, 7]. The AM is also referred to as rapid prototyping (RP), 3D printing, freeform fabrication (FF), layer manufacturing, etc. [1–3, 8]. The AM technologies have important features, including complexity-for-free, tool-less and less-resource intensive, from the viewpoint of sustainability effects [9–12]. The complexity-for-free feature of the AM technologies has created a new research field called design for additive manufacturing (DFAM) [2, 5, 13, 14]. Research issues related to DFAM include freeform shapes, lattice structures and porous objects, topology optimization, part consolidation, non-assembly mechanism, internal channels, segmentation, embedded components, thin and small features, surface features, material choices, multiple materials, infill modifications, process dependent design parameters, etc. [2, 5, 13–22]. As compared to conventional manufacturing (CM) processes, the AM technologies have several promising benefits: (a) decreased the production time and the amount of human intervention due to the reduction of the time-consuming multiple re-fixturing and calibration procedure through the completely automated AM process from design to fabrication of the product in a computer aided design and manufacturing (CAD and CAM)

✉ Dong-Gyu Ahn
smart@chosun.ac.kr

[1] Department of Mechanical Engineering, Chosun University, 309, Pilmun-daero, Dong-gu, Gwangju 61452, South Korea

environment, (b) reduction of cost to fabricate products using expensive materials, such as titanium and nickel based super-alloys, through the improved buy-to-fly (BTF) ratio and the reduced waste, and (c) Improvement of cost-competitiveness and structural integrity through the manufacture of unified structures with arbitrary shapes [2–4, 6, 8, 10, 13, 23–27]. Due to these important features and promising advantages, the AM technologies have attracted attention as emerging technologies from academies and industries in recent years [6, 28, 29].

The usage of AM technologies has significantly changed in the last 30 years [6, 8, 24]. Recently, AM technologies were applied to the direct production of end-use parts and whole products (termed rapid manufacturing (RM)) [2, 6, 8, 28–31]. The AM technologies employ plastics, metals, ceramics, composites, and biological materials as deposited materials [1, 4, 8, 24–28, 30–33]. In order to create metallic parts using a plastic product fabricated by the plastic based AM processes, secondary processes are additionally needed [30, 31]. Metal additive manufacturing (MAM) technologies can directly fabricate a metallic part with a complex shape without an additional manufacturing process [4, 6, 24, 30–33]. The MAM technologies can reduce the lead-time and the cost to create a metallic product from CAD data through the elimination of the secondary process [30–32]. The MAM technologies are promising flexible manufacturing technologies to manufacture a metallic part with complex geometries, controlled properties and desired functionalities [28, 32–35]. In addition, it is very convenient to create a hybrid manufacturing process combining MAM processes with subtractive and forming processes [37–39]. Hence, research into novel processes and applications of the MAM significantly increased in the last decade.

Since Carl Deakard and Professor Joseph Beaman at University of Texas patented a selective laser sintering (SLS) process in 1986, various metal additive manufacturing (MAM) processes, such as a powder bed fusion (PBF) process, a directed energy deposition (DED) process, a sheet lamination (SL) process, etc., were developed [1–8, 24, 28–33, 39–42]. PBF, including selective laser sintering (SLS), direct metal laser sintering (DMLS), selective laser melting (SLM), and electron beam melting (EBM) processes, and DED processes have been widely applied to academic researches, commercialized systems and industrial applications [1–4, 6, 24, 28, 32–34, 39–46]. The deposition rate and the volume density of the DED processes are greater than those of the PBF process, while the layer thickness, the surface roughness and the minimum feature size of the fabricated part by the PBF processes are relatively smaller than those by the DED process [4, 24, 40, 42, 44–48]. The DED processes can create an arbitrary shape on even and uneven substrates through line-by-line deposition of a metallic material, unlike the PBF processes [32, 49, 50]. Because several developed DED systems include multiple powder hoppers and wire feeders to selectively supply powders and wires for different materials, the DED systems can easily fabricate a heterogeneous material with desired properties via successive and simultaneous deposition of different materials [4, 32, 51–54]. Due to the simplified system of the DED apparatus as compared to the PBF apparatus, it is convenient to develop a hybrid process combining DED with different manufacturing processes [24, 36, 38, 55–57]. Hence, research and application of the DED processes has steadily increased in recent years.

This paper reviews recent research trends of DED processes and their applications. Principles, key technologies and the state-of-the art related to the development of process and system, optimization of the deposition conditions and application of the DED process are discussed. In addition, future research issues and opportunities of the DED process are investigated.

2 Principle and Classification of DED Processes

The DED process is defined as "additive manufacturing process in which focused thermal energy is used to fuse materials by melting as they are being deposited" by ISO/ASTM 52900 standard [7]. The principle of the DED process is illustrated in Figs. 1 and 2 [24, 57]. The DED process utilizes the concept of cladding and welding processes [1–4,

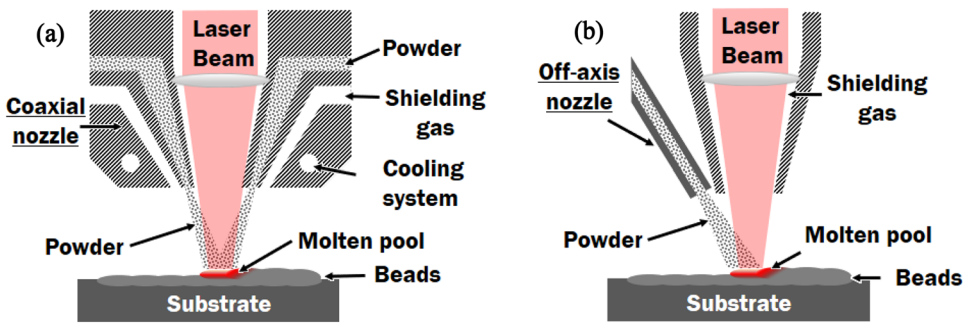

Fig. 1 Powder feeding methodologies of LAM-DED processes (Redrawn and modified figures of reference 57) [57]: (**a**) coaxial feeding and (**b**) off-axis feeding

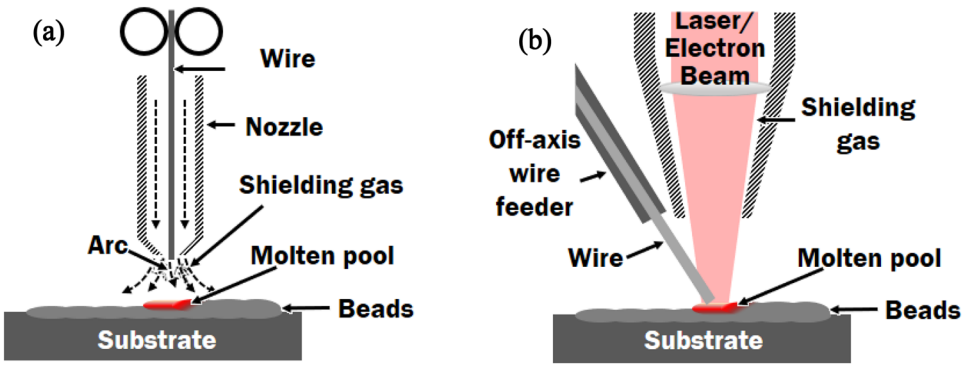

Fig. 2 Wire feeding methodologies of DED processes (Redrawn and modified figures of reference 24) [24]: (**a**) co-axial feeding (WAAM) and (**b**) off-axis feeding (WLAM and WEAM)

6, 8, 24, 32, 42–51, 56–60]. Thermal energy, such as a laser, electron beam, welding heat flux, etc., is focused on the previous layer, as shown in Table 1 [1–4, 6, 8, 24, 32, 42–51, 56–62]. Simultaneously, the feedstock with types of wires and powders is fed to the focused region of the thermal energy [40, 42, 58]. The molten pool is formed by melting of both the previous layer and the feedstock in and around the spot of the focused thermal energy [40, 42, 58]. The deposition bead is created by cooling of the molten pool. Through repetition of the above procedure, a 3D metallic part is fabricated. A typical cooling rate of the DED process ranges from 10^3 to 10^5 °C/s [58].

The DED process can be classified into powder and wire feeding types according to the feedstock, as shown in Table 1 and Fig. 3 [1–4, 6, 8, 24, 42, 46, 56–67]. The developed powder feeding type DED processes uses a laser as a thermal energy, while the wire feeding type DED processes utilizes an electric arc, a plasma arc, a laser, and an electron beam as a thermal energy, as shown in Table 1 and Fig. 3 [1–4, 6, 8, 24, 42, 46, 56–62]. In order to deliver the feedstock into the molten pool, the DED process uses co-axial and lateral types of feeding technologies, as shown in Table 1 and Fig. 2 [1–4, 6, 8, 24, 42, 46, 57–61]. The DED process consisting of a powder feeding device and a laser is known as a laser additive manufacturing (LAM)-DED process [60]. The wire feeding type DED processes are classified into wire and arc additive manufacturing (WAAM), wire and laser additive manufacturing (WLAM), and wire and electron beam additive manufacturing (WEAM) processes according to used thermal energies [1, 4, 6, 24, 46, 58–67]. The DED process with off-axial feeding devices of the feedstock relative to the focused thermal energy is sensitive to feed orientations and deposition conditions [59]. The sensitivity greatly increases for the case of a wire laser additive manufacturing (WLAM) process [24, 59] (Figs. 4, 5, 6).

Energy densities of the laser, the arc and the electron beam for the DED processes are on the order of 10^6, 10^4 and 10^8 W/mm^2, respectively, as shown in Table 2 [46]. The LAM-DED, WAAM and WLAM processes use a shield gas to prevent oxidation of the molten pool during the deposition [6, 24, 34, 40, 42, 44, 56–60, 64–68]. The WEAM processes are operated in a vacuum furnace unlike the LAM-DED, WAAM and WLAM processes [4, 46, 62, 63, 69–72]. The investment cost of the WAAM process is relatively cheaper than that of the LAM-DED, WLAM and WEAM processes [24, 46]. The surface roughness (R_a) of the fabricated part by LAM-DED processes is greater than that by WLAM processes by nearly 20–30% in a plane deposition [59, 73]. The deposition rate and the layer thickness of the wire feeding type DED processes are remarkably greater than those of the powder feeding type DED processes, while the dimensional accuracy and the residual stress of the fabricated part by the wire feeding type DED processes

Table 1 Feedstock, feeding type, thermal energy, classification, and deposition mechanism of DED processes

Feedstock	Feeding type	Thermal energy	Classification	Deposition mechanism	References
Powders	Co-axial and off-axis (lateral) feeding	Laser (CO_2, Nd:YAG, Fiber, etc.)	LAM-DED	Cladding	[1, 4, 6, 32, 42, 44, 57–60]
Wire	Co-axial and off-axis (lateral) feeding	Electric arc	WAAM	Welding (GMAW, GTAW, etc.)	[1, 4, 6, 24, 40, 56, 58, 59, 65]
	Co-axial and off-axis (lateral) feeding	Plasma arc		Welding (PAW and PTAW)	[24, 40, 42, 57, 64, 65]
	Co-axial and off-axis (lateral) feeding	Laser	WLAM	Cladding and Welding	[1, 4, 24, 57, 66, 67]
	Co-axial and off-axis (lateral) feeding	Electron beam (Thermionic and Plasma)	WEAM	Welding	[1, 4, 40, 46, 57, 59, 61, 62]

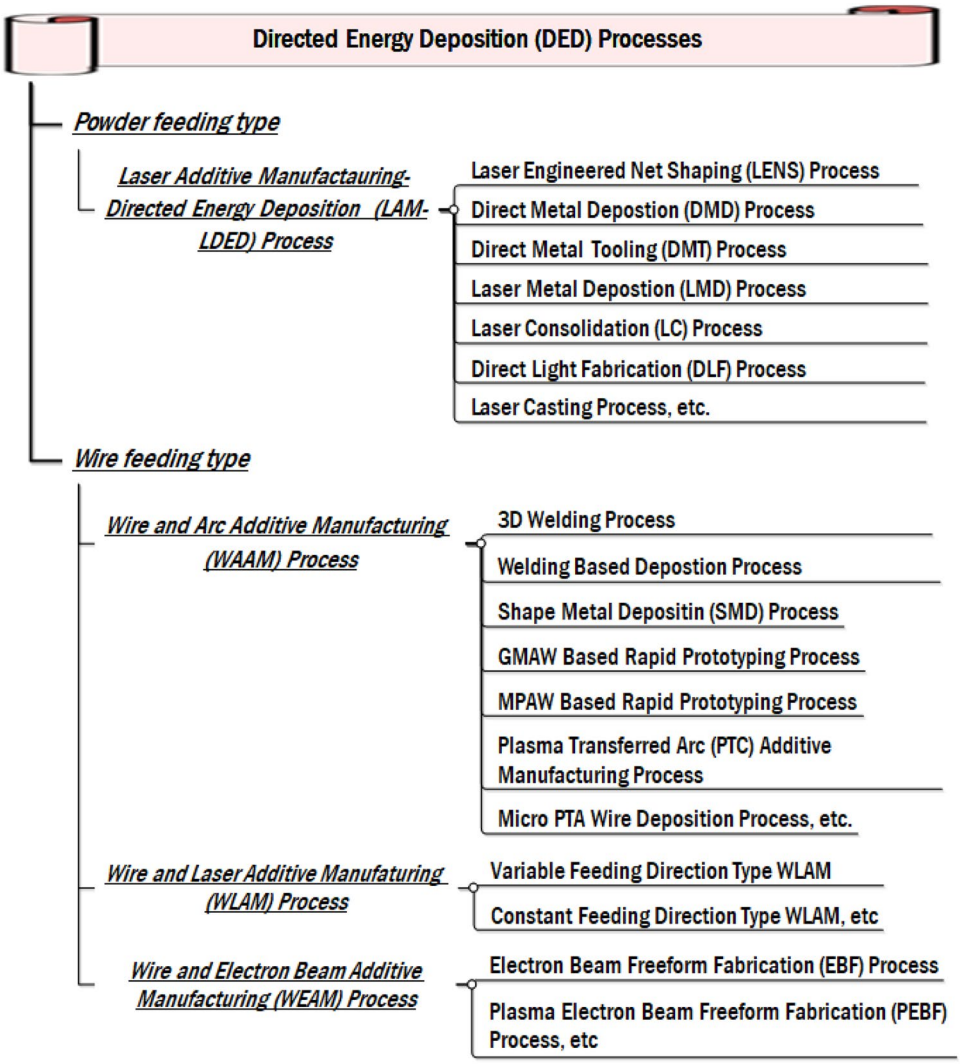

Fig. 3 Classification of DED processes [1–4, 6, 8, 24, 42, 46, 56–67]

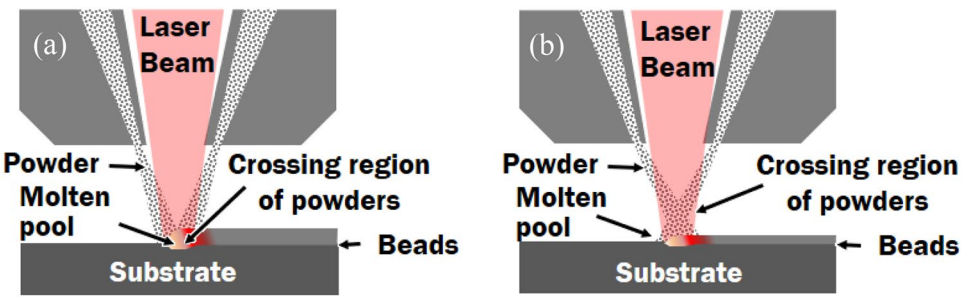

Fig. 4 Typical crossing regions of fed powders for conventional LAM-DED and HELA technology (redrawn and modified figures of reference 90) [90]: (**a**) conventional LAM-DED process and (**b**) HELA technology

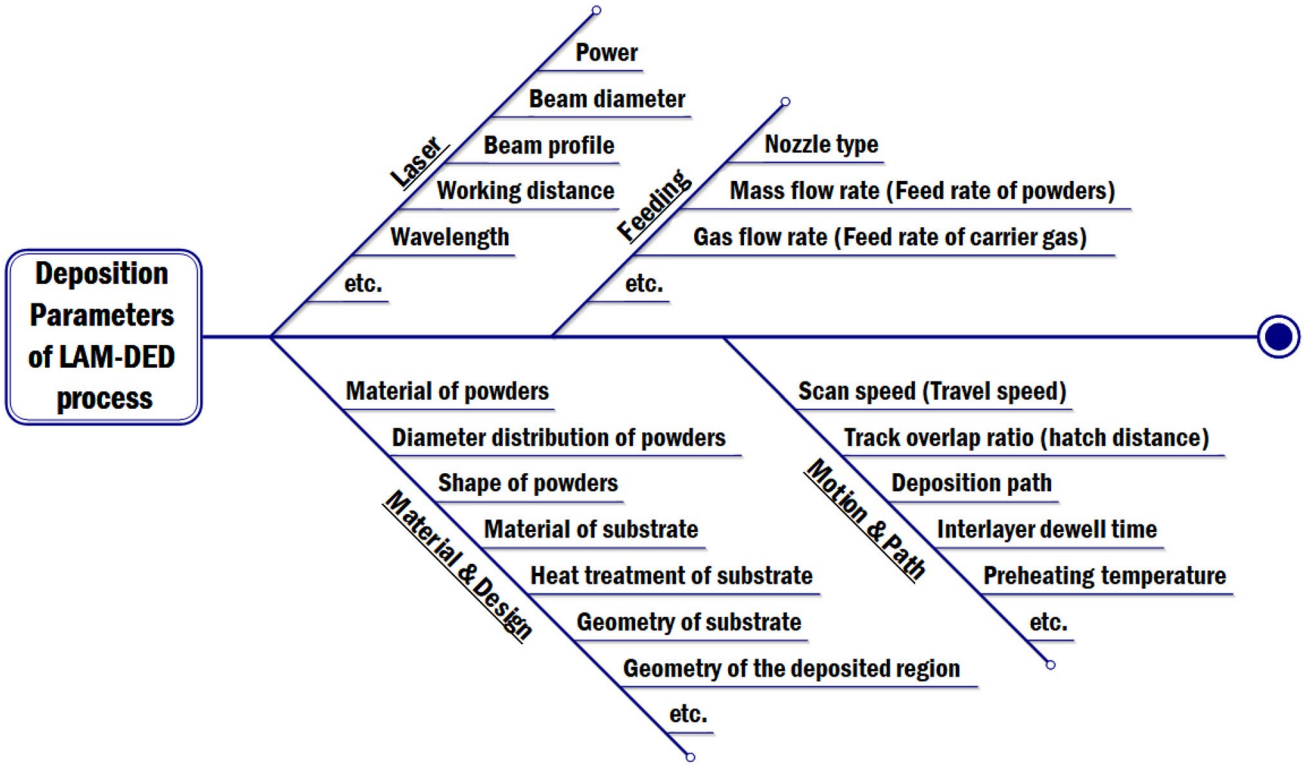

Fig. 5 Deposition parameters of LAM-DED processes [42, 57–60, 94–97]

are inferior to those by of the powder feeding type DED processes, as shown in Table 2 [4, 42, 46, 56–60].

3 Powder Feeding Type DED (LAM-DED) Processes: State-of-the Art

3.1 Characteristics and Principle of LAM-DED Processes

Powder feeding type DED (LAM-DED) processes use the concept of the laser cladding process, as shown in Fig. 1 and Table 1 [1, 4, 6, 32, 40, 42, 47, 48, 58–60, 73, 74]. Sandia National Laboratories in United States developed the first LAM-DED process. In addition, the process was patented as the laser engineered net shaping (LENS) process [4, 40, 59, 60, 75]. The LENS process was commercialized by Optomec Inc. [4, 76]. Since the LENS process was introduced, various LAM-DED processes, such as direct metal deposition (DMD) process, direct metal tooling process, laser metal deposition (LMD) process, laser consolidation (LC) process, direct light fabrication (DLF) process, laser casting process, etc., were developed [4, 58, 77–83]. Mazumder et al. developed the DMD process [4, 32, 58, 77]. The DMD process integrated the closed-loop control unit, including CCD (Charge coupled device) cameras, into the DMD system to maintain the deposited thickness through monitoring of the deposited region [58, 77–79]. The DMD process was commercialized by POM Group (DM3D Inc.) [4, 58, 77–79]. The DMT process with a similar process concept to the DMD process was commercialized by InssTek Inc. in Korea [4, 32, 80, 84].

The LMD process was commercialized by several companies, such as Trumpf Inc., EFESTO Inc., and RPM Inc., [4, 81, 82, 85–89]. The LMD process of Trumpf Inc. optionally provided an extreme high speed-laser material deposition (EHLA) technology to improve the surface creation rate and the quality of the deposited bead [81, 90]. Typical DED processes formed a crossing region of the fed powders from the feeding nozzle into the molten pool, while the EHLA technology created a focal region of the fed powders above the molten pool to melt fed powders before hitting the powders to the molten pool [81, 90]. With EHLA technology, the powder particles no longer need to be melted in the molten pool due to melting of the fed powders above the molten pool, unlike typical DED processes [81, 90]. The typical layer thickness, the minimum feature size and the maximum deposition rate of the LAM-DED are 250–500 μm, 380–1000 μm and 8.3 g/min, respectively, as shown in Table 2 [4, 40, 44, 48, 58, 76]. The maximum layer thickness of the LENS process is nearly 1000 μm [58, 76].

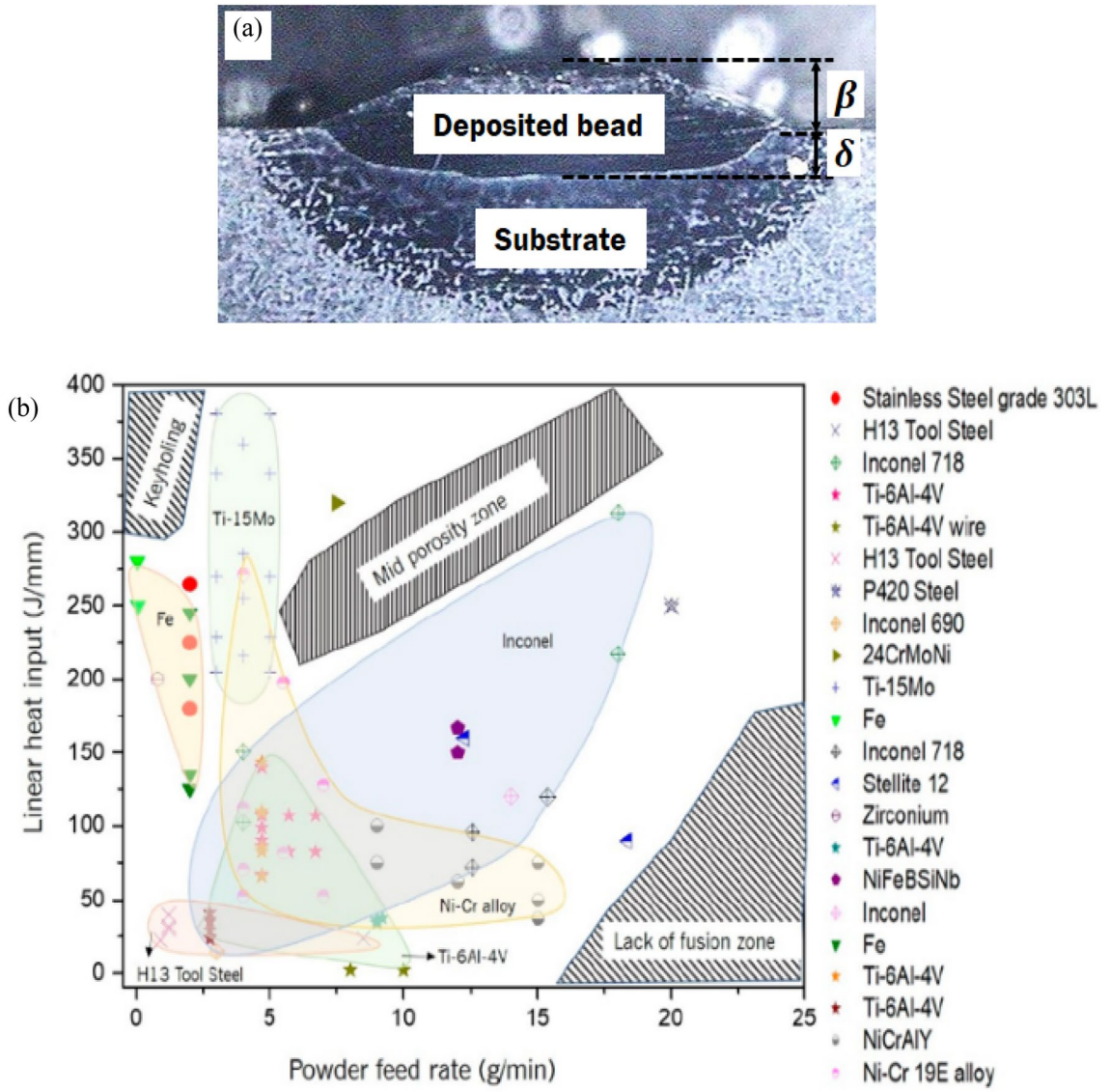

Fig. 6 Deposited region and optimal processing map for LAM-DED process: (**a**) typical formation of the deposited region and (**b**) optimal processing maps for different materials [adapted from reference 42 (Open Access)] [42]

Table 2 Characteristics of representative DED processes

Process [References]	Typical layer thickness (μm)	Minimum feature (width) size (μm)	Density of heat flux (W/mm^2)	Energy efficiency (%)	Working environments	Deposition rate (g/min)	Capture efficiency of feedstock (%)
LAM-DED [4, 42, 44, 46–48, 57–59, 73, 74, 76]	200–500	380–1000	≈ 10^6	< 40	Shielding gas	< 8.3	< 90
WAAM [4, 24, 44, 46, 57, 58, 65, 154]	1000–2000	1000–2000	≈ 10^4	< 90		16.7–66.7	≈ 100
WLAM [24, 46, 57–59, 67, 186, 201]	> 1000	5–15 times of wire diameter	≈ 10^6	2–5		1.5–48.0	
WEAM [4, 24, 40, 44, 46, 57, 58, 69–72]	< 3000	<1,600	≈ 10^8	15–20	Vacuum furnace	< 330	

Table 3 Features of representative commercialized LAM-DED processes

Process	Company	Laser	Moving of deposition head	Type of nozzle	No. of hopper (EAs)	Monitoring of molten pool	References
LENS	Optomec	Fiber	Gantry type (3 and 5 axes)	Co-axial (3 and 4 tip)	≥ 2	1 vision camera (Melt pool sensor)	[4, 32, 40, 59, 60, 76]
DMD	DM3D	Diode/disc/fiber	Gantry type and Robot arm (3 and 5 axes)	Co-axial	≥ 2	2 vision camera	[4, 32, 58, 77–79]
DMT	Inssteck	Fiber	Gantry type (3 and 5 axes)	Co-axial	≥ 2	2 vision camera	[4, 32, 80, 84]
LMD	Trumpf	Diode/disc/fiber	Gantry type (3 and 5 axes)	Co-axial (3 tip)	≥ 2	1 vision camera	[81, 90]
DED	MAXROTEC	Fiber	Robot arm (≥ 5 axes)	Co-axial (4 tip)	≥ 2	IR camera	[92]

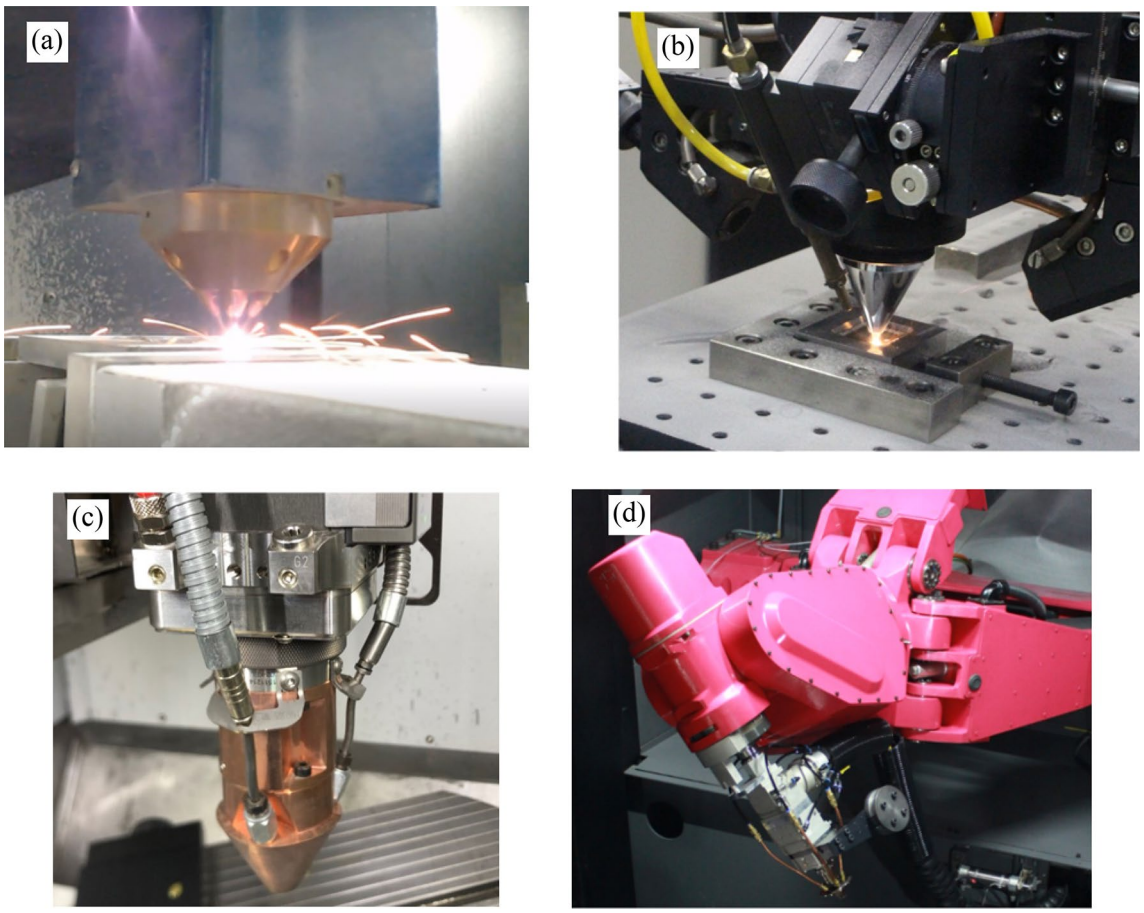

Fig. 7 Deposition heads for different commercialized DED process: (**a**) LENS process (reprinted from figure provided by Ph.D Yong Son and Ph.D Hyub Lee of KITECH with permission), (**b**) DMT process, (**c**) LMD process (Trumph Inc., reprinted from figure provided by Doosan Machine Tools Inc. with permission), and (**d**) DED process (MAXROTEC Inc., reprinted from figure provided by MAXROTECH Inc. with permission) [92]

3.2 Development of Processes and Systems

Table 3 shows features of commercialized LAM-DED processes. The LENS process uses a fiber laser and a gantry type deposition head, as shown in Table 3 and Fig. 7a [4, 32, 59, 60, 76]. A recently developed LENS system includes a melt pool sensor with a vision camera for a feedback control through real time monitoring of the variation of the molten pool during the deposition [76]. The Optomec Inc. developed a LENS modular print engine to integrate the deposition head into a conventional CNC machine tool [76]. The modular print engine provided a promising direction related to technical progress of the LAM-DED process for a hybrid system [91]. The DMD process uses three types of laser, including diode, disc and fiber lasers, as well as gantry and robot arm types of deposition head, as shown in Table 3 [4, 32, 77, 79]. The DMT process utilizes a fiber laser and a gantry type deposition head, as shown in Table 3 and Fig. 7b [4, 32, 80]. In addition, the DMT process employs two vision cameras for a closed-loop control of the layer thickness [80]. The LMD process of Trumpf Inc. includes three types of laser, including diode, disc and fiber lasers, and a gantry type deposition head, as shown in Table 3 and Fig. 7c [81]. In addition, the LMD process of Trumpf Inc. employs a vision camera for monitoring the formation of the molten pool during the deposition. MAXROTEC Inc. in Korea developed a robot arm type DED system, as shown in Table 3 and Fig. 7d [92]. The system uses a fiber laser as a thermal energy source. In addition, the system employs an infrared (IR) camera for closed-loop control through monitoring of the width of the molten pool [92]. Most commercialized DED processes uses two or more hoppers for feeding of powders to deposit heterogeneous materials through selective mixing of different powders [93]. The feature allows the DED process to easily produce a functionally graded material and structure (FGM&S) [93].

3.3 Effects of Deposition Parameters

Deposition parameters of LAM-DED process can be classified into laser, feeding, material and design, and motion and path parameters, as shown in Fig. 5 [42, 57–60, 94–97]. The power of the laser, the scan speed of the laser and the feed rate (mass flow rate) of powders are major parameters affecting the bead formation, joining between successive layers, the porosity, the microstructure, and the residual stress [42, 60, 98]. Several researchers proposed a laser energy per unit length (LEL, Π) and a powder feed per unit length (PFL, Γ) to reflect the influence of the correlation between the three parameters, as shown in Eqs. (1) and (2) [42, 60, 98]. The beam diameter and the profile of the laser beam affect the minimum size of the feature and the formation of the molten pool [60, 94]. The catchment efficiency of powders generally depends on the feed rate of powders, the flow rate of carrier gas, the diameter distribution of powders, the beam profile of the laser, the scan speed of the laser, etc. [42, 72, 94]. Despite the maximum catchment efficiency of powders was reported to be nearly 90% for a specific case, the material usage efficiency of LAM-DED process is generally less than 30% [42, 57, 74]. The energy efficiency of the laser for LAM-DED process is less than 40%, as shown in Table 2 [42, 74]. A dilution layer with mixed chemical compositions is formed between successive layers, as shown in Fig. 6a [42, 57].

$$\Pi(\mathrm{J/mm}) = P/v \tag{1}$$

$$\Gamma(\mathrm{J/mm}) = m_p/v \tag{2}$$

The dilution ratio (α) is defined as given in Eq. (3) [42, 57]. Several researchers proposed the optimal range of the dilution ratio as 10–30% to obtain a proper dilution between the first layer and the substrate [42, 99]. The amount of porosity in the fabricated part was used as an important measure to estimate the optimal deposition conditions [42, 60, 98]. Dass et al. investigated the effects of the LEL and the powder feed rate on the occurrence of the porosity. In addition, they predicted optimal processing regions for different alloys, as shown in Fig. 6b. The global energy density (GED, ω) was introduced to investigate the porosity in the fabricated part by the LAM-DED process, as shown in Eq. (4) [42, 100]. Wolff et al. illustrated that interlayer and intralayer porosities were taken place for regions of low and high values of the GED, respectively [42, 100]. Dass et al. reported that the possibility of lack of fusion defect induced by less dilution increases with decreasing GED in the region of low GED, while the possibility of keyhole porosity induced by high dilution decreases with increasing GED in the region of high GED [42, 100]. In addition, they reported that the keyhole takes place when the dilution ratio exceeds 30%, while the lack of fusion occurs when the dilution ratio is under 10% [42]. The track overlap ratio affected the porosity of the fabricated part by the LAM-DED process [42, 60, 98]. The track overlap ratio of the LAM-DED process is typically 25% of the width of the deposited bead [58]. Paul et al. defined a transverse traverse index (TTL, Ω) to consider the influence of the track overlap ratio on the porosity of the fabricated part, as shown in Eq. (5) [60, 98]. They estimated an experimental equation, including LEL, PFL and TTL, to predict the porosity of the fabricated Inconel 625 specimen by the LAM-DED process [60, 98]. In addition, they reported that dense parts are fabricated when the TTI is close to 0.6, while porous structures are created when the TTL is greater than 0.7 [60, 98].

$$\alpha(\%) = [\delta/(\beta + \delta)]100 \tag{3}$$

$$\omega\left(\mathrm{J/mm^2}\right) = P/\left(vd_l\right) \tag{4}$$

$$\Omega = \xi/\varpi \tag{5}$$

The particle diameter of the fed powders for the LAM-DED process generally ranges from 30 to 200 μm [57, 59, 95]. Spherical powders are preferred for the feedstock in terms of flowability, layer spreading, and loose powder packing [101]. The deposition path affects the residual stress distribution, the microstructure, the anisotropy, the porosity, and the mechanical properties of the fabricated part [96, 102–105]. Uni-directional, alternative directional (zig-zag), chessboard, and contour paths are used to fabricate parts using the LAM-DED process [96, 100]. Riberiro et al. [102] investigated the influence of the deposition path on the shape, the morphology, the surface roughness, the microstructure, and the microhardness of the AISI 316 deposited region. Wolff et al. examined anisotropic characteristics of a Ti–6Al–4V block fabricated by the LENS process using an alternative directional path [103]. Li and Soshi studied the effects of the deposition path on grain morphologies of the fabricated specimen by a DED coating process using a Kinetic Monte Carlo (KMC) Potts model [104]. Soshi et al. investigated the influence of a trochoidal deposition path on the preheating effect, the molten pool size, the power catchment efficiency, the material addition rate, the porosity, and the post deformation for the DED process [105]. Denlinger et al. studied the effects of inter-layer dwell time on distortion and residual stress of a wall structure fabricated by a DED process using Ti-6Al-4 V and Inconel 625 powders [97].

3.4 Applications and Fabricated Parts

Although LAM-DED processes are mainly used to fabricate metallic parts with a near-net shape in the early stage, applications of the LAM-DED processes have been expanded to repair, restoration, remanufacturing, porous coating, tailored materials, tailored structures, and thermal management in recent years, as shown in Table 4 [4, 32, 35, 50, 51, 79–81, 106–151].

3.4.1 Repair, Restoration and Remanufacturing

LAM-DED processes have various advantageous characteristics, such as relatively lower heat input, less distortion, lower dilution rate, excellent metallurgical bonding, excellent mechanical performance, relatively higher geometrical accuracy, suitability for full automation, and precise thermal control, in terms of repair, restoration and remanufacturing (3R) of products as compared to welding processes [107, 109]. Therefore, research on application of the LAM-DED process to repair, restoration and remanufacturing remarkably increased for the purpose of decreasing lead time, cost and greenhouse gas (GHG) emissions through recycling of used materials and the simple modification of used parts [4, 32, 35, 50, 106–112]. Restoration and remanufacturing using the LAM-DED process can potentially improve the properties and the reproduction of discontinued parts [4, 32,

Table 4 Features of representative commercialized LAM-DED processes

Application		Purpose	References
Repair, restoration and remanufacturing	Repair of damaged parts Restoration and remanufacturing of parts with desired shapes and properties	Reduction of lead time, cost and GHG emission Recycle of used materials and parts Production of discontinued parts Improvement of properties and functionalities	[4, 32, 35, 50, 79–81, 106–123]
Porous coating	Metal foam Porous structures on bio-medical materials	Fabrication of metal foam Improvement of bio-compatibility Improvement of BTF	[42, 80, 86, 124–128]
Tailored materials and structures	Functionally graded materials and structures (FGM&S) Multi-layer coating of heterogeneous materials Hardfacing	Control of material properties Improvement of wear and corrosion resistances as well as service life Reduction of material cost	[4, 42, 51, 52, 93, 129–144]
Thermal management	Moulding and forming tools with conformal cooling channels (CCCs) Thermal management mould Heat sink (Cooling fin)	Control of temperature distributions Uniform and rapid cooling characteristics Reduction of cooling and cycle times Improvement of product quality	[4, 32, 76–80, 84, 117, 143, 145–151]

35, 106, 108, 109, 111, 112, 117]. Most of previous studies related to the 3R of parts using LAM-DED processes were focused on repair and remanufacturing of components of power plants and engines [4, 79–81, 106–112]. Hot sections, knife-edges, blades, and compressor seals were repaired by LAM-DEM processes to reduce cost and lead time [4, 32, 106, 107, 109–111]. Diaz et al. examined deposition characteristics of Stellite6 using a LAM-DED process to repair steam circuit components in thermal power stations [106, 110]. Petrat et al. [113] repaired a gas turbine burner, which was fabricated from a SLM process, using a LMD process. Kimi Inc. remanufactured four stroke marine pistons for not only the restoration of the parts but also the improvement of the wear resistance of grooves [107, 109, 114]. Willson et al. [112] reported that there was nearly a 72.5% decrease in GHG emissions and a 68.1% decrease in energy consumption as compared to the fabrication of a new replacing turbine blade when 5% volume of the turbine blade was repaired by a LAM-DED process. InssTek Inc. [80] in collaboration with Korean Air Force repaired the air seal of a jet engine.

LAM-DED processes, including LENS, DMD, DMT, and LMD processes, were used for the sake of repair, restoration and remanufacturing of molding, forming and die

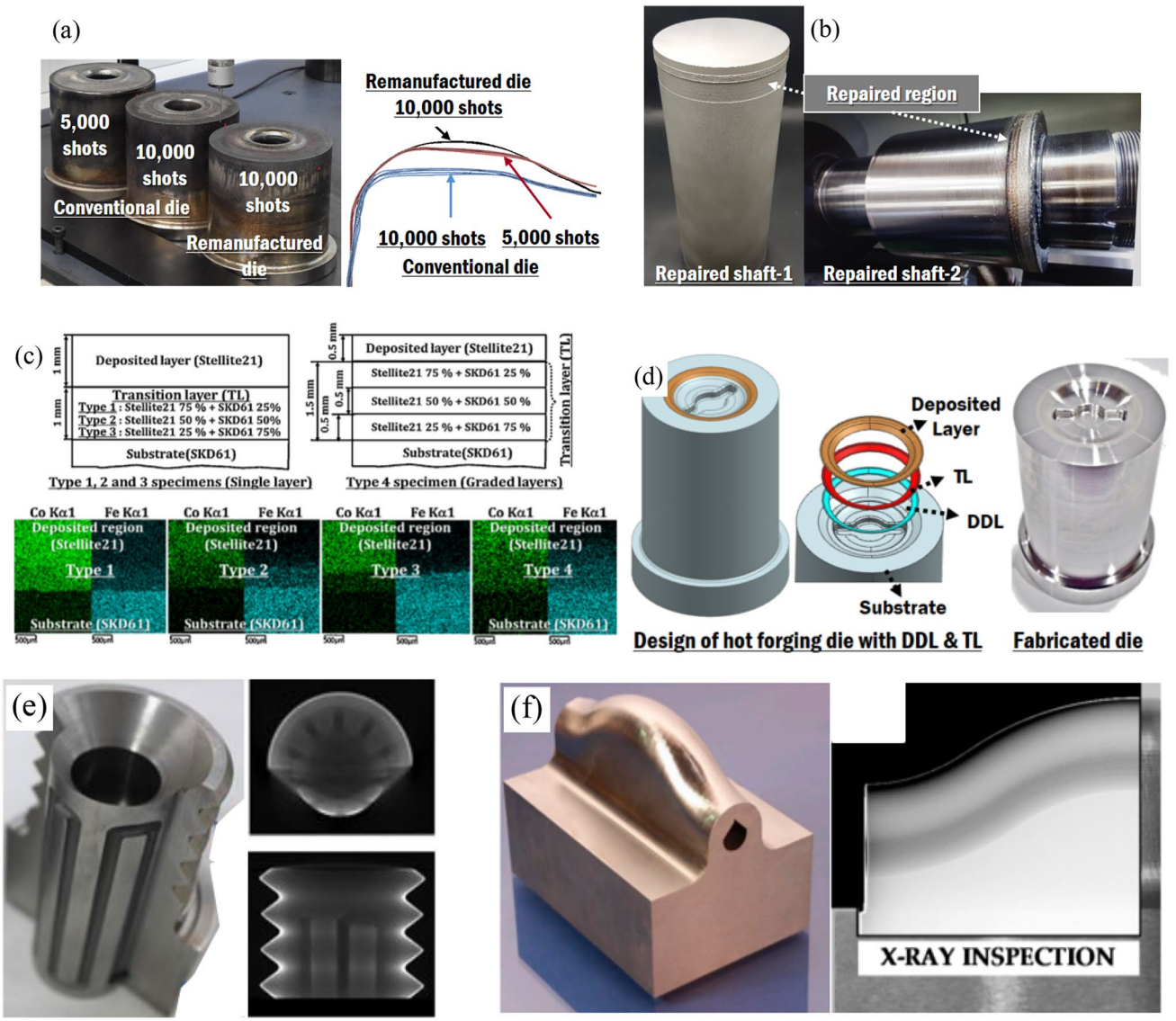

Fig. 8 Fabricated parts by LAM-DED processes: (**a**) comparison of external contours of remanufactured hot forging dies with those of conventional dies, (**b**) repaired weapon components (adapted from figures provided by Naval Shipyard of R.O.K and 3D Printing Center of KITECH with permission), (**c**) example of compositional graded interlayers (adapted from figures of reference 119 with permission) [119], (**d**) example of hot forging die with DDL and TL, (**e**) injection molds incorporating CCCs (adapted from figures reference 149 with permission) [149], and (**f**) hot stamping dies incorporating CCCs [adapted from figures reference 151 (Open Access)] [151]

casting tools from the viewpoint of economic efficiency [4, 32, 35, 51, 76, 77, 79–81, 106, 107, 109, 115–120]. Several researchers reported that the LAM-DED process can provide sharper and smaller deposition with focused high laser energy and improved metallurgical properties as compared to traditional repair technology, such as TIG welding, plasma welding and GTAW welding, [107, 115, 116]. Bennett et al. [116] revealed that the service life of dies repaired by the LAM-DED process is longer than that by a traditional repair process by factors of 3.4–8.0 times. Research on the 3R of molding, forming and die casting tools started from only the repair of tools with different types of defects, while those extended to remanufacturing of tools with improved functionality and performance [4, 32, 35, 76, 77, 79, 80, 106, 107, 116–120]. Ahn et al. remanufactured several hot forging dies with the wear resistance using a selective deposition technology based on the LAM-DED process [4, 119]. They demonstrated that the wear resistance and the service life can be greatly improved when remanufacturing technology based on the LAM-DED process is applied to the hot forging die, as shown in Fig. 8a [119]. Hong et al. [120] remanufactured trimming dies with 23F858 tool steel deposited on S45C structural steel using a DMT process owing to the improved service life of the dies. InssTek Inc. [80] remanufactured the mold of a headlamp to reduce cost and lead time using the DMT process. Morrow et al. addressed that LAM-DED processes can greatly reduce energy consumption, GHG emissions and manufacturing costs for repair and remanufacturing of molds and dies [4, 106, 117].

LAM-DED processes were used to repair various industrial and military parts. Lewis et al. applied the LAM-DED process to repair rail track. They reported that the LAM-DED process is highly recommended to repair track parts with a simple geometry [107, 120]. Rooyen et al. repaired austenitic stainless steel vessels using a LAM-DED process [107]. Liu et al. applied the LMD process to repair the sprocket of a scraper conveyor [109, 122]. Oh et al. [123] applied the DMT process to repair of damaged parts, which were fabricated from a PBF process. Recently, LAM-DMD processes were widely used to repair military parts. The military parts require a long delivery time and an expensive cost. Occasionally, the military parts are discontinued by the manufacturer. Hence, the repair of military parts has attracted attention as a promising application field of the LAM-DED process. The 3D printing center of KITECH (Korea) in collaboration with Navy Shipyard of R.O.K (Republic of Korea) repaired several military parts, as shown in Fig. 8b.

3.4.2 Porous Materials and Coating

Porous materials and coating technologies are emerging as an important application of LAM-DED processes [42, 80, 86, 124–128]. Carcel et al. [86] researched the fabrication of aluminum and titanium foamed layers on Ti–6Al–4V sheet by a LMD process. Koike et al. [124] investigated the manufacture of stainless steel foam with titanium hydride using a LAM-DED process. Recently, the LAM-DED process was applied to a porous coating for implants [42]. Dass and Moridi [42] reported that the porous coating technology using LAM-DED process offers benefits to fabricate porous implants as compared to conventional casting. Xu et al. fabricated porous titanium samples for implants from a LENS process [42, 124]. They also performed in vivo biocompatibility studies using the fabricated porous titanium samples [42, 124]. Bernard et al. [126] examined the fatigue behavior of a porous NiTi alloy for implants in a cyclic compression loading. They manufactured the porous NiTi alloy from a LENS process [126]. Bandyopadhyay et al. [127, 128] applied a LENS process to fabricate porous and functionally graded structures for load bearing implants. In addition, they investigated the in vivo response of porous titanium implants [128]. InssTek Inc. [80] in collaboration with Corentec Inc. developed porous coating technologies for customized implants using a DMT process.

3.4.3 Tailored Materials and Structures

The developed LAM-DED process employs multiple hoppers for feeding of different powders [4, 32, 51–54]. The feeding of different materials enables in situ synthesizing alloys with a location-dependent chemical compositions through mixing of different powders [4, 93, 129, 130]. The in situ synthesizing characteristics of the LAM-DED process can fabricate tailored materials [42, 52, 129, 130]. In addition, inherent deposition characteristics of the LAM-DED process, including line-by-line and layer-by-layer depositions of different materials, allow the manufacture of tailored structures in the material [4, 42, 52, 129, 130]. Representative examples of tailored materials and structures using the LAM-DED process are functionally graded materials and structures (FGM&Ss) with the graded composition as a function of position [4, 42, 52, 129, 130].

Three deposition strategies, including direct joining method (DJM), gradient path method (GPM) and intermediate section method (ISM), were utilized to create the FGM&S using the LAM-DED process [129]. The DJM deposits a successive layer with heterogeneous materials on a substrate or a previous layer without any interlayer between successive layers [51, 129]. The DJM was widely used to create bimetallic materials and structures as a common technology [4, 51, 131, 132]. Yadroitsev et al. [131] applied the DJM to deposition of Stellite12 on stainless steel 316. They investigated the influence of the layer thickness on gradient transition characteristics. They have estimated that the minimum thickness of FGM is 200 μm [131]. In addition,

they fabricated thin wall structures with the combination of bronze with stainless steel 430 L [131]. Park and Ahn [132] used the DJM to create bimetallic materials with a wear resistance layer through the deposition of Stellite6 and NOREM02 on SKD61 hot working tool steel. The DJM provided a key concept for restoration and remanufacturing of products through the deposition of heterogamous materials on even and uneven substrates [4, 35, 50, 51, 123, 133]. Several researchers and industries applied the DJM to the fabrication of bimetallic parts with volumetric heat sinks, wear resistance and the corrosion resistance [4, 32, 51, 77, 79, 80, 117, 120]. Cortina et al. [134] manufactured bimetallic hot stamping tools with a H13 coated layer on AISI 1045 steel from a LAM-DED process to apply a cheaper material to tools.

The DJM can cause cracking in the interface between different materials owing to the difference of lattice structures, thermal expansion coefficient and mechanical properties [4, 51, 119, 129, 132, 135]. The GPM and the ISM were used to overcome the cracking in the interface during the creation of FGM&S [4, 51, 119, 129, 130]. The GPM creates compositionally graded interlayers between different materials, as shown in Fig. 8d [51, 53, 93, 119, 130, 131, 136–140]. Ocylok et al. fabricated functionally graded multi-layers with mixed compositions between bottom and top layers using a LAM-DED process for the sake of improving the wear and corrosion characteristics of a die casting mold [51, 136]. Articek et al. [137] manufactured a continuously graded material consisting of H13 tool steel and Cu from a LENS process. Caroll et al. created a bulk part with compositionally graded interlayers between 304 L stainless steel and Inconel 625 using a RPM 557 laser deposition system [52, 131, 138]. Durejko et al. fabricated thin wall tubes with a Fe3Al/SS316L graded structure in the radial direction using a LENS process [129, 139]. Heer et al. developed a compositionally graded magnetic-nonmagnetic bimetallic structure consisting of 316 and 430 stainless steels using a LENS process [129, 140]. Ahn et al. [119] investigated the influence of the design of compositionally graded interlayers on wear characteristics, as shown in Fig. 8c. In addition, they manufactured hot working dies with a compositionally graded interlayer between SKD61 substrate and Stellite21 deposited layer for the purpose of improving wear characteristics and service life of the die [119].

The ISM creates an intermediate bonding layer, including additional materials, between different materials to avoid undesirable phases, which may be easily formed in the GPM [129]. A brittle intermetallic layer was formed in the interface when the titanium alloys is deposited on stainless steel and Inconel alloy [129, 141, 142]. An intermediate bonding layer with additional materials was required to improve joining characteristics through the elimination of a brittle intermetallic layer [129, 141, 142]. Saharabudhe et al. [141] fabricated a metallic structure with an intermediate bonding layer of NiCr to prevent delamination and cracks via the deposition of Ti–6Al–4V on 410 stainless steel. Several studies used graded vanadium, vanadium, chromium, and iron as materials of the intermediate bonding layer to deposit Ti–6Al–4V on stainless steel [129]. Onuike et al. [142] successfully deposited Ti–6Al–4V on an Inconel 718 substrate through the creation of an intermediate bonding layer with vanadium using a LENS process. Ahn and Kim [143] applied an intermediate bonding layer with Monel 400 between P21 and ampcoloy 940 to the fabrication of a thermal management mould using a DMT process. Kim et al. [144] adopted a damage diminution layer (DDL) between successive layers to improve the ductility of the deposited region. They also used transition layers (TLs) with graded compositions between successive layers to prevent cracking induced by the differences in thermal and mechanical properties [144]. Figure 8d shows an example of a hot forging die with DDL and TL.

3.4.4 Thermal Management

Various studies on applications of the LAM-DED process to the development of structures and parts related to a thermal management are performed. Representative applications of the LAM-DED process to the thermal management are the fabrication of conformal cooling channels (CCCs) and heat sinks for molding, forming and die casting tools [4, 32, 76–80, 84, 117, 143, 145–151]. Mazumder et al. and DM3D Inc. manufactured various injection molds with CCCs and volumetric heat sinks from a DMD process to reduce cooling and cycle times through improvement of the cooling rate [4, 32, 77, 79, 117]. Kolleck et al. [145] fabricated hot stamping dies incorporating CCCs using a DMD process. Vollmer et al. manufactured press-hardening tools with CCCs from a LMD process of Trumpf Inc. for the sake of reducing the tool temperature and the elimination of hot spots in the tools [147]. Ahn et al. developed thermal management molds with volumetric heat sinks using a DMT process for the purpose of uniform and rapid cooling of the molds [32, 143]. Ahn et al. in collaboration with Woosung Inc. developed several injection molds incorporating CCCs, including molds for a fan of a refrigerator, a window button of a car, a drawer of a refrigerator, etc., using a DMT process for the sake of improving the production efficiency and the product quality together [4, 32, 147]. They reported that injection molds incorporating CCCs can greatly enhance the production efficiency and the product quality [4, 32, 147]. Ahn et al. [147] patented design and fabrication technologies related to CCCs on curved surfaces. Soshi et al. [148] developed an injection mold incorporating a coolant grid using a DMG Mori LASERTEC 65 3D. They revealed that the injection mold incorporating a coolant grid can improve

cooling efficiency [148]. Extreme Fabrication Technology Group (EFTG) of KITECH manufactured various injection and blow molding molds, including molds for a TPE boot, a wheel hub cap, etc., to reduce cooling and cycle times, as shown in Fig. 8e [149]. In addition, the EFTG developed a direct metal tooling process for injection mold with curved CCCs [150]. Cortina et al. [151] have fabricated hot stamping dies incorporating CCCs using a LMD process, as shown in Fig. 8f.

4 Wire Feeding Type DED Processes: State-of-the Art

Wire feeding type DED processes are essentially the extension of welding and cladding processes, as shown in Fig. 2 and Table 1 [1, 4, 24, 40, 46, 58–60, 62–73]. The capture efficiency of the feedstock for the wire feeding type DED processes is nearly 100%, as shown in Table 2 [24, 57–59, 152]. The material usage efficiency of the wire feeding type DED process is extremely greater than that of the LAM-DED process [152]. In addition, wires are cheaper than powders [152]. Due to a higher deposition rate and the ability to fabricate larger structures, the wire feeding type DED process is proper to fabricate a part with a large volume [24, 42, 65, 152, 153]. The wire feeding type DED process is effective for simple geometries and a surface coating [58].

4.1 Wire and Arc Additive Manufacturing (WAAM) Process

4.1.1 Characteristics and Principle of WAAM Processes

The WAAM combines an arc, including electric and plasma arcs, as heat energy and a wire as a feed stock [4, 24, 42, 43, 59, 65, 154]. The WAAM process can be classified into three types according to the principle of the welding process: (a) gas metal arc welding (GMAW), (b) gas tungsten arc welding (GTAW) and (c) plasma arc welding (PAW) [24, 42, 43, 65, 154–157]. Table 5 shows merits and demerits for different WAAM processes [24, 65, 165]. Because the feeding direction of the wire is co-axial with the welding torch, the deposition path is easily created, as shown in Table 5 [24, 65, 157]. The set-up cost of the GMAW is cheaper than that of the GTAW and the PAW [165]. However, the GMAW includes several disadvantages, including residual stress, distortion and deterioration induced by an excessive heat input, [158]. Cold metal transfer (CMT) technology is the modified GMAW using the controlled dip transference [24, 65, 157]. The CMT technology can provide several advantages, such as a very low heat input, spatter-free metal transference, extremely stable electric arc, and sound welds, [24, 65, 157, 165]. In addition, the CMT technology can control the arc length on its own [157]. The GTAW and the PAW are more stable and reliable process than the GMAW [157].

The WAAM process based on GTAW can fabricate metallic parts with relatively smooth surface and high strength [54, 165]. The GTAW can greatly reduce porosity as compared to the GMAW [158]. The high temperature region of the arc of the PAW is narrower than that of GTAW. Hence, the WAAM based on PAW can create relatively narrower deposition bead [24]. WAAM processes based on GTAW

Table 5 Merits and demerits for different WAAM processes [24, 65, 156, 157, 159, 160]

Type	Merits	Demerits	Electrode	Deposition rate (kg/h)
GMAW	High efficiency and low cost Low initial set-up cost Relatively less complex process Co-axial feeding of wire Relatively easier deposition path	Unstable process in uneven deposition surfaces Low arc stability High spattering Excessive heating Excessive residual stress and deterioration Poor surface roughness Relatively greater distortion	Consumable	3–4 (CMT : 2–3)
GTAW	Smooth surface finish High strength of the deposited part Reduced porosity Relatively reliable process	Off-axis feeding of wire Change of welding direction Sensitive to arc length Complicated deposition path	Non-consumable	1–2
PAW	Narrow high temperature zone as compared to GTAW (Narrow weld beads) Relatively reliable process Relatively high welding speed	Necessity of rotation of torch		2–4

and PAW are used to deposit titanium due to the arc wandering problem of the WAAM process based on GMAW [65]. Unlike the WAAM process based on GMAW, WAAM processes based on GTAW and PAW off-axially feed the wire [4, 24, 65, 152–157]. The off-axial feeding of wire leads to a change of the welding direction and excessive sensitivity of the arc length [157]. The WAAM processes based on GTAW and PAW require rotation of the torch to maintain an identical feeding direction of the wire [65, 159]. The WAAM processes based on GTAW and PAW need a complicated path program [65, 157].

The WAAM process employs CNC gantries and robot systems for manipulating the motion of the welding torch and the wire feeder [65]. A typical layer thickness and the minimum feature size ranges from 1000 to 2000 μm together, as shown in Table 2 [24, 65, 154]. The energy efficiency of WAAM is less than 90%, as shown in Table 2 [4, 24]. The BTF ratio of WAAM can be reduced to 1.2 [65, 154]. The WAAM process can greatly reduce the waste of material due to a low BTF ratio as compared to conventional subtractive manufacturing (SM) processes [65, 154, 155, 157, 159]. The deposition rate of the WAAM process typically ranges from 16.7 to 66.7 g/min [24, 65]. The surface roughness of the fabricated part by the WAAM process is nearly 200 μm of R_a [59]. Deposition rates of WAAM processes based on GMAW, GTAW and PAW lie in ranges of 3–4 kg/h, 1–2 kg/h and 2–4 kg/h, respectively, as shown in Table 5 [160]. Wu et al. [160] summarized materials used in WAAM processes, as shown in Table 6.

4.1.2 Development of Processes and Systems

Table 7 summarizes representative research groups and used thermal energy sources for WAAM processes. Cranfield University (U.K), University of Sheffield (U.K), University of Wollongong (Australia), Tennessee Technological University (U.S.A), Oak Ridge National Laboratory (U.S.A), Indian Institute of Technology (India), and Harbin Institute of Technology (China) are representative active research groups working on WAAM processes, as shown in Table 7 [24, 44, 65, 161, 170]. In the early 1990s, Williams et al. in the Welding Engineering Center (WEC) of Cranfield University began to research the development of a WAAM process based on GMAW to increase the BTF ratio of expensive and high performance alloys through cooperation with Rolls-Royce plc [65, 155, 170]. They continuously developed advanced WAAM processes and their applications [65, 155, 159, 170]. WAAM3D was incorporated to commercialize WAAM technologies of Cranfield University [162]. Advanced Manufacturing Research Center (AMRC) at the University of Sheffield in collaboration with seven partners initiated Rapid Product of Large Aerospace

Table 6 Used materials by WAAM process for different WAAM processes [4, 24, 65, 157–160, 166]

Applications	Aerospace	Automotive	Marine	Corrosion resistance	High temperature	Tool and molds
Alloy	Ti, Al, Ni	A1, Steel	Ti, Steel, Bronze	Ti, Ni	Ti, Ni	Steel

Table 7 Representative research groups and used thermal energy sources of WAAM process

Research group	Country	Thermal energy source	References
Cranfield Univ. (WAAM3D Inc.)	U.K	GMAW, GTAW, PAW	[24, 44, 65, 154, 155, 158, 159, 161, 162, 170, 173]
Univ. of Nottingham	U.K	GMAW	[24, 44, 160, 173]
Univ. of Sheffield (Advanced manufacturing research center)	U.K	GTAW	[24, 44, 65, 153, 155, 160, 161, 170]
Univ.of Wollongong	Australia	GMAW, GTAW	[24, 44, 160, 161, 170, 174]
Ock Ridge National Laboratory	U.S.A	GMAW, GTAW	[115, 163, 164]
Tennessee Technological Univ.	U.S.A	GMAW (CMT), GTAW	[54, 165]
RAMLAB Inc.	Netherlands	GMAW	[166]
MX3D Inc	Netherlands	GMAW	[167, 172]
Indian Institute of Technology	India	GMAW, PTA	[24, 44, 161, 175]
Harbin Institute of Technology	Chania	GMAW, GTAW	[24, 44, 161, 175]
Beijing Institute of Technology	Chania	GTAW	[152]
Federal Univ. of Parana	Brazil	Micro-PTA	[64]
IK4-LORTEK Inc.	Spain	GMAW (CMT), GTAW (TopTIG)	[157]
Norsk Titanium Inc.	Norway	PAW	[42, 57, 169]

Components (RAPOLAC) in 2005 [65, 153, 155, 170]. The project was focused on the WAAM process based on cold wire-fed GTAW to fabricate large parts with a variety of aerospace material [155, 170]. University of Wollongong developed a robot WAAM process integrated a closed loop control system [24, 160, 161]. Kim et al. et al. of Tennessee Technological University developed a robot WAAM process based on CMT and GTAW, as shown in Fig. 10a [54, 165]. Oak Ridge National Laboratory (ORNL) in collaboration with Wolf Robotics and Lincoln Electric developed a robot WAAM process based on the GMAW for a metal big area additive manufacturing (MBAAM), as shown in Fig. 10b [162, 163]. Rodriguez et al. [157] developed WAAM processes based on CMT and TopTIG for stainless steel. Norsk Titanium commercialized a WAAM process based on PAW, which is a Rapid Plasma Deposition (RPD) process, to fabricate a large part using titanium alloys [42, 57, 169]. Several WAAM machines, such as GTarc300-3 WAAM machine (Gefertec GmbH, Germany), VARIAXISj-600 AM (Mazak, Japan), Addilan V0.1 (Addilan, Spain), ArcMan-600 (Nanjing Enigma Automation, China), RC-WAAM-3000 (Nanjing Zhongke Raycham Laser Technology, China), etc., were commercialized [162, 169].

4.1.3 Effects of Deposition Parameters

Representative deposition parameters of the WAAM process are arc current, arc voltage, working distance, travel speed, feed rate of wire, flow rate of shielding gas, deposition path, interpass time, dwell time between successive layers, material of wire, diameter of wire, etc., as shown in Fig. 9 [58, 152–161, 168, 171–181]. Ji et al. [152] investigated the influence of heat input, layer thickness, deposition path, and wire curvature on the formation and the mechanism of defects to control macro defects for the fabrication of TC4 alloy using a WAAM process based on GTAW. Rodriguez et al. [157] examined the effects of deposition parameters, including the arc current, the wire feed rate, the arc voltage, the travel speed, the arc length, the deposition rate, and the deposition path, on bead formations, temperature histories during deposition and tensile properties for WAAM processes based on CMT and TopTIG. In addition, they performed building experiments of large parts using selected proper deposition conditions for the WAAM processes based on CMT and TopTIG [157]. Dinovitzer et al. [171] investigated the effects of the wire feed rate, the travel speed, the arc current, and the argon flow rate on the bead geometry and the microstructure of the fabricated HASTELLOY X part by a WAAM process based on GTAW through a design of experiments (DOEs) . They reported that the bead height is greatly dependent on the feed rate of the wire, while the melting depth and the surface roughness are independent on the feed rate [158, 171].

Yehorov et al. [176] studied on the effects of the travel speed, the deposition rate, and the wire feed rate on the surface quality of a thin wall part fabricated by a WAAM process based on GMAW. Shen et al. [177] examined the influence of the arc current and the interpass temperature on the morphology, the phase change, the hardness, the chemical composition, and the tensile property of a Fe3Al-based

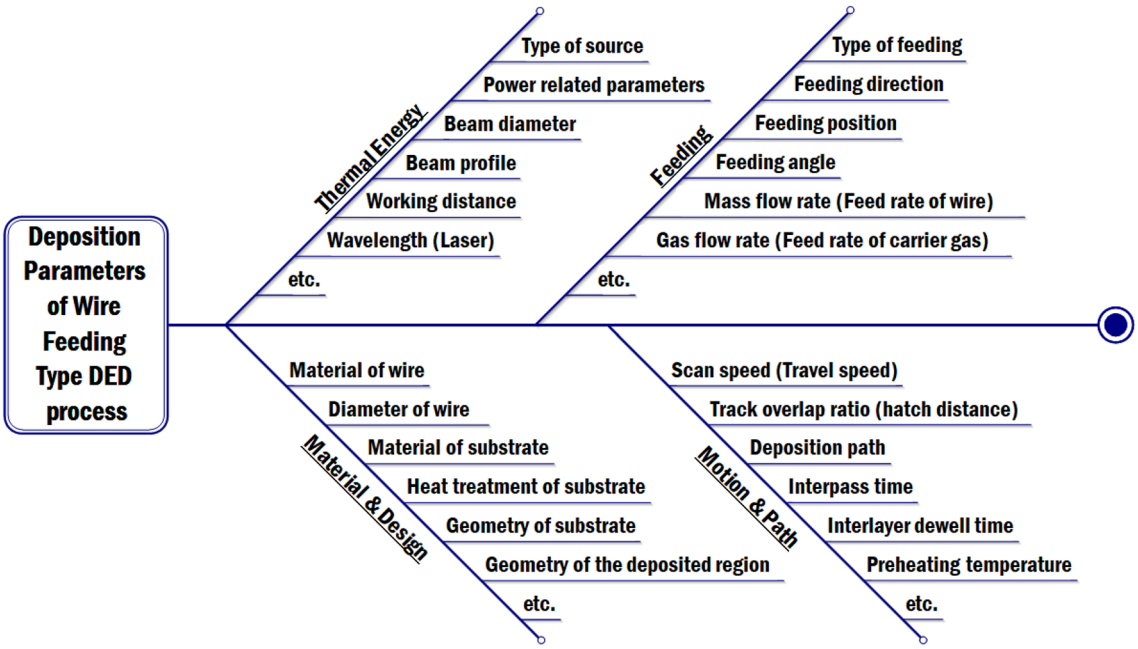

Fig. 9 Deposition parameters of wire feeding type DED processes [24, 46, 58, 66–68, 71, 73, 152, 154–165, 168, 170–181, 185, 188, 189, 191, 194, 200, 203, 204, 212, 217–219, 221–224]

iron aluminide part fabricated by a WAAM process based on GTAW. Wu et al. [178] examined the influence of the heat accumulation on arc characteristics and metal transfer behavior during deposition in WAAM of Ti–6Al–4V parts. Gokhale et al. investigated the effects of the arc current, the torch speed, the wire feed rate, and the torch angle on the formation of the bead to fabricate a thin wall structure using a WAAM process based GTAW [158, 179]. They reported that the torch angle is a dominant parameter to determine the formation of the bead. Martina et al. [159] investigated the influence of the wire feed rate, the arc current and the travel speed on the bead formation and the surface waviness of the deposited part to obtain a processing map for a WAAM process based on PAW. Jhavar et al. [175] examined the effects of the plasma power, the travel speed and the wire feed rate on the formation and the quality of the deposited bead by a WAAM process based on a micro PTA.

Rodrigues et al. [172] reported that the deposition path greatly affects defects, including the porosity, the surface waviness, the hump, recurrent macrostructural problems, etc., and residual stress distributions of the fabricated part by a WAAM process. Li et al. [168] investigated the influence of the overlap ratio of in-plane and out-of-plane and the deposition path of out-of-plane on the surface profile of the fabricated part by a robot WAAM process based on GMAW. Ding et al. [180] proposed a tangent overlap model to improve the surface profile and roughness of the fabricated part by a robotic WAAM process. Ma et al. [181] employed weaving techniques for improving the surface flatness of a large and thin wall structure. Wu et al. [174] studied the effects of forced interpass cooling on the bead geometry, the surface oxidation, the macrostructure, the microstructure, the hardness, the mechanical properties, and the fracture behavior of the fabricated Ti–6Al–4V part by a WAAM process based on GTAW.

4.1.4 Applications and Fabricated Parts

The WAAM processes widely applied to the fabrication of a large-sized part using expensive materials, as shown in Table 8 [65, 162, 166, 167, 169, 172, 182]. The WEC of Cranfield University fabricated large-sized aerospace components, including a Ti–6Al–4V wing spar, a Ti–6Al–4V external landing gear rib, an aluminum wing rib, and a Ti–6Al–4V pylon mount, using WAAM processes based on PAW and CMT, as shown in Table 8 [65, 162, 172, 182]. The WEC reported that the WAAM processes can greatly reduce the BTF and the fabrication cost as compared to conventional manufacturing, such as conventional and high-speed machining, processes as shown in Table 8 [65, 172, 183]. In addition, in order to reduce the lead time, the WEC of Cranfield University fabricated a wing for wind tunnel test and a profiled cone using a WAAM process based on CMT, as shown in Table 8 [65]. Clark et al. investigated the

Table 8 Applications of WAAM processes

Applications	Dimension/weight	Based process	Materials	Deposition rate (kg/h)	BTF of CM	BTF of WAAM	Cost reduction (%)	References
Wing spar	1.2×0.2 m^2 (In-plane)/17 kg	PAW	Ti–6Al–4V	0.8	6.5	2.15	29	[65, 162, 172, 182]
External landing gear rib	0.8×0.7 m^2 (In-plane)/24 kg	PAW	Ti–6Al–4V	0.8	12	2.3	69	[65, 162, 172, 182]
			Steel	0.8	12	2.3	55	
Wing rib (Conventional machining)	2.5 m (Length)/15 kg	CMT (two torches)	Al	1.1	45	2.9	65	[65, 162, 172, 182]
Wing rib (High speed machining)	2.5 m (Length)/15 kg	CMT (two torches)	Al	1.1	45	2.9	61	[65, 162, 172, 182]
Wing for wind tunnel test	0.8 m (Length)	CMT	High strength steel	3.5	–	–	–	[65]
Pylon mount (Original design)	7.6 kg	–	Ti–6Al–4V		5.1	1.5	7	[65, 162, 172, 182]
Pylon mount (Topologically optimized)	3.9 kg	–	Ti–6Al–4V	–	6	1.5	29	[65, 162, 172, 182]
Profiled cone	0.4 m (Diameter)	CMT	Mild steel	2.6	–	1.25	–	[65]
Propeller	1.35 m (Diameter)/180 kg	GMAW	Bronze alloy	–	–	–	–	[166]

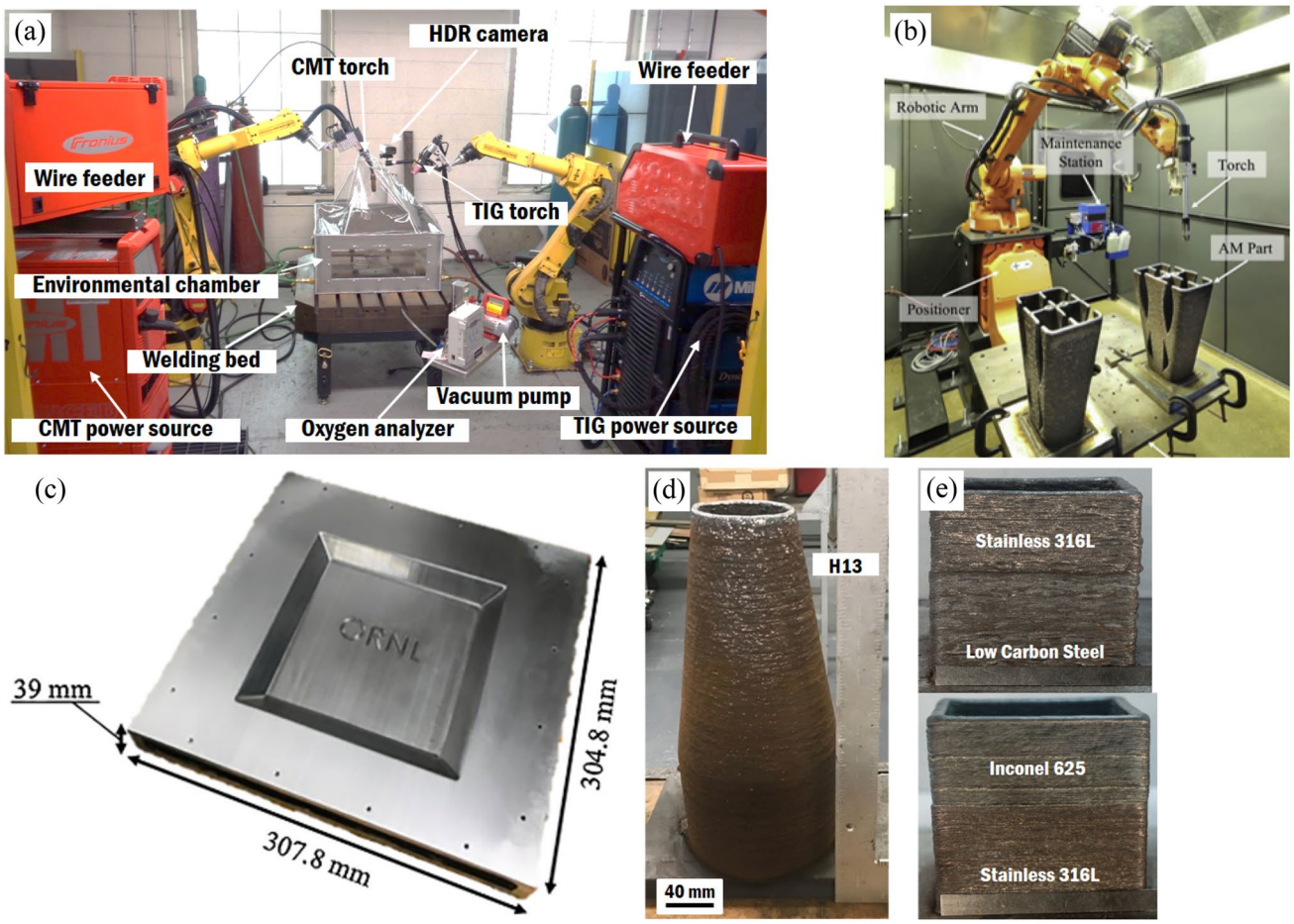

Fig. 10 WAAM systems and fabricated parts: (**a**) WAAM system of Tennessee Technological University (reprinted from figure provided by Prof. Duck Bong Kim of Tennessee Technological University with permission), (**b**) MBAAM system and fabricated parts of ORNL (reprinted from figure of reference 164 with permission) [164], (**c**) fabricated mould for compression molding by MBAAM system (reprinted from figure of reference 164 with permission) [164], (**d**) fabricated part with a large volume (reprinted from figure provided by Prof. Duck Bong Kim of Tennessee Technological University with permission) and (**e**) examples of BAMS (reprinted from figures provided by Prof. Duck Bong Kim of Tennessee Technological University with permission)

application of a shape metal deposition (SMD) process to the fabrication of a nickel alloy part for aero engine components [183]. RAMLAB Inc. [166] successfully manufactured a ship propeller with a diameter of 1350 mm, dubbed WAAMpeller, from a WAAM process based on GMAW. A bronze alloy, Nickel Aluminum Bronze (NAB), was used as the deposition material [166]. Norsk Titanium Inc. produced the FAA approved structural components of Boeing 787 Dreamliner using a WAAM process using PAW [169, 184]. RAMLAB and Norsk Titanium forecasted that WAAM processes can greatly reduce the lead time, the cost and the waste [166, 169]. In addition, Norsk Titanium predicted that the RPD process can reduce the used titanium alloys by nearly 25–75% as compared to forging and metal working processes [169]. ONRL fabricated a big metallic part with a large volume, as shown in Fig. 10b, c [164]. Kim et al. of Tennessee Technological University fabricated various parts with a large volume using high entropy alloy, as shown in Fig. 10d. Li et al. [56] manufactured stiffened panels from a WAAM process based on a tandem GMAW. They created Al 2325 stiffeners with a thin wall on an Al2219 alloy.

Several researchers fabricated bimetallic additively-manufactured structures (BAMS) through mixing of the material using a dual wire feeding into the molten pool [54]. Kim et al. of Tennessee Technological University fabricated BAMS from a WAAM process based on CMT, as shown in Fig. 10e [54, 165]. Kim et al. deposited different materials in bottom and top regions to create a BAMS. Wu et al. [156] manufactured a different type BAMS, in which a Ni deposited region is parallel to a steel deposited region in the horizontal direction, from a WAAM process based on GTAW.

4.2 Wire and Laser Additive Manufacturing (WLAM) Process

4.2.1 Characteristics and Principle of WLAM Processes

The WLAM process is one of the MAM processes to produce metallic parts without porosity using a laser, such as diode, disc, Nd:YAG, CO_2, and fiber lasers, as a thermal energy source and an metallic wire [4, 24, 61, 67, 73, 153, 185–202]. The WLAM process fundamentally uses the concept of laser cladding and welding, as shown in Table 1 [4, 24, 66, 67]. As compared to the LAM-DED process using powders, the WLAM process provided promising advantages, such as a clean fabrication environment without metal dust pollution, reduced cost to produce wire, reduced material wastage, improved surface roughness, and a high deposition rate, from the viewpoint of a green technology [188, 189]. The deposition rate of the WLAM generally ranges from 1.5 to 48.0 g/min, as shown in Table 2 [24]. The layer thickness of the WLAM process is typically greater than 1000 μm [186, 201]. The WLAM process is widely applied to surface protection, surface treatment, repair and feature addition [190–192]. Recently, the application of the WLAM process area was extended to the mBAAM for the manufacture of metallic parts with an extremely large volume due to characteristics of a high deposition rate [190, 191]. Ti-based, Ni-based, Fe-based, and Al-based alloys are utilized as the material of the wire [24, 61, 185–191]. Many researches focused on Ti–6Al–4V to develop applications of the WLAM process to the aerospace industry in recent years [24, 153]. The diameter of the used wire by the WLAM process normally ranges from 0.2 to 1.2 mm [24, 186]. The WLAM process employs a high power laser for melting the substrate and the wire [4, 24, 191]. The width of the bead deposited by the WLAM process usually lies in the range of 5–15 times of the wire diameter [59, 186]. Hence, in order to decrease the minimum feature size of the WLAM process, the wire diameter should be reduced [186]. The mean surface roughness of the WLAM part ranges from 40 μm of R_a to 60 μm of R_a for the case of flat deposition [73, 185]. The travel speed of the laser commonly lies in the range of 0.05–2.4 m/min in the WLAM process [24]. Unlike the WAAM process, a hardness gradient within the top region of the deposited part by the WLAM process manifests due to repeated rapid heating, melting, solidification, and cooling cycles during the deposition process [153, 187, 193]. The hardness gradients affect the increased tensile strength of the top region [153, 187]. The tensile strength in the deposition direction is greater than that in the building direction [153, 187, 193]. Anisotropic characteristics with different mechanical properties in the deposition and building direction appear in the fabricated part by the WLAM process [153, 187, 191, 193].

4.2.2 Development of Processes and Systems

Various types of WLAM processes and systems have been developed [24, 61, 66, 153, 187–193]. The WLAM process can be classified into lateral and co-axial types according to the feeding type of the wire [24, 59, 61, 153, 185, 188–195, 198]. Lateral feeding of the wire is a common method to deliver the wire to the molten pool in the WLAM process [24, 59, 66, 73, 185, 194–197, 199]. Miranda et al. [194] developed a WLAM set-up for rapid prototyping using a Ti–6Al–4V wire. The system included a Yb fiber laser with a maximum power of 8 kW, a fiber coupler and a five axis rig [194]. EDAS Innovation Works Inc. devised an experimental set-up consisting of a lateral wire feeder (Weldaix Inc.), Nd:YAG laser with a maximum power of 3.5 kW, a

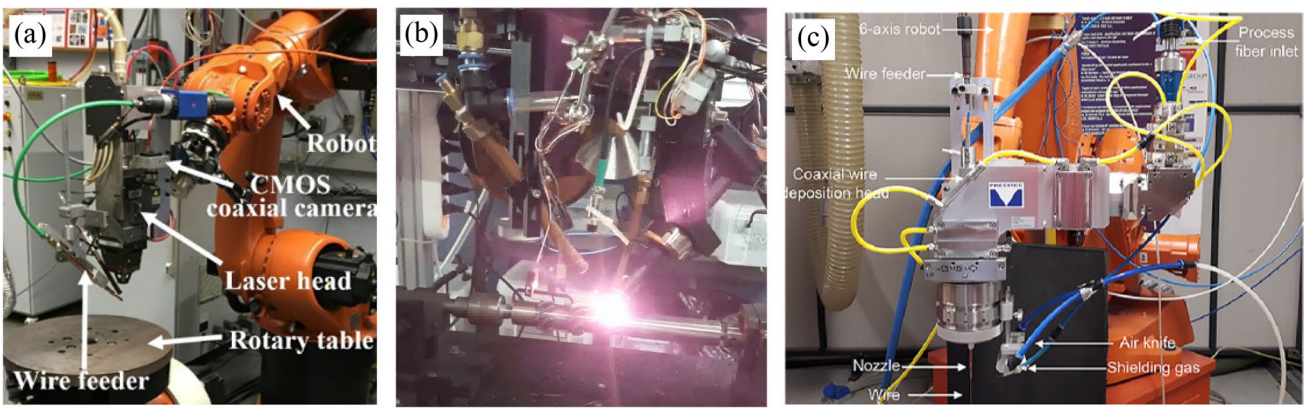

Fig. 11 Developed WLAM systems: (**a**) robotized laser-wire direct metal deposition system (reprinted from figure of reference 191 with permission) [191], (**b**) WLAM system with a rotating wire feeder (reprinted from figure provided by Ph.D Jae Gu Kim of KIMM with permission) and (**c**) LMWD system with a coaxial wire deposition head (reprinted from figure reference 61 with permission) [61]

high accuracy 6-axis robot (KR 100, KUKA Inc.), a COMS camera, and a thermography camera for the WLAM process [153, 187]. Research Center for Advanced Manufacturing at Southern Methodist University developed a robotized laser-wire direct metal deposition system, including a 6-axis robot (KR-60) with a 2-axis rotary table, an fiber laser with a maximum power of 4 kW (IPG Inc.), a wire feeding system (Binzel Inc.), and a CMOS camera (Prosilica GC640), as shown in Fig. 11a [191].

ORNL in cooperation with GKN aerospace Inc. developed a WLAM system, including a laser with a maximum power of 20 kW, a lateral wire feeder, and an online monitoring camera, for mBAAM using a titanium alloy [190, 191]. Su et al. [196] devised a WLAM system using a pulsed Nd:YAG laser. The system included an infrared thermograph and a CNC worktable [196]. Lincoln Electric Company (USA) developed a work cell, including a laser hot wire (LHS) system mounted on a Fanuc robot, for near-net shaping using metallic wires [197]. The LHS system offered potential for a high deposition rate using a low laser power owing to resistive preheating of the wire [197, 198]. In addition, the LHS could provide several advantages, including low melt-back of the diluted region, thermal stability and metallurgical control, for additive manufacturing of metals [196]. In order to improve the process stability through the reduction of the risk of process stoppage induced by wire oscillation and the productivity through the application of additional wires, the diameter of the laser beam was larger than that of the wire for the case of a conventional WLAM process [68, 185, 194]. Kim and Lee [195] developed a novel WLAM process with a rotating metal wire feeder to ensure front feeding of the wire irrespective of the deposition path, as shown in Fig. 11b. Demir [186] investigated a micro laser metal wire deposition (MLMWD) process for additive manufacturing of thin-wall structure. The MLMWD process employed a pulsed Nd:YAG laser and an in-house built wire feeder for precise control of the deposited region [186]. In the MLMWD process, the beam diameter was comparable to that of the wire to allow correct positioning of the laser over the deposited wire unlike a conventional WLAM process [186].

Although the lateral feeding type easily implements the concept of the designed WLAM process, the lateral feeding type of WLAM process is greatly sensitive to wire feeding and deposition conditions [24, 59, 73, 153, 189, 195]. With the lateral feeding type WLAM process, it is difficult to create the deposition path considering the proper feeding direction and location of the wire during the deposition of a complex shape as compared to the co-axial feeding type [191]. In addition, the lateral feeding of the wire causes anisotropic deposition problems, limited mobility of the deposition head and reduced flexibility of the deposition geometry [61, 153]. In order to overcome disadvantages of the lateral feeding type WLAM process, several co-axial feeding type WLAM processes with vertical feeding of the wire have been introduced [61, 199–203]. The wire is vertically fed to the laser focus for the case of the co-axial wire feeder. Several split separate beams and an axisymmetric multi-laser beam source are focused on a focal point through lateral irradiation of the laser beam for the case of the laser cladding head with a co-axial wire feeder [191, 201]. The co-axial feeding type WLAM process allows omni-directional deposition [191, 201]. Wang et al. [200] devised a co-axial feeding type of directed laser deposition (DL) system with vertical wire feeding inside of an annular laser beam.

Fraunhofer Institute for Material and Beam Technology (IWS) commercialized a novel laser cladding head with a co-axial wire feeder (COAXwire) [191, 201]. ORNL in collaboration with GKN aerospace developed a WLAM process using a COAX laser wire feeding system [190]. Brueckner et al. [201] employed a COAXwire cladding head consisting of an IPG fiber laser with maximum power of 400 W and a modified DINSE wire feeding system for fabricating a small-sized part. Motta et al. [61] developed a laser metal wire deposition (LMWD) system. The system consisted of a coaxial wire deposition head (CoaxPrinter) a multi-mode active fiber laser with a maximum power of 3 kW (YLS-300), a 6 axis anthropomorphic robot with a rotary table (ABB IRB 2400-10), and a high speed imaging system (Fastcam Mini AX200), as shown in Fig. 11c [61]. Kotar et al. [202] devised an experimental set-up to investigate the initial transient phase and the stability of the annular laser beam direct wire deposition (ALB-DWD) process. Fu et al. [199] developed a WLAM process using an axisymmetric multi-laser source and vertical wire feeding. They used three laser beams and a coaxial wire feeder [199].

4.2.3 Effects of Deposition Parameters

The quality and the properties of parts fabricated by the WLAM process are dependent on the laser power, the travel speed, the beam diameter, the track overlap ratio, the deposition path, the interpass time, the interlayer dwell time, the wire feeding direction, the feeding angle, the wire tip position, etc., as shown in Fig. 9 [24, 66–68, 73, 185, 188, 189, 191, 193, 200, 201, 204]. Several researchers reported that the wire tip should be immersed in the molten pool to create continuous and smooth beads with a uniform surface aspect [66, 194]. The combination of the wire feeding direction and the wire tip position in the molten pool remarkably affected the droplet transfer and the bead quality [24, 61, 67, 73, 185, 189, 199, 205]. Most previous research works revealed that front and side feeding can fabricate a good deposition bead as compared to back feeding [24, 67, 73, 185, 199, 205]. In addition, it was suggested that the proper feeding

angle of the wire ranges from 20 ° to 60 ° [67, 73, 185]. Syed and Li [205] reported that pores hardly appear in the multi-layer deposited part when front feeding of the wire is adopted. Xiao et al. reported that rear feeding of the wire is more effective than front and side feeding for the case of the aluminum welding using a CO_2 laser [24, 205]. Syed and Li [205] suggested that the trail edge is a proper position of the wire in the molten pool for the case of rear feeding.

The laser power, the travel speed and the wire feed rate are major deposition parameters to determine the deposition rate of the material, the characteristics of the deposited region and the occurrence of defects [24, 61, 66, 185, 188, 189, 194]. The feed rate of the wire is limited by the LEL [24, 188, 189]. The intermittent dripping phenomenon in the deposited bead occurs when the feed rate of the wire is very low for a high LEL, while a stubbing phenomenon in the deposited bead takes place when the feed rate of the wire is excessively high for a low LEL [24, 61, 188, 189]. Motta et al. [61] predicted the process feasibility map to estimate an appropriate LEL for the deposition of AISI 308 stainless steel using the LMWD process with a coaxial wire deposition head. In addition, they reported that power decay strategies or close-loop temperature control is needed to maintain a stable molten pool size through the prevention of heat accumulation during multi-layer deposition [61]. Kotar et al. [202] developed process-stability windows to predict an appropriate combination of initial laser power and workpiece irradiation proportion (WIP) of each wire feed rate for the deposition of SS 316 wire on a SS 304 substrate using the ALB-DWD process. Deposition rate and area can be estimated by the ratio of the wire feed rate to the travel speed when the diameter of the wire is fixed [24, 186, 194]. Demir [186] defined equations to predict the deposited volume of the wire, the delivered volume of the wire and the material use efficiency for the deposition of single and multiple layers. Chua et al. [203] investigated the influence of the laser power, the travel speed and the bead length on the temperature distribution and the residual stress. Caiazzo [206] derived an equation to estimate the deposition rate of wire. The porosity of the deposited region was considered in the equation [206].

Characteristic dimensions of the deposited region, the diluted region and the HAZ for the WLAM process are greatly influenced by the three major deposition parameters [24, 67, 186, 188, 189, 197, 200, 206]. Mok et al. reported that the height of the bead is mainly influenced by the travel speed, whereas the width of the bead is significantly dependent on the laser power [24, 67]. Demir [186] estimated empirical equations related to relationships between process parameters, including the laser energy, the pulse duration and travel speed, on characteristics dimensions of the deposited bead and the diluted region for the deposition of AISI 301 wire on the AISI 316 substrate using the pulsed Nd:YAG laser. Kottman et al. [197] estimated process maps for dilution as a function of the laser power and the hot wire power when the Ti–6Al–4V wire is deposited by the laser hot wire process. Caiazzo [206] examined the effects of the laser power, the travel speed, and the wire feed rate on the formation of the bead, the fusion zone and the pores in the vicinity of the deposited region. Brandl et al. [207] extensively investigated the influence of the laser power, the travel speed, and the wire feed rate to the travel on dimensions and hardness of the bead, the fusion zone and the HAZ for the deposition of Ti–6Al–4V using a Nd:YAG laser.

The deposition path, the interpass time and the interlayer dwell time (interlayer cooling time and interlayer time interval) greatly affected residual stress distributions, mechanical properties and microstructures in the vicinity of the deposited region [191, 193, 203, 204]. Akbari and Kovacevic [191] examined the effects of the interlayer time interval on the thermal history, the microstructure and the mechanical properties of the fabricated part by the robotized LWDMD process. Bandari et al. investigated the influence of the interlayer cooling time on distortion and mechanical properties in

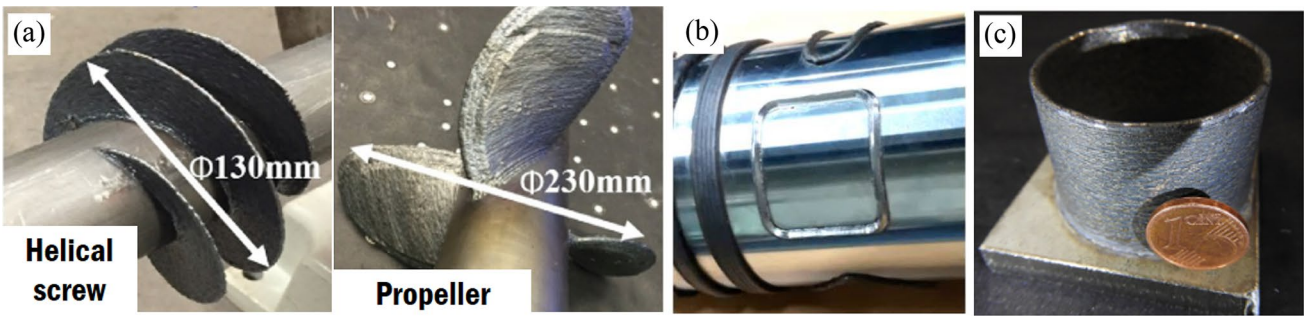

Fig. 12 Fabricated parts by the developed WLAM systems: (**a**) helical screw and propeller fabricated by the robotized laser-wire direct metal deposition system (reprinted from figures of reference 191 with permission) [191], (**b**) Ti–6AL–4V structures on curved surfaces fabricated by the WLAM process with a rotary wire feeder (reprinted from figure provided by Ph.D. Jae Gu Kim of KIMM with permission) and (**c**) cylindrical thin wall structure with a small volume fabricated by a LMWD system with a coaxial wire deposition head (reprinted from figure of reference 61 with permission) [61]

the WLAM process to deposit Ti–6Al–4V [193, 208]. They reported that a longer interlayer cooling time increases the distortion of the fabricated part, while the interlayer cooling time hardly affects the mechanical properties of a large scale part [193]. Chua et al. [204] examined the effects of the deposition path, the deposition direction, and the interpass time on thermo-mechanical characteristics for Ti–6Al–4V thin wall deposition through a three-dimensional finite element analysis (FEA). Chua [209] proposed a control scheme of the interpass time to make a uniform interpass temperature during successive deposition of the bead in a plane using FEAs. Ding et al. [210] developed a path planning program based on Matlab software to deposit a complex part using an 8-axis robotized WLAM system.

4.2.4 Applications and Fabricated Parts

The WLAM process is not actively applied to industrial parts yet. Feasibility studies are in progress to fabricate metallic parts using developed WLAM systems. Brandl et al. [153] fabricated a Ta-200 cylinder and Ti–6Al–4V thruster using a laser beam based deposition process. Akbari and Kovacevic [191] created several thin wall structures with a medium volume, such as a ball structure, a helical screw structure, a propeller structure, etc., on thin plates and cylindrical bar from a robotized laser-wire direct metal deposition system, as shown in Fig. 12a. Kim and Lee [195] deposited several Ti–6Al–4V structures on flat and curved surfaces using a WLAM process with a rotary wire feeder, as shown in Fig. 12b. Kottman et al. [197] applied a WLAM process using a hot wire to repair of a shot block for die casting. Fu et al. [199] fabricated several test parts using a WLAM process with a vertical wire feeder. WLAM processes with a coaxial wire feeder frequently used to fabricate small metallic parts with a thin wall structure. Motta et al. [61] manufactured a cylindrical thin wall structure with a small volume from a LMWD system, as shown in Fig. 12c. Demir [186] created a small-sized thin wall structure with an aspect ratio of up to 20 on an AISI 316 substrate using the μLMWD process. Brueckner et al. [201] fabricated a near-net-shape pin structure with an extremely small volume.

4.3 Wire and Electron Beam Additive Manufacturing (WEAM) Process

4.3.1 Characteristics and Principle of WEAM Processes

The WEAM process uses an electron beam (ebeam) as a thermal energy source. The ebeam is a stream of accelerated electrons with kinetic energy unlike the laser [211]. A thermal energy is generated by a collision between electrons and materials when the ebeam is applied to the material processing [211]. The ebeam is applicable to highly reflective and conductive materials, such as copper, aluminum, etc., [41, 46, 212]. The energy density, the energy efficiency, the scan speed, the penetration depth, and the deposition rate of the ebeam are significantly greater than those of the laser, as shown in Table 2 [24, 46, 62, 63, 69–71, 213, 214]. The deposition rate and the layer thickness of the WEAM process are less than 330 g/min and 3000 μm, respectively, as shown in Table 2 [24, 40, 69–71]. The WEAM process is also suitable for the fabrication of parts with a large volume. The ebeam gun included a vacuum environment to prevent electron scattering induced by the collisions between electrons and molecules of elements of air [46, 63, 69–72, 211]. In addition, a vacuum furnace with a protective environment is needed to prevent both electron scattering in the furnace and X-ray irradiation to the operator [46, 63, 69–72, 211, 214]. The deposition of the material in a vacuum environment ensures clean operation without a consumable shield gas [212]. The vacuum environment can reduce impurities [215].

Two types of ebeam gun, including thermionic and plasma Ebeam guns, are adopted for the WEAM process. Table 9 shows features of a thermionic ebeam (T-ebeam) and a plasma ebeam (P-ebeam). The T-ebeam and the P-ebeam use hot and cold cathodes to generate a stream of free electrons, respectively, as shown in Table 9 [41, 46, 211, 212]. Free electrons are emitted by heating of the filament in the T-ebeam gun, while they are emitted by the collision of the activated ions from the plasma gas into the cold cathode [41, 211, 212]. The emission temperature of the hot cathode is greater than 2200 °C, while that of the cold cathode is nearly room temperature [211]. Hence, the service life of the hot cathode is remarkably short than that of the cold cathode due to evaporation and erosion of the hot cathode, as shown

Table 9 Comparison of features of a thermionic ebeam with those of a plasma ebeam [41, 46, 211, 213]

Features	Thermionic electron beam (T-ebeam)	Plasma electron beam (P-ebeam)
Cathode	Hot cathode	Cold cathode
Emission temperature (°C)	> 2,200 (for tungsten)	≈ room temperature
Service life of cathode (hours)	< 50	> 100
Vacuum (Torrs)	10^{-4}–10^{-6}	10^{-2}–10^{-4}
Cost of gun	Relatively expensive	Relatively cheap
Acceleration voltage (keV)	1–150 (commercialized system)	1-30 (commercialized system)

in Table 9 [41, 46, 211, 212]. The T-ebeam gun requires a high level vacuum environment in the range of 10^{-4} to 10^{-6} Torrs to avoid oxidation of the cathode material, while the P-ebeam gun needs a low level vacuum environment in the range 10^{-2} to 10^{-4} Torrs, as shown in Table 9 [41, 46, 211, 212]. The WEAM system using P-ebeam is cheaper than that using T-ebeam [46]. The typical diameter of the wire for the WEAM ranges from 0.5 mm to 3.0 mm [46]. A coating of the wire using a corrosion-resistive material is needed to prevent oxidation of the wire [46].

4.3.2 Development of Process and System

Research on the WEAM process was initiated by Dave et al. of MIT in U.S.A. [213, 216]. NASA Langley Research Center (LaRC, U.S.A) patented the electron beam free-form fabrication (EBF^3) process [24, 46, 69, 212, 214]. The EBF^3 process used a T-ebeam gun to weld materials [46, 214, 217]. NASA LaRC developed two types of EBF^3 system, including ground-based and portable systems [46, 217]. The ground-based consisted of T-ebeam guns with a maximum acceleration voltage of 60 keV and a dual wire feeder, respectively [46, 217]. The dual wire feeder of the ground-based EBF^3 system used to feed either fine or coarse wires to fabricate parts with different feature sizes or two different alloys to create the product with gradient properties [217]. The portable EBF^3 system, including a maximum acceleration voltage of 20–30 keV and a single wire feeder, was developed to investigate the influence of the microgravity on the fabrication characteristics [217, 218]. The EBF^3 process used an off-axis feeding method of the wire [46, 218]. The EBF^3 process has been applied to the deposition of Ni, Ti, Cu, and Al alloys for aerospace application [218].

Sciaky Inc. (U.S.A) patented an electron beam additive manufacturing (EBAM) process using a T-ebeam gun, as shown in Table 10 [46, 69]. Sciaky Inc. collaborated with NASA LaRC to develop the EBAM system [69, 218]. Sciaky Inc. developed several EBAM systems with different deposition volumes to fabricate parts with medium, large and mega scales, as shown in Fig. 13a [46, 69, 215]. The maximum acceleration voltage was more than 60 keV [46, 69, 214]. The maximum power of the EBAM system ranged from 15 kW to 42 kW, as shown in Table 10 [46, 69]. The EBAM systems included a dual wire feeder to create a functionally graded material (FGM) [46, 215]. The structure and the configuration of the EBAM system of Sciaky Inc. were similar to those of the EBF^3 system. Sciaky Inc. developed five types of EBAM systems, as shown in Table 10 [46, 69].

Table 10 Characterizes of ebeam guns and wire feeders of different WEAM systems [46, 63, 69–71, 214, 217–219]

Process	Company/institute	Type of ebeam	Feeding type	Power (kW)	Acceleration voltage (keV)	Model
EBF^3	NASA LaRC	T-ebeam (Siacky ebeam welder)	Off-axis	15-42	20-60	Ground-based system, portable system
EBAM	Siacky Inc.	T-ebeam	Off-axis	15-42	30-60	EBAM68, EBAM88, EBAM110, EBAM150, EBAM330
	Nuclear AMRC	T-ebeam (Pro-beam ebeam welder)	Off-axis	40	80	K2000 based system
xBeam	Xbeam Inc.	P-ebeam	Co-axial	< 5	10-15	xBeam Lab., xBeam Works, xBeam Grand

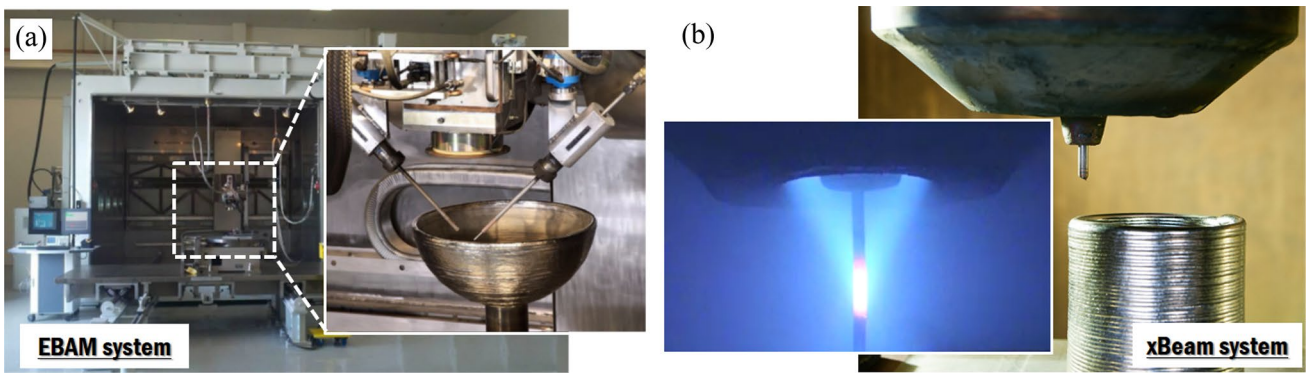

Fig. 13 Developed WEAM systems: (**a**) EBAM system of Siacky Inc. (adapted from figures provided by Siacky Inc. with permission) [69] and (**b**) xBeam systems of xBeam Inc. (adapted from figures provided by xBeam Inc. with permission) [70]

Nuclear Advanced Manufacturing Research Center (Nuclear AMRC) of University of Sheffield (U.K) in collaboration with Pro-beam Inc. developed EBAM systems based on the K2000 T-ebeam welding facility [46, 71, 219]. A T-ebeam gun with an acceleration voltage of 80 keV and a maximum power of 40 kW was mounted on a 3-axis CNC controlled gantry system [46, 71, 219]. In addition, a 2-axis rotation table, including turn and tilt table, was installed in the K2000 facility [71, 219]. The deposition rate and the layer thickness of the EBAM system lay in ranges of 0.6–5.7 kg/h and 0.4–1.7 mm, respectively [71, 219]. An off-axis wire feeding method was applied to the EBAM system [71, 219].

NVO Chervona Hvilya Inc. in Ukraine patented a method and a system for manufacturing of three-dimensional objects, referred to as the xbeam process, [46, 63, 70, 220]. Figure 13b illustrates the deposition concept of xBEAM systems [70]. The xbeam system had two key features: (a) a voltage P-ebeam with a hollow conical cathode and (b) a coaxial wire feeding system [46, 63, 70, 214, 220]. The voltage P-ebeam with a conical cathode could reduce vacuum levels of the furnace, X-rays during the deposition, protective facilities for the X-rays, and system costs, while that could improve the service life of the cathode [63, 70, 214]. The coaxial wire feeding system overcame disadvantages of the off-axis feeding system, including porosity in the deposited region and forming of non-uniform metal structures induced by an asymmetrical thermal field as well as difficulties in accurate and stable feeding of the wire caused by internal thermal stress, through omni-directional deposition [63, 214]. The coaxial wire feeding allowed the metal to continuously transfer from the fused end of the wire to the molten pool [214]. The acceleration voltage of the P-ebeam gun for the xBeam system lay in the range of 10–15 keV [214]. The spot diameter of the P-ebeam for the xBeam process was nearly 1 mm [214]. Kovalchuk et al. reported that the service life of the cathode is greater than 1000 h [214]. A low acceleration voltage of the P-ebeam gun created a rather shallow molten pool on the substrate [214]. A low specific power input of the xBeam process greatly decreased residual stresses of fabricated parts [214]. The deposition rate and the surface roughness of the xBeam process were less than 2000 cm^3/h and 1 mm, respectively [63, 70]. The minimum wall thickness of the fabricated part by the xBeam process was nearly 1.5 mm [70]. The xBeam process focused on the application of titanium alloy [63, 70, 214]. Kang's research group of Korea Institute of Industrial Technology (KITECH in Korea) performed fundamental research into the development of a WEAM process using a P-ebeam system.

4.3.3 Effects of Deposition Parameters

The product quality of the WEAM process is influenced by the acceleration voltage, the beam current, the travel speed, the beam diameter, the track overlap ratio, the deposition path, the interpass time, the interlayer dwell time, the wire feeding direction, the feeding angle, the wire tip position, etc., as shown in Fig. 9 [24, 46, 62, 71, 72, 218, 219, 221–224]. However, so far a few research works on the effects of deposition parameters have been carried out to improve the product quality and the deposition efficiency for WEAM. Taminger et al. investigated the effects of the beam power, the travel speed and the wire feed rate on microstructures and tensile properties of 2219 Al and Ti–6Al–4V parts fabricated by the EBF^3 process [212, 217, 218]. They performed feasibility studies on the ability to carry out a post finishing process of parts deposited by the EBF^3 process [212, 217, 218]. Wanjara et al. [221] examined the influence of the travel speed and a consecutive re-melting pass on the porosity of the deposited region, the efficient growth rate of the buildup and the height to width ratio of the buildup for the deposition of BNi-2 brazing paste on a stainless steel type 321 substrate using a Sciaky EBAM system. Węglowski et al. [72] studied the effects of the beam current, the acceleration voltage, the travel speed, and the wire feed rate on the width and the height of reinforcement for an EBAM process. Baufeld et al. obtained proper deposition conditions for different materials and shapes using an EBAM process based on K2000 [71, 219]. Kovalchuk and Ivaishin [63] investigated the influence of the deposition length on the residual distortion for the xBeam process. Tarasov et al. [222] examined the effects of the deposition path on microstructure, crystalline lattice parameter and residual strain for the deposition of 304 stainless steel using an experimental EBAM machine. Denlinger et al. [223] developed a thermo-mechanical analysis method based on a finite element analysis to estimate residual stress and distortion of the EBAM process for Ti–6Al–4V. They proposed a reset scheme of the stress and strain to account for stress relaxation during the deposition [223]. They also carried out an inverse simulation to determine the absorption efficiency, the emissivity and the stress relaxation temperature through the comparison of experimental results using a Sciaky system and analytical results [223]. Chen et al. [224] investigate the deposition path in the building direction and the beam current on temperature, distortion and residual stress distributions of a thin-walled Ti–6A–4V part fabricated by the EBF^3 process.

4.3.4 Applications and Fabricated Parts

NASA LaRC fabricated aluminum, titanium and nickel alloys parts using the EBF^3 process for aerospace applications [212, 217, 218]. Brice et al. [213] successfully

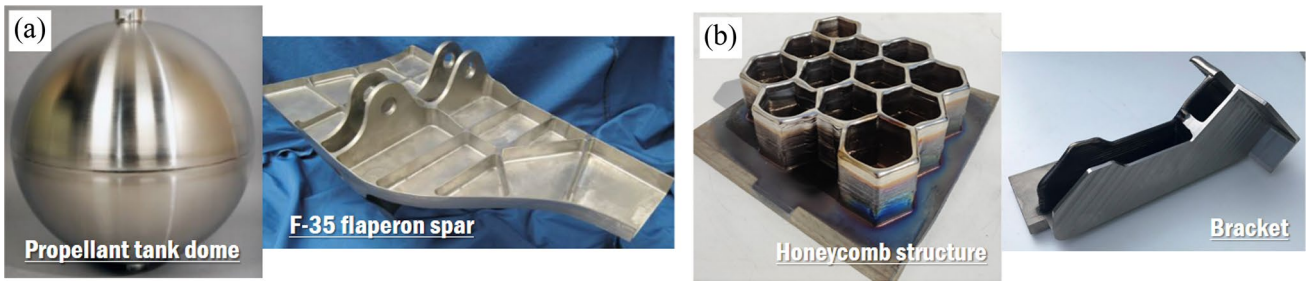

Fig. 14 Fabricated parts by the developed WEAM systems: (**a**) fabricated parts by a EBAM system of Siacky Inc. (adapted from figures provided by Siacky Inc. with permission) [69] and (**b**) fabricated parts by xBeam systems of xBeam Inc. (adapted from figures provided by xBeam Inc. with permission) [70]

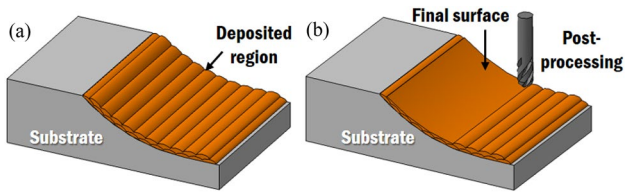

Fig. 15 Schematic diagram of hybrid AM (HAM) process combining AM with SM processes: (**a**) as built and (**b**) as post-processing

produced a Ti–6Al–4V F-22 AMAD bracket using the EBF^3 process. NASA LaRC manufactured several generic rocket nozzles with a thin wall, a gradual transition angle and a large volume using the EBF^3 process [218]. NASA LaRC produced three types of generic rocket nozzles with a near-net shape, including an In 718 rocket nozzle with a height of 457 mm, a Ti–6Al–4V rocket nozzle with a height of 360 mm, and a Cu–Ni bimetallic nozzle with a height of 460 mm, [218]. In addition, in order to improve the energy efficiency, the stiffness and the acoustic damping, NASA LaRC created Al 2219 stiffened panels with linear and curvilinear stiffeners for aircraft structures and launch vehicles using the EBF^3 process [218].

Sciaky Inc. fabricated various large sized titanium parts using an EBAM system [69, 225]. Sciaky Inc. cooperated with Lockheed Martin Aeronautics and Airbus to fabricate titanium components for US Air Force [46, 69, 225]. Lockheed Martin Aeronautics Inc. in collaboration with Sciaky Inc. developed titanium propellant tanks with a thin wall structure using an EBAM system of Sciaky, as shown in Fig. 14a [69]. They reported that the lead time, the cost and the waste to produce the titanium propellant tanks can be reduced by 80%, 55% and 75%, respectively, when the EBAM system is used [69]. Sciaky Inc. in collaboration with Lockheed Martin Aeronautics Inc. fabricated a F-35 flaperon spar using an EBAM system, as shown in Fig. 14a [69]. Sciaky Inc. forecasted that the manufacturing cost of the flaperon spar can be greatly reduced as compared to the traditional manufacturing process when the EBAM process is adopted [69]. Sciaky Inc in collaboration with Airbus produced a large sized titanium rear upper spar to reduce the lead time and the cost [225]. Nuclear AMRC applied the developed EBAM system to fabricate Ti–6Al–4V, high strength corrosion resistance steel and stainless steel 316L parts [71, 219]. Nuclear AMRC produced several Ti–6Al–4V ducts, a Ti–6Al–4V bowl, a HSCR (High strength corrosion resistant) steel duct, a stainless steel trefoil, etc. using the developed EBAM system [71, 219]. In addition, Nuclear AMRC created steel features on a cylinder [219]. xBeam Inc. fabricated several examples, such as Ti–6Al–4V honeycomb structure, Ti–6Al–4V frame structure, titanium stiffened structure, titanium bracket, etc., using an xBeam system, as shown in Fig. 14b [63, 70, 214]. xBeam Inc. began to develop industrial applications in recent years [70].

5 Current Research Issues

5.1 Hybrid AM Processes and Systems

The DED process needs additional post-processing to improve the surface roughness and the geometrical accuracy of the fabricated part, as shown in Fig. 15 [36, 42, 55, 57, 119, 143, 147, 226, 227]. An additional post-process is generally performed on a different apparatus in separate shop floors [55, 57, 227]. Hence, the additional post-processing can increase the lead time and the cost to produce a final product [55, 57, 227]. The hybrid AM (HAM) process combining DED and SM processes can overcome disadvantages of the additional post-processing, which are induced by using different machines in separate shop floors through the realization of multi-tasking in the integrated system [57, 206, 227]. Cortina et al. [227] summarized the benefits of the hybrid system; (a) no need to change part during manufacturing, (b) reduction of material movement inside the factory, (c) manufacture of parts with higher complexity, (d) decrease in BTF, (e) reduced factory space, (f) simplicity

Table 11 Features of HASM processes and systems

Process	Research group and industry	Combination	Machine tool type	System	Position of deposition head	References
Shape deposition manufacturing (sdm)	Carnegie Mellon Univ. and Stanford Univ.	Microcasting + machining	CNC (5-axis)	–	Fixed to side of spindle	[24, 36, 228]
Hybrid manufacturing	Mazak	WAAM (GMAW) + machining	5-axis vertical	VARIAISj -600 M	Fixed to side of spindle	[172]
Controlled metal buildup (CMB)	Fraunhofer Institute	LAM-DED or WLAM + machining	5-axis vertical	–	Fixed to side of spindle	[57, 58, 229]
Hybrid manufacturing	De Montfort Univ.*	LAM-DED + machining	3-axis vertical	RECLAIM Machine	In spindle (AM) Stored in tool magazine (SM)	[36, 57, 111]
Hybrid manufacturing	Hamuel Maschinenbau GmbH*	LAM-DED + machining	Retrofit to machine tool	HSTM-1000	In spindle (AM) Stored in tool magazine (SM)	[36, 57, 230, 231]
Hybrid manufacturing	DMG Mori Seiki	LAM-DED + machining	5-axis vertical	LASERTEC 65 3D hybrid	In spindle (AM) Stored in own compartment (SM)	[36, 57, 95, 226, 227, 231]
Hybrid manufacturing	Mazak*	LAM-DED + machining	5-axis horizontal	INTEGREX i-400 AM	In spindle (AM) Stored in tool magazine (SM)	[36, 57, 227, 232]
LENS	Opotomec	LAM-DED + machining	Retrofit to machine tool	MTS500, MTS860	Fixed to side of spindle	[55, 57, 76]
Hybrid manufacturing	ELB-Schliff*	LAM-DED + machining	Grinding (Creep feed: 5- axis)	milGrind	Fixed to side of spindle	[57, 233]
Hybrid manufacturing	Okuma**	LAM-DED + machining	5-axis vertical	MU-8000 V LASER EX	Fixed to side of spindle	[227, 234]
Hybrid manufacturing	Doosan machine tool**	LAM-DED + machining	5-axis vertical	DVF8000-AML	Fixed to side of spindle	–
Hybrid manufacturing	MAXROTEC	LAM-DED + machining	Robot arm (6-axis)	MDP-1000	In spindle (AM) Stored in own compartment (SM)	[92]
3D welding and milling	KIST and KIMM	WAAM (GMAW) + machining	3-aixs vertical	–	Fixed to side of spindle	[24, 235]
Hybrid WAAM & milling (HWM)	Beijing Univ. of Technology	WAAM (Tandem GMAW) + machining	Robot arm	–	Fixed to side of spindle	[56]
Hybrid WAAM and milling (HWM)	Beihang Univ.	WAAM (GMAW) + machining	Robot arm	RASM	Fixed to side of spindle	[181]
Hybrid plasma deposition and milling (HPDM)	Wuhan Univ. of Technology	WAAM (PAW) + machining	3-aixs vertical	–	Fixed to side of spindle	[236, 237]

*Collaboration with Hybrid Manufacturing Technology Inc

**Collaboration with Trumpf Inc

for operator, (g) lower overall investment, and (h) reduced cost of the final part. Most research works and developed systems related to the HAM process were focused on the combination of DED with machining processes [24, 36, 42, 55, 57, 119, 143, 147, 226, 227]. Features of HAM processes and systems are summarized in Table 11. Since a shape deposition manufacturing (SDM) process was developed by Carnegie Mellon University in U.S.A, various HAM processes based on DED processes were introduced, as shown in Table 11 and Fig. 16 [36, 55, 57, 226, 227].

HAM processes based on LAM-DED processes can be classified into in spindle and side of spindle types

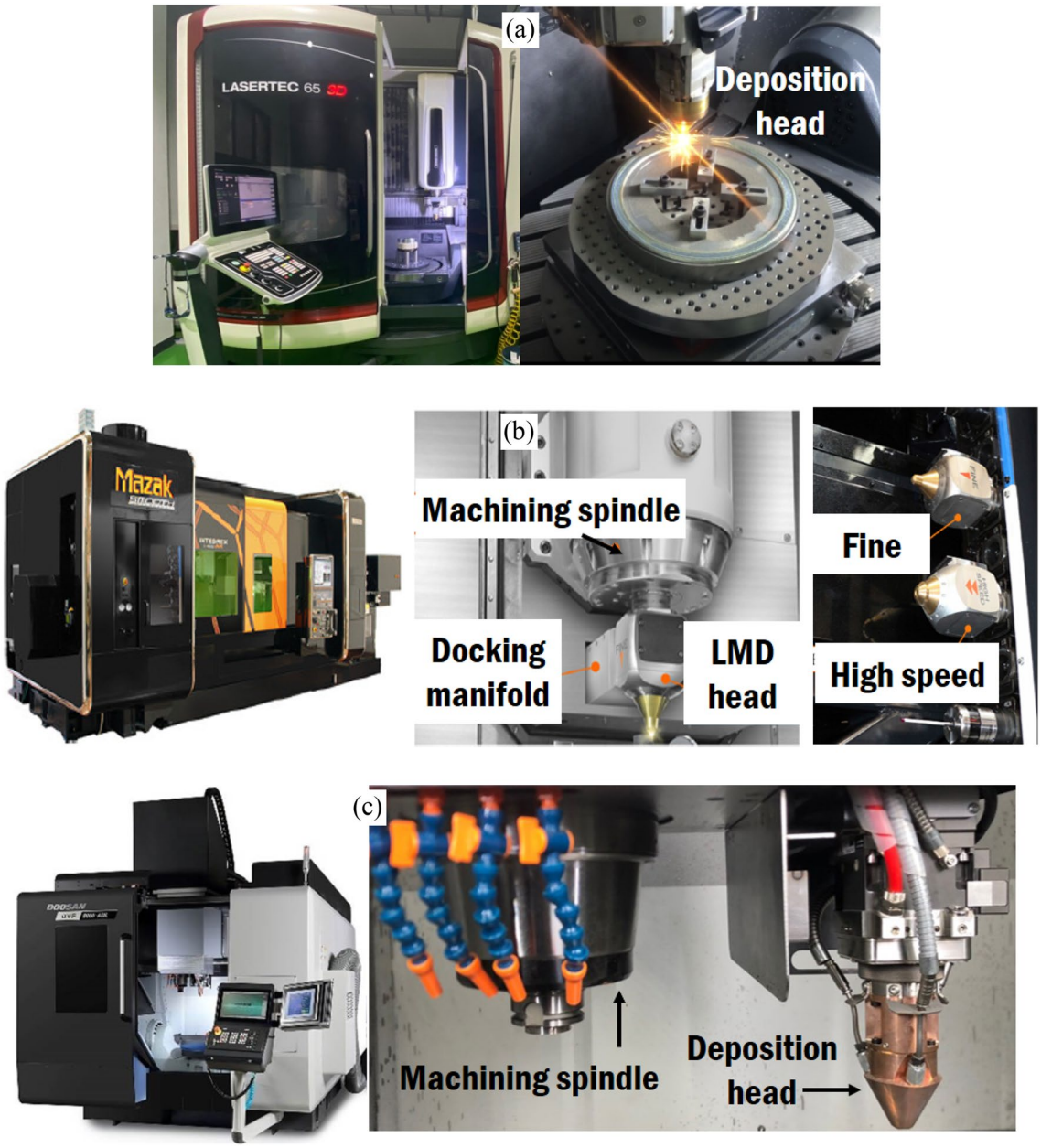

Fig. 16 Examples of commercialized HAM system based on DED processes: (**a**) LASERTEC 65 3D hybrid system of DMG Mori Seiki Inc. (adapted from figures provided by Partners Lab. Inc. with permission) [238] (**b**) INTEGREX i-400 AM system of Mazak Inc. (adapted from figures of reference 232 with permission) [232] and (**c**) DVF8000-AML system of Doosan Machine Tool Inc. (adapted from figures provided by Doosan Machine Tool Inc. with permission)

according to the position of the deposition head [36, 57]. In the in spindle type, an automatic tool changer (ATC) is employed for automatically attaching the deposition head and the machining tools to the spindle [36, 57, 232, 233]. The deposition head is stored in the tool magazine and its own compartment during the SM process [57, 92, 232]. RECLAIM Machine (De Mont fort University), HSTM-1000 (Hamuel Maschinenbau GmbH), INTEGREX i-1400 AM (Mazak), and milGrind (ELB-Schliff) used AMBIT™ laser-based DED heads (Hybrid Manufacturing Technology Inc.) as the deposition head. The AMBIT™ laser-based DED head can be stored in the tool magazine of the machining center [239]. The deposition head is always located in the side of spindle type HAM systems, unlike in spindle type HAM systems [57, 76, 229, 234]. MU-8000 V LASER EX (Okuma) and DVF8000-AML (Doosan Machine Tool) adopted the DED head of Trumpf Inc. to improve the reliability for operation of

the DED head [227, 234]. A LENS modular print engine (Optomec) can be easily integrated in the CNC machine [36]. The LENS modular print engine was used to retrofit a legacy CNC machine tool in recent years [36]. The HAM system based on LAM-DED processes commonly utilized a 5-axis CNC system [36, 55, 57, 227]. One of the important research issues related to the HAM system based on LAM-DED process is the development of appropriate CAM (Computer aided manufacturing) software, including identification of a suitable build orientation, the part decomposition, the collision avoidance algorithm, the path planning, etc., to optimize the fabrication procedure of parts [36, 42, 227].

HAM processes based on wire feeding type DED processes can be classified into 3 axis CNC and robot arm types according to the machine tool system [36, 57]. The development of HAM systems based on the WAAM process were refocused due to a relatively higher deposition rate and cheaper cost of the system in recent years [56, 172]. Hence, most of the developed HAM processes based on wire feeding type DED processes adopted the WAAM process as the deposition process, as shown in Table 11 [24, 56, 181, 236, 237]. In order to enhance the production efficiency and the fabrication volume of the HAM process, multiple robot based HAM systems, including multi-deposition heads and multi machining tools, were adopted in recent research works [65, 181]. Relatively excessive residual stress distributions occurred in the vicinity of the deposited region due to the relatively higher deposition rate for the case of the WAAM process [65, 172]. WEC of Cranfield University developed a hybrid process, including high pressure interlayer rolling in a WAAM process, for the sake of refinement and overall improvement of microstructures [65, 160, 172, 240]. The hybrid process was used to reduce the residual stress and the distortion of the fabricated part by the WAAM process [65, 172, 241–245]. In addition, the hybrid process was used for the purpose of decreasing the porosity and improving the surface finish [172, 245, 246].

5.2 In-situ Monitoring

The process optimization is one of the hot research issues related to the DED process and system for the purpose of improving the product quality and the process reliability. In-situ monitoring is one of the major research directions in term of the process optimization of the DED process [36, 42, 65, 172, 227]. In-situ monitoring techniques are applied to DED processes for the sake of enhancing product qualities and decreasing material discontinuities through the process optimization [42, 247–250]. Visible cameras, pyrometers, infrared (IR) cameras, thermocouples (TCs), and X-rays are commonly employed for monitoring DED processes, as shown in Table 12 [48, 61, 75, 77, 79–81, 92, 191, 196, 201, 251–265].

The visible cameras used for in situ monitoring include a charge coupled device (CCD) camera, a complementary metal–oxide–semiconductor (CMOS) camera, and a high speed camera, as shown in Table 12. Most of the commercialized LAM-DED processes have employed CCD cameras for monitoring the formation of the molten pool, as shown in Tables 1 and 2. The visible cameras are generally used to investigate the geometry of the molten pool, the temperature distribution in the molten pool, the deposition height, and particle effects for the case of a LAM-DED process, as shown in Table 12 and Fig. 17a [75, 77, 79–81, 251, 253, 256]. In addition, the visible cameras were employed for monitoring the deposition height of the fabricated part by DMD and DMT processes, as shown in Table 12 [77, 79, 80]. The measured data were used for feedback control of the layer thickness [77, 79, 80]. The visible cameras were adopted to measure the geometry of the molten pool, the temperature distribution of the molten pool, the interaction between the wire tip and the molten pool, and the formation of the droplet for the case of a WLAM process, as shown in Table 12 and Fig. 17b [61, 191, 201, 252, 255]. Heralić et al. employed visible cameras for monitoring the formation of the molten pool and the height of the bead for a WLAM process [252, 255]. They applied measured data to the control of the height and the width of the deposited bead through an iterative learning controller [252, 255]. In order to measure temperature distributions in the molten pool, IR and near IR (NIR) filters were attached to visible cameras [192, 254].

IR cameras were employed for in situ monitoring of the temperature distributions of the molten pool. Clamir Inc. developed a closed-loop control system based on an IR camera to control the laser power [258, 259]. Taminger et al. [254] applied visible and IR cameras to the EBF^3 process for the sake of monitoring the temperature distribution of the molten pool. Optomec Inc. in collaboration with STRATONICS Inc. developed a Melt-pool Sensor based on pyrometer and a thermal imager based on a Thermalviz software to control the laser power by monitoring the temperature distributions of the molten pool [261, 262]. Pyrometers to measure the temperature at a spot and temperature distribution in a line were used through combination of the other monitoring device in recent years [266, 267]. Thermocouples (TCs) were used to directly measure temperature at a spot in the vicinity of the molten pool [48]. X-ray have been adopted to monitor the occurrence of defects, the dynamics of the molten pool, and the interaction between powders and the molten pool during the deposition [263–265].

Recently, combinations of different monitoring devices were used for in-process monitoring of the DED process, as shown in Table 12 [78, 94, 160, 178, 202, 266–270]. Combinations of a visible camera and a pyrometer were used to

Table 12 Classification of in situ monitoring methodologies of DED process according to measurement devices

Devices	Monitoring/goals	DED process	Feedback	References
Visible camera (CCD and CMOS)	Geometry of molten pool	LENS	No	[75]
	Deposition height (Layer thickness)	DMD	Yes	[77, 79]
	Geometry of molten pool and deposition height	DMT	Yes	[80]
	Geometry of molten pool (Trumpf Inc.)	LMD	No	[81]
	Geometry and temperature of molten pool (using IR filter)	WLAM	No	[191]
	Temperature of molten pool	LAM	No	[251]
	Geometry of molten pool and control of bead geometry	WLAM	Yes	[252]
	Deposition height	LAM	No	[253]
	Temperature distribution of molten pool (using NIR filter)	EBF^3	No	[254]
	Interaction between the wire tip and the molten pool Control of deposition height using iterative learning controller	WLAM	Yes	[255]
Visible camera (High speed)	Geometry of molten pool and droplet formation	WLAM	No	[61]
	Droplet formation	WLAM	No	[201]
	Geometry of molten pool, particle effects (using 4 cameras)	LENS	No	[256]
IR camera	Temperature distribution of molten pool (MAXROTEC Inc.)	LAM	No	[92]
	Temperature distribution of molten pool	WAAM	No	[190, 257]
	Temperature distribution of molten pool	WLAM	No	[196]
	Temperature distribution of molten pool and control of power	LAM	Yes	[258, 259]
	Temperature distribution of molten pool	LMD	No	[260]
	Temperature distribution of molten pool (Short-wave IR)	EBF^3	No	[254]
Pyrometer	Temperature distribution of molten pool and control of power (Melt-Pool Senor, Thermal Imager based on Thermal Viz.)	LENS	Yes	[261, 262]
Thermocouple	Temperature history in the vicinity of the molten pool	LENS	No	[48]
X-ray	Probing the phase evolution	LAM	No	[263]
	Defects and molten pool dynamics	LAM	No	[42, 264]
	Defects, molten pool dynamics and powder-molten pool interaction	LAM	No	[42, 265]
Visible camera + pyrometer	Control of molten pool temperature and deposition height	DMD	Yes	[78]
	Effects of heat accumulation on arc characteristics and metal transfer behavior	WAAM	No	[178]
Visible camera + IR camera	Geometry and temperature of molten pool	WAAM	Yes	[160]
IR camera + pyrometer	Temperature distributions and histories of molten pool Effects of temperature distribution on microstructure formation	LENS	No	[250, 266]
	Temperature distributions of molten pool Prediction of porosity	LENS	No	[250, 267]
Visible came + pyrometer + IR camera	Intensity distribution of beam and geometry of molten pool	LAM	No	[94]
	Interaction between wire and molten pool Estimation of process map	WLAM	No	[202]
	Temperature distribution of molten pool Particles-in-flight tracks and particle transport	LMD	No	[268, 269]
	Particles-in-flight tracks and mass flow rate Temperature distributions and histories of molten pool	LAM	No	[270]

control the temperature of the molten pool and the deposition height of part for the DMD process and to investigate the effects of the temperature distribution on the microstructure formation of the WAAM process [78, 178]. Wu et al. [160] employed a combination of a visible camera and an IR camera for monitoring the geometry and the temperature of the molten pool of a WAAM process. Several researchers utilized the combination of an IR camera and a pyrometer to investigate temperature distributions and histories of the molten pool as well as the effects of heat accumulation on arc characteristics and metal transfer behaviors for the LENS process [250, 266, 267]. In addition, the combination of an IR camera and a pyrometer were used to predict the porosity of the deposited region by the LENS process [267]. In several research works, a combination of triple monitoring devices consisting of a visible camera, a pyrometer and an

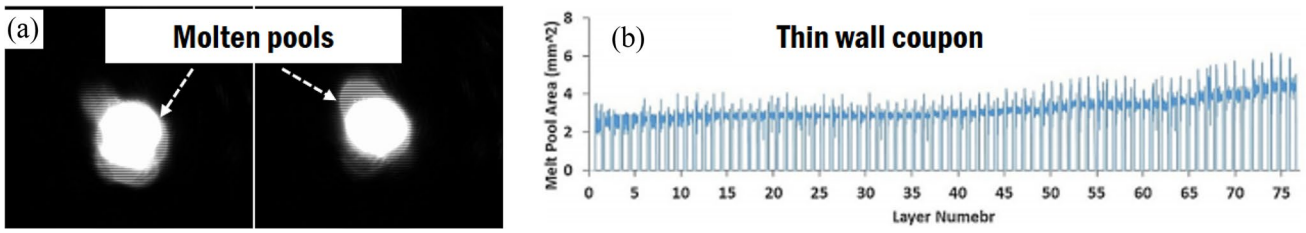

Fig. 17 Examples of in situ monitoring of DED processes: (**a**) formation of the molten pool for LENS process (adapted from figures provided by Ph.D. Yong Son and Ph.D Hyub Lee of KITECH with permission) (**b**) variation of the molten pool area according to number of layer for a robotized WLAM process (adapted from figures of reference191 with permission) [191]

IR camera was adopted to examine temperature distributions, temperature histories and geometries of the molten pool as well as intensity distributions of the laser beam for LAM-DED processes [94, 268–270]. The combination of triple monitoring devices was used to investigate particles-in-flight tracks, the particle transport and the mass flow rate for LAM-DED processes [268–270]. In addition, the combination of triple monitoring devices was adopted to investigate the interaction between the wire and the molten pool and to estimate the process map for a WLAM process [202].

5.3 Thermo-Mechanical Analysis

In order to reduce residual stresses in the fabricated part by DED processes, various experimental and analytical approaches were performed [97, 203, 204, 223, 224, 271–286]. Recently, researches on thermo-mechanical analyses steadily increased to predict the desired deposition method through the control of heat transfer characteristics and the reduction of residual stress evolution, as shown in Table 13.

Research related to thermo-mechanical analyses to investigate residual stress and distortion during the fabrication of the part using the DED process can be classified into four categories; (a) modeling and validation, (b) effects of deposition and geometry parameters, (c) effects of deposition paths and times, (d) preheating and post cooling, as shown in Table 13. In general, in situ monitoring of temperature distributions, distortions and deflections is carried out to obtain an appropriate model for thermo-mechanical analysis using a TC, an IR camera, a digital image camera (DIC), a X-ray diffraction (XRD), and a linear displacement sensor (LDS), as shown in Table 13 [97, 223, 224, 274, 275, 277, 281–283, 286]. In addition, a scanner, a neutron diffraction (ND), a hole drilling (HD), an optical microscope, a XRD, a table encoder, and a coordinate measuring machine (CMM) are commonly employed for comparing the results of thermo-mechanical analyses to those of experiments from viewpoints of residual stress, distortion and deflection, as shown in Table 13 [203, 204, 223, 271–273, 276, 279, 281, 284, 285].

Thin wall structures are generally adopted to perform modeling and validation for thermo-mechanical analyses with different shapes [223, 271–274, 276]. Stender et al. [275] studied the workflow of a thermo-mechanical analysis for a LENS process. Heigel et al. [276] investigated the effects of the convection model on the residual stress and the distortion of the fabricated part by a LENS process. Denlinger et al. [223] examined the effects of the stress relaxation temperature on the distortion of the created part by a WEAM process to predict a proper relaxation temperature and residual stress distribution. Several researchers investigated the effects of deposition parameters, including the laser power, the scan speed and the feeding rate, on residual stress distributions of fabricated parts by WLAM and LAM processes, as shown in Table 13 [203, 277–279]. Vundru et al. [278] predicted relationships between non-dimensional deposition parameters, including non-dimensional power, feed rate and scan speed, and the non-dimensional stress parameter to obtain a process map for the residual stress through thermo-mechanical analyses. In addition, they estimated the relationship between non-dimensional deposition parameters and the normalized dilution [278]. In order to obtain proper designs of fabricated parts by DED processes, the influence of geometry parameters, including the bead length, the up-lift height, the wall height, the wall thickness, the radius, etc., on residual stress and deflection distributions was examined using thermo-mechanical analyses for DED processes [203, 277, 280]. Zhang et al. [280] studied the effects of radius and height of a circular thin wall part on residual distortion distributions for a LAM-DED process.

Deposition strategies, including the deposition path, the interpass time, the inter-layer dwell time, etc., greatly affected residual stress distributions and final shapes for the case of DED processes. Hence, various research works based on thermo-mechanical analyses were performed to estimate appropriate deposition paths and characteristic times for DED processes [97, 204, 224, 281–284]. Chua et al. [204] investigated the effects of the deposition path, the interpass time and the cooling time on residual stress and deflection distributions for a WLAM process. Chen et al. [282] studied the influence of the deposition path on

Table 13 Researches on thermo-mechanical analyses related to the residual stress and the distortion

Researches	Analysis/goal	Shape	Measurement device		DED	References
			In-situ	Post		
Modeling and validation	Modeling/prediction of residual stress	Rectangular hollow wall	–	Scanner	LENS	[271]
		Thin wall	–	ND	LAM	[272, 273]
	Modeling/prediction of distortion and bulging	Airfoil (Thin wall)	TC + DIC	–	LAM	[274]
	Workflow of thermo-mechanical analysis	Cylinder	IR camera	–	LENS	[275]
	Effects of convection model on deflection and residual stress	Thin wall	TC,LDS	HD	LENS	[276]
	Effects of stress relaxation temperature on distortion, Prediction of residual stress	Sloped thin wall	TC,LDS	HD	WEAM	[223]
Deposition and geometry parameters	Effects of laser power, scan speed and bead length on residual stress distribution	Single line	–	OM	WLAM	[203]
	Effects of deposition parameters on distortion and residual stress distributions	Thin wall	TC + IR + DIC	–	LAM	[278]
	Relationship between non-dimensional parameters on residual stress, process map	Single line	–	–	LAM	[278]
	Effects of laser power and scan speed on residual stress	Plane	–	XRD	LENS	[279]
	Effects of radius and height of circular thin wall on residual distortion	Circular thin wall	–	–	LAM	[280]
Deposition path and time	Effects of deposition path and interpass time on residual stress and deflection	Thin wall	–	Table encoder	WLAM	[204]
	Effects of deposition path on distortion and residual stress	Thin wall	XRD	–	EBF^3	[224]
	Effects of pattern of zig-zag deposition on residual stress	Plate	IR	XRD	LAM	[281]
	Effects of deposition path on residual stress	Block	TC	–	DMT	[282]
	Effects of inter-layer dwell time and material on distortion and residual stress	Thin wall	TC + LDS	–	LAM	[97, 283]
	Effects of inter-layer dwell time on residual stress	Cylindrical hollow wall	–	HD	WAAM	[284]
Pre heating and post cooling	Effects of number of pre-heating on distortion and residual stress	Thin-wall	–	CMM, HD, ND	BEAM	[285]
	Effects of preheating method and cooling rate on distortion and residual stress	Rectangular hollow and S-shape wall	TC + LDS	–	LAM	[286]

residual stress and distortion of a thin wall part fabricated by the EBF^3 process. Denlinger et al. examined the effects of the inter-layer dwell time on distortion and residual stress of Inconel 625 and Ti–6Al–4V thin wall parts fabricated by a LAM-DED process [97, 283]. Li and Xiong [284] studied the influence of the inter-layer dwell time on residual stress distributions of a cylindrical hollow part fabricated by a WAAM process. Several studies related to thermo-mechanical analyses have focused on preheating and post cooling technologies to reduce the residual stress

and the distortion for DED processes. Cao et al. [285] examined the effects of the number of preheating on distortion and residual stress distributions of a thin wall part fabricated by a BEAM process. Lu et al. [286] investigated the influence of preheating temperature and post cooling rate on distortion and residual stress distributions of rectangular and S-shaped Ti–6Al–4V parts fabricated by a LAM-DED process.

6 Summary

This paper reviewed recent research trends of DED processes and their applications. Key technologies and the state-of-the art for different DED processes were investigated from viewpoints of the development of process and system, the optimization of the deposition strategy, and the application. Through the literature survey, important processing data to manufacture metallic products from different DED processes were examined. In addition, significant applications and benefits of the DED process were discussed. Most of research works related to DED processes concentrated on the improvement of the product quality, the reduction of the fabrication time, the increase in the building volume, and the diversity of the material. Researches related to the LAM-DED process were focused on the enhancement of the quality and the reliability of the product as well as the decrease in the fabrication time through the process optimization. WAAM processes were considered to be applicable to industrial parts with a large volume from viewpoints of the cost efficiency and the process flexibility. WEAM processes were suitable to the fabrication of large sized aerospace and military components using expensive high performance alloys for the sake of reducing the BTF, the lead time and the cost. Common research themes of powder and wire feeding types of DED processes were the usage of high functionality materials, the prevention of defects and the mitigation of the residual stress. The LAM-DED process provided various impressive applications from the viewpoint of green technology: (a) repair, restoration and remanufacturing, (b) porous materials and coatings, (c) FGM&s and (d) thermal management.

Important current research issues related to DED processes were investigated. Researches related to HAM systems concentrated on the development of novel HAM systems based on LAM-DED processes and their operation software, including programs for path generation and collision avoidance, due to various merits of HAM systems. A robot based WAAM system was used to develop a HAM system for the fabrication of a large-sized part. In addition, a hybrid process, including a high pressure interrolling in a WAAM process, was proposed for the sake of reducing the residual stress and distortion of the fabricated part through the refinement, and improving the microstructure. Various in situ monitoring technologies using visible cameras, IR cameras, pyrometers, TCs and XRDs were employed for improving the product quality and the process reliability together. Most of researches related to the in situ monitoring were focused on in-process investigation of temperature distributions of the molten pool, dynamics of the molten pool, interactions between fed materials and the molten pool, and the occurrence of defects during the deposition. In order to improve the process reliability, the in situ monitoring technologies were applied to feedback control of process parameters. Thermo-mechanical analyses for DED processes were mainly focused on the influence of deposition strategies, including deposition parameters, deposition paths, characteristic times, preheating conditions, post cooling rates, and product geometries on residual stress, deflection and distortion distributions

Table 14 Future research issues and opportunities of DED processes

Novel processes and systems	Development of novel HAM processes and systems Development of software for HAM systems (including programs for path generation) Retrofit of machine tool Development of processes and systems for the fabrication of a large-sized part (BAAM)
Process optimizations	Development of process map Development of methodologies of in situ monitoring Feedback control of process parameters through in situ monitoring Development of algorithm for feedback control (including machine learning) Thermo-mechanical analyses to estimate deposition strategies
Sustainable applications	Repair, restoration and remanufacturing Porous materials and coatings Functionally graded materials and structures (FGM&S) Thermal management Near-net shaping of metallic parts with a large volume

of the fabricated parts. In-situ monitoring technologies were adopted to obtain an appropriate model for thermo-mechanical analyses.

Through the investigation of the state-of-the art and important current research issues, future research issues and opportunities of DED processes were identified from viewpoints of novel processes and systems, process optimizations, and sustainable applications, as shown in Table 14.

Acknowledgements This work was supported by the National Research Foundation of Korea (NRF) grant funded by the Korea government (MSIT) (NRF-2019R1A2C1006741).

Compliance with Ethical Standards

Conflict of interest The author declares that there is no conflict of interest.

Open Access This article is licensed under a Creative Commons Attribution 4.0 International License, which permits use, sharing, adaptation, distribution and reproduction in any medium or format, as long as you give appropriate credit to the original author(s) and the source, provide a link to the Creative Commons licence, and indicate if changes were made. The images or other third party material in this article are included in the article's Creative Commons licence, unless indicated otherwise in a credit line to the material. If material is not included in the article's Creative Commons licence and your intended use is not permitted by statutory regulation or exceeds the permitted use, you will need to obtain permission directly from the copyright holder. To view a copy of this licence, visit http://creativecommons.org/licenses/by/4.0/.

References

1. Frazier, W. E. (2014). Metal additive manufacturing: A review. *Journal of Materials Engineering and Performance, 23*(2), 1917–1928.
2. Thompson, M. K., Moroni, G., Vaneker, T., Fadel, G., Campbell, R. I., Gibson, I., et al. (2016). Design for additive manufacturing: Trends, opportunities, constructions, and constraints. *CIRP Annals—Manufacturing Technology, 65*(2), 737–760.
3. Gao, W., Zhang, Y., Ramanujan, D., Ramani, K., Chen, Y., Williams, C. B., et al. (2015). The status, challenges, and future of additive manufacturing in engineering. *Computer-Aided Design, 69,* 65–89.
4. Ahn, D. G. (2016). Direct metal additive manufacturing processes and their sustainable applications for green technology: A review. *International Journal of Precision Engineering and Manufacturing-Green Technology, 3*(4), 381–395.
5. Renjith, S. C., Park, K., & Okudan Kremer, G. E. (2020). A design framework for additive manufacturing: Integration of additive manufacturing capabilities in the early design process. *International Journal of Precision Engineering and Manufacturing, 21*(2), 329–345.
6. Schmidt, M., Merklein, M., Bourell, D., Dimitrove, D., Hausotte, T., Wegner, K., et al. (2017). Laser based additive manufacturing in industry and academia. *CIRP Annals—Manufacturing Technology, 66*(2), 561–583.
7. International Organization for Standardization (2018). Additive manufacturing—General principles—Terminology. ISO/ASTM 52900, https://www.iso.org/obp/ui/#iso:std:iso-astm:52900:dis:ed-2:v1:en.
8. Guo, N., & Leu, M. C. (2013). Additive manufacturing: Technology, applications and research needs. *Frontiers of Mechanical Engineering, 8*(3), 215–243.
9. Ford, S., & Despeisse, M. (2016). Additive manufacturing and sustainability: An exploratory study of the advantages and challenges. *Journal of Cleaner Production, 137,* 1573–1587.
10. Attaran, M. (2017). The rise of 3D printing: The advantages of additive manufacturing over traditional manufacturing. *Business Horizons, 60*(5), 677–688.
11. Niaki, M. K., Torabi, S. A., & Nonino, F. (2019). Why manufacturers adopt additive manufacturing technologies: The role of sustainability. *Journal of Cleaner Production, 222,* 381–392.
12. Niaki, M. K., Nonino, F., Palombi, G., & Torabi, S. A. (2019). Economic sustainability of additive manufacturing: Contextual factors driving its performance in rapid prototyping. *Journal of Manufacturing Technology Management, 30*(2), 353–365.
13. Pradel, P., Zhu, Z., Bibb, R., & Moultrie, J. (2018). Investigation of design for additive manufacturing in professional design practice. *Journal of Engineering Design, 29*(4–5), 165–200.
14. Nguyen, C. H. P., Kim, Y., & Choi, Y. (2019). Design for additive manufacturing of functionally graded lattice structures: A design method with process induced anisotropy consideration. *International Journal of Precision Engineering and Manufacturing-Green Technology*. https://doi.org/10.1007/s40684-019-00173-7.
15. Gibbons, G. J., & Hansell, R. G. (2005). Direct tool steel injection mould inserts through the arcam EBM free-form fabrication process. *Assembly Automation, 25*(4), 300–305.
16. Schmelzle, J., Kline, E. V., Dickman, C. J., Reutzel, E. W., Jones, G., & Simpson, T. W. (2015). (Re) Designing for part consolidation: Understanding the challenges of metal additive manufacturing. *Journal of Mechanical Design, 137*(11), 111404. https://doi.org/10.1115/1.4031156.
17. Langelaar, M. (2016). Topology optimization of 3D self-supporting structures for additive manufacturing. *Additive Manufacturing, 12,* 60–70.
18. Chung, H., Lee, N., Ko, J., Lee, T., Lee, P.-H., & Choi, J. Y. (2019). Optimal powder deposition process to develop a new direct-write additive manufacturing system. *International Journal of Precision Engineering and Manufacturing., 20*(6), 1057–1067.
19. Park, J., Goo, B., & Park, K. (2019). Topology optimization and additive manufacturing of customized sports item considering orthotropic anisotropy. *International Journal of Precision Engineering and Manufacturing., 20*(8), 1443–1450.
20. Lebaal, N., Zhang, Y., Demoly, F., Roth, S., Gomes, S., & Bernard, A. (2019). Optimised lattice structure configuration for additive manufacturing. *CIRP Annals—Manufacturing Technology, 68*(1), 117–120.
21. Zhu, Y., Zhao, J., Zhang, M., Li, X., Wang, L., & Hu, C. (2020). An improved density-based design method of additive manufacturing fabricated inhomogeneous cellular-solid structures. *International Journal of Precision Engineering and Manufacturing, 21*(1), 103–116.
22. Liu, J., Zheng, Y., Ma, Y., Qureshi, A., & Ahmad, R. (2020). A topology optimization method for hybrid subtractive–additive remanufacturing. *International Journal of Precision Engineering and Manufacturing-Green Technology, 7*(5), 939–953.
23. Atzeni, E., & Salmi, A. (2020). Economics of additive manufacturing for end-usable metal parts. *The International Journal of Advanced Manufacturing, 62*(9–12), 1147–1155.
24. Ding, D., Pan, Z., Cuiuri, D., & Li, H. (2015). Wire-feed additive manufacturing of metal components: Technologies,

developments and future interests. *The International Journal of Advanced Manufacturing, 8*(1–4), 465–481.
25. Orme, M. E., Gschweitl, M., Ferrari, M., Vernon, R., Madera, I. J., Yancey, R., et al. (2017). Additive manufacturing of lightweight, optimized, metallic components suitable for space flight. *Journal of Spacecraft and Rockets, 54*(5), 1050–1059.
26. Froes, F., & Boyer, R. (2019). Review of additive manufacturing technologies and applications in the aerospace industry. *Additive Manufacturing for the Aerospace Industry* (pp. 7–31). Amsterdam: Elsevier.
27. Berman, B. (2012). 3-D printing: The new industrial revolution. *Business Horizons, 55*(2), 155–162.
28. Eyers, D. R., & Potter, A. T. (2017). Industrial additive manufacturing: A manufacturing system and perspective. *Computers in Industry, 92–93,* 208–218.
29. Galantucci, L. M., Guerra, M. G., Dassisti, M., & Lavecchia, F. (2019). Additive manufacturing: New trends in the 4th industrial revolution. In *Proceedings of the 4th International Conference on the Industry 4.0 Model for Advanced Manufacturing* (pp. 153–169).
30. Levy, G. N., & Schindel, R. (2002). Overview of layer manufacturing technologies, opportunities, options and applications for rapid tooling. *Proceedings of the Institution of Mechanical Engineers, Part B: Journal of Engineering Manufacture, 216*(12), 1621–1634.
31. Levy, G. N., Schindel, R., & Kruth, J. P. (2003). Rapid manufacturing and rapid tooling with layer manufacturing (LM) technologies, state of the art and future perspectives. *CIRP Annals—Manufacturing Technology, 52*(2), 589–609.
32. Ahn, D. G. (2011). Applications of laser assisted metal rapid tooling process to manufacture of molding & forming tools—State of the art. *International Journal of Precision Engineering and Manufacturing, 12*(5), 925–938.
33. Lewandowski, J. J., & Seifi, M. (2016). Metal additive manufacturing: A review of mechanical properties. *Annual Review of Materials Research, 46,* 151–186.
34. Osakada, K., & Shiomi, M. (2006). Flexible manufacturing of metallic products by selective laser melting of powder. *International Journal of Machine Tools and Manufacture, 46*(11), 1188–1193.
35. Yang, D. Y., Bambach, M., Cao, J., Duflou, J. R., Groche, P., Kuboki, T., et al. (2018). Flexibility in metal forming. *CIRP—Annals Manufacturing Technology, 67*(2), 743–765.
36. Flynn, J. M., Shokrani, A., Newman, S. T., & Dhokia, V. (2016). Hybrid additive and subtractive machine tool—Research and industrial developments. *International Journal of Machine Tools and Manufacture, 101,* 79–101.
37. Meyer, D., & Wielki, N. (2019). Internal reinforced domains by intermediate deep rolling in additive manufacturing. *CIRP Annals—Manufacturing Technology, 68*(1), 579–582.
38. Pragana, J. P. M., Cristino, V. A. M., Bragança, I. M. F., Silva, C. M. A., & Martins, P. A. F. (2020). Integration of forming operations on hybrid additive manufacturing systems based on fusion welding. *International Journal of Precision Engineering and Manufacturing-Green Technology, 7*(3), 595–607.
39. Dickens, P. M. (1995). Research developments in rapid prototyping. *Proceedings of the Institution of Mechanical Engineers, Part B: Journal of Engineering Manufacture, 209*(4), 261–266.
40. Sames, W. J., List, F. A., Pannala, S., Dehoff, R. R., & Babu, S. S. (2016). The metallurgy and processing science of metal additive manufacturing. *International Materials Review, 61*(5), 315–360.
41. Ahn, D. G., & Lee, H. J. (2019). Investigation of novel metal additive manufacturing process using plasma electron beam based on powder bed fusion. *CIRP Annals—Manufacturing Technology, 68*(1), 245–248.
42. Dass, A., & Moridi, A. (2019). State of the art in directed energy deposition: From additive manufacturing to materials design. *Coatings, 9*(7), 418. https://doi.org/10.3390/coatings9070418.
43. Yap, C. Y., Chua, C. K., Dong, Z. L., Zhang, D. Q., Loh, L. E., & Sing, S. L. (2015). Review of selective laser melting: Materials and applications. *Applied Physics Reviews, 2*(4), 041101. https://doi.org/10.1063/1.4935926.
44. Byun, J. G., & Cho, S. M. (2016). Trend of metal 3D printing by welding. *Journal of Welding and Joining, 34*(4), 1–8.
45. Liu, S., & Shin, Y. C. (2019). Additive manufacturing of Ti6Al4V alloy: A review. *Materials and Design, 164,* 107552. https://doi.org/10.1016/j.matdes.2018.107552.
46. Negi, S., Nambolan, A. A., Kapil, S., Joshi, P. S., Karunakaran, K. P., & Bhargava, P. (2020). Review on electron beam based additive manufacturing. *Rapid Prototyping Journal, 26*(3), 485–498.
47. Jinoop, A. N., Paul, C. P., Mishra, S. K., & Bindra, K. S. (2019). Laser additive manufacturing using directed energy deposition of Inconel718 wall structures with tailored characteristics. *Vacuum, 166,* 270–278.
48. Li, Z., Chen, J., Sui, S., Zhong, C., Lu, X., & Lin, X. (2020). The microstructure evolution and tensile properties of Inconel 718 fabricated by high-deposition-rate laser directed energy deposition. *Additive Manufacturing, 31,* 100941. https://doi.org/10.1016/j.addma.2019.100941.
49. Alya, S., Vundru, C., Ankamreddy, B., & Singh, R. (2019). Characterization and modeling of deposition geometry in directed energy deposition over inclined surface. *Procedia Manufacturing, 34,* 695–703.
50. Oh, W. J., Son, Y., Son, J. Y., Shin, G. W., & Shim, D. S. (2020). Effect of groove shapes on mechanical properties of STS316L repaired by direct energy deposition. *Transactions of Materials Processing, 29*(2), 103–111.
51. Ahn, D. G. (2013). Hardfacing Technologies for improvement of wear characteristics of hot working tools: A review. *International Journal of Precision Engineering and Manufacturing, 14*(7), 1271–1283.
52. Loh, G. H., Pei, E., Harrison, D., & Monzón, M. D. (2018). An overview of functionally graded additive manufacturing. *Additive Manufacturing, 23,* 34–44.
53. Schneider-Maunoury, C., Weiss, L., Perroud, O., Joguet, D., Boisselier, D., & Laheurte, P. (2019). An application of differential injection to fabricate functionally graded Ti–Nb alloys using DED-CLAD process. *Journal of Materials Processing Technology, 268,* 171–180.
54. Ahsan, M. R. U., Tanvir, A. N. M., Seo, G.-J., Bates, B., Hawkins, W., Lee, C., et al. (2020). Heat-treatment effects on a bimetallic additively-manufactured structure (BAMS) of the low-carbon steel and austenitic-stainless steel. *Additive Manufacturing, 32,* 101036. https://doi.org/10.1016/j.addma.2020.101036.
55. Sealy, M. P., Madireddy, G., Williams, R. E., Rao, P., & Toursangsaraki, M. (2018). Hybrid processes in additive manufacturing. *Journal of Manufacturing Science and Engineering, 140*(6), 060801. https://doi.org/10.1115/1.4038644.
56. Li, F., Chen, S., Shi, J., Tian, H., & Zhao, Y. (2017). Evaluation and optimization of hybrid manufacturing process combining wire arc additive manufacturing with milling for the fabrication of stiffened panels. *Applied Sciences, 7*(12), 1233. https://doi.org/10.3390/app7121233.
57. Lorenz, K. A., Jones, J. B., Wimpenny, D. I., & Jackson, M. R. (2015). A review of hybrid manufacturing. In *Proceeding of solid freeform fabrication* (pp. 96–108). http://utw10945.utweb.utexas.edu/sites/default/files/2015/2015-8-Lorenz.pdf.
58. Gibson, I., Rosen, D., & Strucker, B. (2015). Directed energy deposition process,. *Additive manufacturing technology* (pp. 245–268). Berlin: Springer.

59. Singh, A., Kapil, S., & Das, M. (2020). A comprehensive review of the methods and mechanisms for powder feedstock handling in directed energy deposition. *Additive Manufacturing, 35,* 11388. https://doi.org/10.1016/j.addma.2020.101388.
60. Jinoop, A., Paul, C., & Bindra, K. S. (2019). Laser-assisted directed energy deposition of nickel super alloys: A review. *Proceedings of the Institution of Mechanical Engineers, Part L: Journal of Materials: Design and Applications, 223*(11), 2376–2400.
61. Motta, M., Demir, A. G., & Previtali, B. (2018). High-speed imaging and process characterization of coaxial laser metal wire deposition. *Additive Manufacturing, 22,* 497–507.
62. Stawovy, M. T. (2018). Comparison of LCAC and PM Mo deposited using Sciaky EBAM™. *International Journal of Refractory Metals and Hard Materials, 73,* 162–167. https://doi.org/10.1016/j.ijrmhm.2018.02.009.
63. Kovalchuk, D., & Ivasishin, O. (2019). Profile electron beam 3D metal printing. *Additive manufaturing for the aerospace industry* (pp. 213–233). Amsterdam: Elsevier.
64. Alberti, E. A., Bueno, B. M. P., & D'Oliveira, A. S. C. M. D. (2015). Additive manufacturing using plasma transferred arc. *The International Journal of Advanced Manufacturing, 83*(9–12), 1861–1871.
65. Williams, S. W., Martina, F., Addison, A. C., Ding, J., Parda, G., & Colegrove, P. (2016). Wire + arc additive manufacturing. *Materials Science and Technology, 32*(7), 641–647.
66. Moures, F., Cicală, E., Sallamand, P., Grevey, D., Vannes, B., & Ignat, S. (2005). Optimisation of refractory coatings realised with cored wire addition using a high-power diode laser. *Surface & Coatings Technology, 200,* 2283–2292.
67. Mok, S. H., Bi, G., Folkes, J., & Pashby, I. (2008). Deposition of Ti–6Al–4V using a high power diode laser and wire, part I: Investigation on the process characteristics. *Surface & Coatings Technology, 202,* 3933–3939.
68. Chua, B. L., Lee, H. J., Ahn, D. G., & Kim, J. G. (2018). Investigation of penetration depth and efficiency of applied heat flux in a directed energy deposition process with feeding of Ti–6Al–4V wires. *Journal of Korean Society of Precision Engineering, 35*(2), 211–217.
69. Siacky Inc. https://www.sciaky.com/additive-manufacturing/electron-beam-additive-manufacturing-technology.
70. xBeam Technology. https://xbeam3d.com/technology.
71. Baufeld, B., Widdison, R., Dutilleul, T., & Bridger, K. (2016). Electron beam additive manufacturing at the nuclear AMRC. *Elektronika ir Elektrotechnika, 51,* 25–30.
72. Węglowski, M. S., Błacha, S., Pilarczyk, J., Dutkiewicz, J., & Rogal, Ł. (2018). Electron beam additive manufacturing with wire—Analysis of the process. *Proceedings of AIP Conference*. https://doi.org/10.1063/1.5035007.
73. Syed, W. U. H., Pinkerton, A. J., & Li, L. (2005). A comparative study of wire feeding and powder feeding in direct diode laser deposition for rapid prototyping. *Applied Surface Science, 247,* 268–276.
74. Liu, S., Zhang, Y., & Kovacevic, R. (2015). Numerical simulation and experimental study of powder flow distribution in high power direct laser cladding process. *Lasers in Manufacturing and Materials Processing., 2,* 199–218.
75. Keicher, D. (1998). Beyond rapid prototyping to direct fabrication: Forming metallic hardware directly from a CAD solid model. *Materials Technology, 13*(1), 5–7.
76. Optomec Inc. https://optomec.com/3d-printed-metals/lens-technology/.
77. Mazumder, J., Dutta, D., Kikuchi, N., & Ghosh, A. (2000). Closed loop direct metal deposition: Art to part. *Optics and Lasers in Engineering, 34*(4–6), 397–414.
78. Song, L., Bagavath-Singh, V., Dutta, B., & Mazumder, J. (2011). Control of melt pool temperature and deposition height during direct metal deposition process. *The International Journal of Advanced Manufacturing Technology, 58*(1–4), 247–256.
79. DM3D Inc. http://www.pomgroup.com/.
80. InssTek Inc. http://www.insstek.com/.
81. Laser metal deposition (LMD). https://www.trumpf.com/en_SG/applications/additive-manufacturing/laser-metal-deposition-lmd/.
82. Gasser, A., Backes, G., Kelbassa, I., Weisheit, A., & Wissenbach, K. (2010). Laser additive manufacturing. *Laser Technik Journal, 7*(2), 58–63. https://doi.org/10.1002/latj.201090029.
83. Milewski, J. O., Lewis, G. K., Thoma, D. J., Keel, G. I., Nemec, R. B., & Reinert, R. A. (1998). Directed light fabrication of a solid metal hemisphere using 5-axis powder deposition. *Journal of Materials Processing Technology, 75*(1), 165–172.
84. Jee, H., & Suh, J. (2013). Software supports and E-manufacturing for DMT process. *Journal of Mechanical Science and Technology, 27*(10), 2947–2953.
85. Lakshmi, K. S., & Arumaikkannu. G. (2017). Current trends of additive manufacturing in the aerospace industry. In *Advances in 3D printing & additive manufacturing technologies* (pp. 39–54). Singapore: Spinger. http://doi.org/10.1007/978-981-10-0812-2_4.
86. Carcel, B., Carcel, A. C., Perez, I., Fernandez, E., Barreda, A., Sampedro, J., & Ramos, J. A. (2008). Manufacture of metal foam layers by laser metal deposition. In *Proceedings of XVII international symposium on gas flow, chemical lasers, and high-power lasers*. https://doi.org/10.1117/12.816702.
87. EFESTO Inc. http://www.efesto.us/company/.
88. RPM Innovations Inc. https://www.rpm-innovations.com/.
89. Qiu, C., Ravi, G. A., Dance, C., Ranson, A., Dilworth, S., & Attallah, M. M. (2015). Fabrication of large Ti-6Al-4 V structures by direct laser deposition. *Journal of Alloys and Compounds, 629,* 351–361.
90. Schopphoven, T., Gasser, A., & Backes, Gerhard. (2017). EHLA: Extreme high-speed laser material deposition-economical and effective protection against corrosion and wear. *Laser Technik Journal, 4,* 26–29.
91. Vartanian, K., & McDonald, T. (2016). Accelerating industrial adoption of metal additive manufacturing technology. *JOM Journal of the Minerals Metals and Materials Society, 68*(3), 806–810.
92. MAXROTEC Inc. http://www.maxrotec.com/.
93. Banait, S. M., Paul, C. P., Jinoop, A. N., Kumar, H., Pawade, R. S., & Bindra, K. S. (2020). Experimental investigation on laser directed energy deposition of functionally graded layers of Ni–Cr–B–Si and SS316L. *Optics & Laser Technology, 121,* 105787. https://doi.org/10.1016/j.optlastec.2019.105787.
94. Govekar, E., Jeromen, A., Kuznetsov, A., Levy, G., & Fujishima, M. (2018). Study of an annular laser beam based axially-fed powder cladding process. *CIRP Annals—Manufacturing Technology, 67*(1), 241–244.
95. Kakinuma, Y., Mori, M., Oda, Y., Mori, T., Kashihara, M., Hansel, A., et al. (2016). Influence of metal powder characteristics on product quality with directed energy deposition of Inconel 625. *CIRP Annals—Manufacturing Technology, 65*(1), 209–212.
96. Kono, D., Maruhashi, A., Yamaji, I., Oda, Y., & Mori, M. (2018). Effects of cladding path on workpiece geometry and impact toughness in directed energy deposition of 316L stainless steel. *CIRP Annals—Manufacturing Technology, 67*(1), 233–236.
97. Denlinger, E. R., Heigel, J. C., Michaleris, P., & Palmer, T. A. (2015). Effect of inter-layer dwell time on distortion and residual stress in additive manufacturing of titanium and nickel

alloys. *Journal of Materials Processing Technology, 215,* 123–131.
98. Paul, C. P., Mishra, S. K., Premsingh, C. H., Bhargava, P., Tiwari, P., & Kukreja, L. M. (2011). Studies on laser rapid manufacturing of cross-thin-walled porous structures of Inconel 625. *The International Journal of Advanced Manufacturing Technology, 61*(5–8), 757–770.
99. Spalding, I. J. (1988). Applied laser tooling. *Journal of Modern Optics, 35*(5), 754–755.
100. Wolff, S. J., Lin, S., Faierson, E. J., Liu, W. K., Wagner, G. J., & Cao, J. (2017). A framework to link localized cooling and properties of directed energy deposition (DED)-processed Ti–6Al–4V. *Acta Materialia, 132,* 106–117.
101. Anderson, I. E., White, E. M. H., & Dehoff, R. (2018). Feedstock powder processing research needs for additive manufacturing development. *Current Opinion in Solid State and Materials Science, 22*(1), 8–15.
102. Ribeiro, K. S. B., Mariani, F. E., & Coelho, R. T. (2020). A study of different deposition strategies in direct energy deposition (DED) processes. *Procedia Manufacturing, 48,* 663–670.
103. Li, W., & Soshi, M. (2019). Modeling analysis of grain morphologies in directed energy deposition (DED) coating with different laser scanning patterns. *Materials Letters, 251,* 8–12.
104. Soshi, M., Odum, K., & Li, G. (2019). Investigation of novel trochoidal toolpath strategies for productive and efficient directed energy deposition process. *CIRP Annals Manufacturing Technology, 68*(1), 241–244.
105. Zhang, D., Sun, S., Qiu, D., Gibson, M. A., Dargush, M. S., Brandt, M., et al. (2018). Metal alloys for fusion-based additive manufacturing. *Advanced Engineering Materials*. https://doi.org/10.1002/adem.201700952.
106. Leino, M., Pekkarinen, J., & Soukka, R. (2016). The role of laser additive manufacturing methods of metals in repair, refurbishment and remanufacturing—Enabling circular economy. *Physics Procedia, 83,* 752–760.
107. Saboori, A., Aversa, A., Marchese, G., Biamion, S., Lombardi, M., & Fino, P. (2019). Application of directed energy deposition-based additive manufacturing in repair. *Applied Sciences, 9,* 3316. https://doi.org/10.3390/app9163316.
108. Le, V. T., Paris, H., & Mandil, G. (2018). The development of a strategy for direct part reuse using additive and subtractive manufacturing technologies. *Additive Manufacturing, 22,* 687–699.
109. Wahab, R. D. A., & Azman, A. (2019). Additive manufacturing for repair and restoration in remanufacturing: An overview from object design and systems perspectives. *Processes, 7*(11), 802. https://doi.org/10.3390/pr7110802.
110. Diaz, E., Tabar, M. J., Yáñez, A., García, J., & Taibo, J. (2010). Laser powder welding with a Co-based alloy for repairing steam circuit components in thermal power stations. *Physics Procedia, 5,* 349–358.
111. Jones, J. B., Mcnutt, P., Tosi, R., Perry, C., & Wimpenny, D. I. (2012). Remanufacture of turbine blades by laser cladding, machining and in-process scanning in a single machine. In *Proceedings of 23rd annual international solid freeform fabrication symposium* (pp. 821–827).
112. Wilson, J. M., Piya, C., Shin, Y. C., Zhao, F., & Ramani, K. (2014). Remanufacturing of turbine blades by laser direct deposition with its energy and environmental impact analysis. *Journal of Cleaner Production, 80,* 170–178.
113. Petrat, T., Graf, B., Gumenyuk, A., & Rethmeier, M. (2016). Laser metal deposition as repair technology for a gas turbine burner cade of Inconel 718. *Physics Procedia, 83,* 761–768.
114. https://www.kimi-sa.com/marine-shiprepairs/diesel-engine-machinery/four-stroke-piston-repair/. Retrieved September 14, 2020.
115. Jhavar, S., Paul, C. P., & Jain, N. K. (2013). Causes of failure and repairing options for dies and molds: A review. *Engineering Failure Analysis, 34,* 519–535.
116. Bennett, J., Garcia, D., Kendrick, M., Hartman, T., Hyatt, G., Ehmann, K., et al. (2019). Repair automotive dies with directed energy deposition: Industrial application and life cycle analysis. *Journal of Manufacturing Science and Engineering, 141*(2), 021019. https://doi.org/10.1115/1.4042078.
117. Morrow, W. R., Qi, H., Kim, I., Mazumder, J., & Skerlos, S. J. (2007). Environmental aspects of laser-based and conventional tool and die manufacturing. *Journal of Cleaner Production, 15*(10), 932–943.
118. Chen, C., Wang, Y., Ou, H., He, Y., & Tang, X. (2014). A review on remanufacture of dies and moulds. *Journal of Cleaner Production, 64,* 13–23.
119. Ahn, D. G., Lee, H. J., Cho, J. R., & Guk, D. S. (2016). Improvement of the wear resistance of hot forging dies using a locally selective deposition technology with transition layers. *CIRP Annals—Manufacturing Technology, 65,* 257–260.
120. Hong, M.-P., Kim, W.-S., Sung, J.-H., Kim, D.-H., Bae, K.-M., & Kim, Y.-S. (2018). High-performance eco-friendly trimming die manufacturing using heterogeneous material additive manufacturing technologies. *International Journal of Precision Engineering and Manufacturing-Green Technology, 5*(1), 133–142.
121. Lewis, S. R., Lewis, R., & Fletcher, D. I. (2015). Assessment of laser cladding as an option for repairing/enhancing rails. *Wear, 330–331,* 581–591.
122. Liu, H., Hu, Z., Qin, X., Wang, Y., Zhang, J., & Huang, S. (2017). Parameter optimization and experimental study of the sprocket repairing using laser cladding. *The International Journal of Advanced Manufacturing Technology, 91*(9–12), 3967–3975.
123. Oh, W. J., Lee, W. J., Kim, M. S., Jeon, J. B., & Shim, D. S. (2019). Repairing additive-manufactured 316L stainless steel using direct energy deposition. *Optics & Laser Technology, 117,* 6–17.
124. Koike, R., Matsumoto, T., Kakinuma, Y., Aoyama, T., Oda, Y., Kuriya, T., et al. (2018). A basic study on metal foam fabrication with titanium hydride in direct energy deposition. *Procedia Manufacturing, 18,* 68–73.
125. Xue, W., Krishna, B. V., Bandyopadhyay, A., & Bose, S. (2007). Processing and biocompatibility evaluation of laser processed porous titanium. *Acta Biomaterialia, 3*(6), 1007–1018.
126. Bernard, S., Krishna Balla, V., Bose, S., & Bandyopadhyay, A. (2012). Compression fatigue behavior of laser processed porous NiTi alloy. *Journal of the Mechanical Behavior of Biomedical Materials, 13,* 62–68.
127. Bandyopadhyay, A., Krishna, B. V., Xue, W., & Bose, S. (2008). Application of laser engineered net shaping (LENS) to manufacture porous and functionally graded structures for load bearing implants. *Journal of Materials Science Materials in Medicine, 20*(S1), 29–34.
128. Bandyopadhyay, A., Shivaram, A., Tarafder, S., Sahasrabudhe, H., Banerjee, D., & Bose, S. (2016). In Vivo response of laser processed porous titanium implants for load-bearing implants. *Annals of Biomedical Engineering, 45*(1), 249–260.
129. Yan, L., Chen, Y., & Liou, F. (2019). Additive manufacturing of functionally graded metallic materials using laser metal deposition. *Additive Manufacturing, 31,* 100901. https://doi.org/10.1016/j.addma.2019.100901.
130. Chen, Y., Zhang, X., Parvez, M. M., & Liou, F. (2020). A review on metallic alloys fabrication using elemental powder blends by laser powder directed energy deposition process. *Materials, 13*(16), 3562. https://doi.org/10.3390/ma13163562.
131. Yadroitsev, I., Bertrand, P., Laget, B., & Smurov, I. (2007). Application of laser assisted technologies for fabrication of functionally graded coatings and objects for the International

Thermonuclear Experimental Reactor components. *Journal of Nuclear Materials, 362*(2–3), 189–196.
132. Park, N.-R., & Ahn, D.-G. (2014). Wear characteristics of Stellite6 and NOREM02 hardfaced SKD61 hot working tool steel at the elevated temperature. *International Journal of Precision Engineering and Manufacturing, 15*(12), 2549–2558.
133. Yu, J.-H., Choi, Y.-S., Shim, D.-S., & Park, S.-H. (2018). Repairing casting part using laser assisted additive metal-layer deposition and its mechanical properties. *Optics & Laser Technology, 106,* 87–93.
134. Cortina, M., Arrizubieta, J. I., Ruiz, J. E., & Lamikiz, A. (2020). Thermomechanical analysis of additively manufactured bimetallic tools for hot stamping. *Journal of Manufacturing Processes, 57,* 905–918.
135. Onuike, B., Heer, B., & Bandyopadhyay, A. (2018). Additive manufacturing of Inconel 718—Copper alloy bimetallic structure using laser engineered net shaping (LENS™). *Additive Manufacturing, 21,* 133–140.
136. Ocylok, S., Weisheit, A., & Kelbassa, I. (2010). Functionally graded multi-layers by laser cladding for increased wear and corrosion protection. *Physics Procedia, 5,* 359–367.
137. Articek, M., Mifelner, M., & Anael, I. (2013). Synthesis of functionally graded material H13/Cu by LENS technology. *Advances in Production Engineering & Management, 8*(4), 169–176.
138. Carroll, B. E., Otis, R. A., Borgonia, J. P., Suh, J., Dillon, R. P., Shapiro, A. A., et al. (2016). Functionally graded material of 304L stainless steel and inconel 625 fabricated by directed energy deposition: Characterization and thermodynamic modeling. *Acta Materialia, 108,* 46–54.
139. Durejko, T., Ziętala, M., Polkowski, W., & Czujko, T. (2014). Thin wall tubes with Fe3Al/SS316L graded structure obtained by using laser engineered net shaping technology. *Materials and Design, 63,* 766–774.
140. Heer, B., & Bandyopadhyay, A. (2018). Compositionally graded magnetic-nonmagnetic bimetallic structure using laser engineered net shaping. *Materials Letters, 216,* 16–19.
141. Sahasrabudhe, H., Harrison, R., Carpenter, C., & Bandyopadhyay, A. (2015). Stainless steel to titanium bimetallic structure using LENS™. *Additive Manufacturing, 5,* 1–8. https://doi.org/10.1016/j.addma.2014.
142. Onuike, B., & Bandyopadhyay, A. (2018). Additive manufacturing of Inconel 718—Ti6Al4V bimetallic structures. *Additive Manufacturing, 22,* 844–851. https://doi.org/10.1016/j.addma.2018.06.025.
143. Ahn, D.-G., & Kim, H.-W. (2009). Study on the manufacture of a thermal management mould with three different materials using a direct metal tooling rapid tooling process. *Proceedings of the Institution of Mechanical Engineers, Part B: Journal of Engineering Manufacture, 224*(3), 385–402.
144. Kim, D.-I., Jang, Y.-H., Lee, H.-J., Ahn, D.-G., Song, H., & Seok, C.-S. (2017). Design of overlay coated region with hardfacing, transition and damage diminution layers for the reduction of damages of hot forging tools. *Journal of Mechanical Science and Technology, 31*(12), 5639–5647.
145. Kolleck, R., Pfanner, S., & Warnke, E. P. (2007). Development of cooled tools for press hardening of born steel sheets. *Key Engineering Materials, 344,* 225–232.
146. Hölker-Jäger, R., & Tekkaya, A. E. (2017). Additive manufacture of tools and dies for metal forming. In *Laser additive manufacturing: Materials, design, technologies, and applications* (pp. 439–464). Woodhead Publishing. https://doi.org/10.1016/C2014-0-03891-9.
147. Ahn, D.-G., Park, S.-H., & Kim, H.-S. (2010). Manufacture of an injection mould with rapid and uniform cooling characteristics for the fan parts using a DMT process. *International Journal of Precision Engineering and Manufacturing, 11*(6), 915–924.
148. Soshi, M., Ring, J., Young, C., Oda, Y., & Mori, M. (2017). Innovative grid molding and cooling using an additive and subtractive hybrid CNC machine tool. *CIRP Annals Manufacturing Technology, 66*(1), 401–404.
149. Kim, W. S., Hong, M., Park, J. S., Lee, Y. S., Cha, K. J., Sung, J. H., et al. (2015). Case studies on applications of conformal cooling channel based on DMT technology. *Journal of the Korean Society of Manufacturing Process Engineers, 14*(3), 9–14.
150. Han, J. S., Yu, M. J., Lee, M. G., Lee, Y. S., Kim, W. S., Lee, H. J., et al. (2019). Development of direct metal tooling (DMT) process for injection mold core with curved conformal cooling channel. *Journal of the Korean Society of Manufacturing Process Engineers, 18*(11), 103–108.
151. Cortina, M., Arrizubieta, J., Calleja, A., Ukar, E., & Alberdi, A. (2018). Case study to illustrate the potential of conformal cooling channels for hot stamping dies manufactured using hybrid process of laser metal deposition (LMD) and milling. *Metals, 8*(2), 102. https://doi.org/10.3390/met8020102.
152. Ji, L., Lu, J., Tang, S., Wu, Q., Wang, J., Ma, S., et al. (2018). Research on mechanisms and controlling methods of macro defects in TC4 alloy fabricated by wire additive manufacturing. *Materials, 11*(7), 1104. https://doi.org/10.3390/ma11071104.
153. Brandle, E., Baufeld, B., Leyens, C., & Gault, R. (2010). Additive manufactured Ti–6Al–4V using welding wire: Comparison of laser and arc beam deposition and evaluation with respect to aerospace material specifications. *Physic Procedia, 5,* 595–606.
154. Busachi, A., Erkoyuncu, J., Colegrove, P., Martina, F., & Ding, J. (2015). Designing a WAAM based manufacturing system for defence applications. *Physic Procedia, 37,* 48–53.
155. Yilmaz, O., & Ugla, A. A. (2016). Shaped metal deposition technique in additive manufacturing: A review. *Proceedings of the Institution of Mechanical Engineers, Part B: Journal of Engineering Manufacture, 230*(10), 1781–1798.
156. Wu, B., Pan, Z., Qiu, Z., Carpenter, K., Wang, T., Ding, D., et al. (2020). Enhanced interface strength in steel-nickel bimetallic component fabricated using wire arc additive manufacturing with interweaving deposition strategy. *Journal of Materials Science and Technology, 52,* 226–234.
157. Rodriguez, N., Vázquez, L., Huarte, I., Arruti, E., Tabernero, I., & Alvarez, P. (2018). Wire and arc additive manufacturing: A comparison between CMT and TopTIG processes applied to stainless steel. *Welding in the World, 62*(5), 1083–1096.
158. Karayel, E., & Bozkurt, Y. (2020). Additive manufacturing method and different welding applications. *Journal of Material Research and Technology, 9*(5), 11424–11438.
159. Martina, F., Mehnen, J., Williams, S. W., Colegrove, P., & Wang, F. (2012). Investigation of the benefits of plasma deposition for the additive layer manufacture of Ti–6Al–4V. *Journal of Materials Processing Technology, 212*(6), 1377–1386.
160. Wu, B., Pan, Z., Ding, D., Cuiuri, D., Li, H., Xu, J., et al. (2018). A review of the wire arc additive manufacturing of metals: Properties, defects and quality improvement. *Journal of Manufacturing Processes, 35,* 127–139.
161. Jin, W., Zhang, C., Jin, S., Tian, Y., Wellmann, D., & Liu, W. (2020). Wire arc additive manufacturing of stainless steels: A review. *Applied Sciences, 10,* 1563. https://doi.org/10.3390/app10051563.
162. WAAM3D Inc. https://waam3d.com/.
163. Sridharan, N., Noakes, M. W., Nycz, A., Love, L. J., Dehoff, R. R., & Babu, S. S. (2018). On the toughness scatter in low alloy C-Mn steel samples fabricated using wire arc additive manufacturing. *Materials Science and Engineering A, 713,* 18–27.
164. Hassan, A. A., Noakes, M., Nandwana, P., Kim, S., Kunc, V., Vaidya, U., et al. (2020). Scaling up metal additive manufacturing

process to fabricate molds for composite manufacturing. *Additive Manufacturing, 32,* 101093. https://doi.org/10.1016/j.addma.2020.101093.
165. Ahsan, M. R. U., Tanvir, A. N. M., Ross, T., Elsawy, A., Oh, M.-S., & Kim, D. B. (2019). Fabrication of bimetallic additively manufactured structure (BAMS) of low carbon steel and 316L austenitic stainless steel with wire + arc additive manufacturing. *Rapid Prototyping Journal, 26*(3), 519–530.
166. RAMLAB Inc. https://ramlab.com/waam-as-a-service/.
167. MX3D Inc. https://mx3d.com/.
168. Li, Y., Han, Q., Zhang, G., & Horváth, I. (2018). A layers-overlapping strategy for robotic wire and arc additive manufacturing of multi-layer multi-bead components with homogeneous layers. *The International Journal of Advanced Manufacturing Technology, 96*(9–12), 3331–3344.
169. Norsk Titanium Inc. https://www.norsktitanium.com/technology.
170. Geng, H., Li, J., Xiong, J., Lin, X., & Zhang, F. (2016). Geometric Limitation and tensile properties of wire and arc additive manufacturing 5A06 aluminum alloy parts. *Journal of Materials Engineering and Performance, 26*(2), 621–629.
171. Dinovitzer, M., Chen, X., Laliberte, J., Huang, X., & Frei, H. (2019). Effect of wire and arc additive manufacturing (WAAM) process parameters on bead geometry and microstructure. *Additive Manufacturing., 26,* 138–146.
172. Rodrigues, T. A., Duarte, V., Miranda, R. M., Santos, T. G., & Oliveira, J. P. (2019). Current status and perspectives on wire and arc additive manufacturing (WAAM). *Materials, 12*(7), 1121. https://doi.org/10.3390/ma12071121.
173. Ding, J., Colegrove, P., Martina, F., Williams, S., Wiktorowicz, R., & Palt, M. R. (2015). Development of a laminar flow local shielding device for wire + arc additive manufacture. *Journal of Materials Processing Technology, 226,* 99–105.
174. Wu, B., Pan, Z., Ding, D., Cuiuri, D., Li, H., & Fei, Z. (2018). The effects of forced interpass cooling on the material properties of wire arc additively manufactured Ti6Al4V alloy. *Journal of Materials Processing Technology, 258,* 97–105.
175. Jhavar, S., Jain, N. K., & Paul, C. P. (2014). Development of micro-plasma transferred arc (μ-PTA) wire deposition process for additive layer manufacturing applications. *Journal of Materials Processing Technology, 214*(5), 1102–1110.
176. Yehorov, Y., da Silva, L. J., & Scotti, A. (2019). Balancing WAAM production costs and wall surface quality through parameter selection: A case study of an Al–Mg5 alloy multilayer-non-oscillated single Pass wall. *Journal of Manufacturing and Materials Processing, 3,* 32. https://doi.org/10.3390/jmmp3020032.
177. Shen, C., Pan, Z., Cuiuri, D., Ding, D., & Li, H. (2016). Influences of deposition current and interpass temperature to the Fe3Al-based iron aluminide fabricated using wire-arc additive manufacturing process. *The International Journal of Advanced Manufacturing Technology, 88*(5–8), 2009–2018.
178. Wu, B., Ding, D., Pan, Z., Cuiuri, D., Li, H., Han, J., et al. (2017). Effects of heat accumulation on the arc characteristics and metal transfer behavior in Wire Arc Additive Manufacturing of Ti6Al4V. *Journal of Material Processing Technology, 250,* 304–312.
179. Gokhale, N. P., Kala, P., & Sharma, V. (2019). Thin-walled metal deposition with GTAW welding-based additive manufacturing process. *Journal of the Brazilian Society of Mechanical Sciences and Engineering, 41*(12), 569.
180. Ding, D., Pan, Z., Cuiuri, D., & Li, H. (2015). A multi-bead overlapping model for robotic wire and arc additive manufacturing (WAAM). *Robotics and Computer-Integrated Manufacturing, 31,* 101–110.
181. Ma, G., Zhao, G., Li, Z., Yang, M., & Xiao, W. (2019). Optimization strategies for robotic additive and subtractive manufacturing of large and high thin-walled aluminum structures. *The International Journal of Advanced Manufacturing Technology, 101,* 1275–1292.
182. Clark, D., Bache, M. R., & Whittaker, M. T. (2008). Shaped metal deposition of a nickel alloy for aero engine applications. *Journal of Materials Processing Technology, 203,* 439–448.
183. Martina, F., & Williams, S. (2015). Wire + arc additive manufacturing vs. traditional machining from solid: A cost comparison. In *Report of Welding Engineering and Laser Processing Centre of Cranfield University*, https://waammat.com/documents/waam-vs-machining-from-solid-a-cost-comparison.
184. https://www.aerospacemanufacturinganddesign.com/article/norsk-titanium-structural-components-boeing–041117/.
185. Kam, D. H., Kim, Y. M., & Kim, C. H. (2016). Recent studies of laser metal 3D deposition with wire feeding. *Journal of Welding and Joining, 34*(1), 35–40.
186. Demir, A. G. (2018). Micro laser metal wire deposition for additive manufacturing of thin-walled structures. *Optics and Lasers in Engineering, 100,* 9–17.
187. Baufeld, B., Brandl, E., & van der Biest, O. (2011). Wire based additive layer manufacturing: Comparison of microstructure and mechanical properties of Ti–6Al–4V components fabricated by laser-beam deposition and shaped metal deposition. *Journal of Materials Processing Technology, 211*(6), 1146–1158.
188. Xu, X., Mi, G., Luo, Y., Jiang, P., Shao, X., & Wang, C. (2017). Morphologies, microstructures, and mechanical properties of samples produced using laser metal deposition with 316 L stainless steel wire. *Optics and Lasers in Engineering, 94,* 1–11.
189. Abioye, T. E., Folkes, J., & Clare, A. T. (2013). A parametric study of Inconel 625 wire laser deposition. *Journal of Materials Processing Technology, 213*(12), 2145–2151.
190. Love, L. J., Nycz, A. N., Noakes, M., Post, B., Roschli, A., & Babu, S. (2017). Development and demonstration of large-scale metal additive manufacturing for military vehicle applications, *ORNL/TM-2017/5*, 51–56.
191. Akbari, M., & Kovacevic, R. (2018). An investigation on mechanical and microstructural properties of 316LSi parts fabricated by a robotized laser/wire direct metal deposition system. *Additive Manufacturing, 23,* 487–497.
192. Hussein, N. I. S., Segal, J., McCartney, D. G., & Pashby, I. R. (2008). Microstructure formation in Waspaloy multilayer builds following direct metal deposition with laser and wire. *Materials Science and Engineering A, 497*(1), 260–269.
193. Bandari, Y. K., Lee, Y. S., Nandwana, P., Richardson, B. S., Adediran, A. I., & Love, L. J. (2018). Effect of inter-layer cooling time on distortion and mechanical properties in metal additive manufacturing.In *Proceedings of the 29th annual international solid freeform fabrication symposium* (pp. 425–437).
194. Miranda, R. M., Lopes, G., Quintino, L., Rodrigues, J. P., & Williams, S. (2008). Rapid prototyping with high power fiber lasers. *Materials and Design, 29*(10), 20207-2074.
195. Kim, J., & Lee, C. W. (2018). Laser assisted additive manufacturing by rotating metal wire feeder. *Journal of Korean Society of Precision Engineering, 35*(9), 847–852.
196. Su, J., Xiao, M., Zhang, Z., Ye, Z., Jin, X., & Yang, Y. (2017). Microstructural morphology and evolution of austenite stainless steel deposited using pulsed laser and wire. *The International Journal of Advanced Manufacturing Technology, 93*(9–12), 3357–3370.
197. Kottman, M., Zhang, S., McGuffin-Cawley, J., Denney, P., & Narayanan, B. K. (2015). Laser hot wire process: A novel process for near-net shape fabrication for high-throughput applications.

JOM Journal of the Minerals Metals and Materials Society, 67(3), 622–628.
198. Nie, Z., Wang, G., McGuffin-Cawley, J. D., Narayanan, B., Zhang, S., Schwam, D., et al. (2016). Experimental study and modeling of H13 steel deposition using laser hot-wire additive manufacturing. *Journal of Materials Processing Technology, 235,* 171–186.
199. Fu, J., Gong, L., Zhang, Y., Wu, Q., Shi, X., Chang, J., et al. (2017). Microstructure and mechanical properties of Ti–6Al–4V fabricated by vertical wire feeding with axisymmetric multi-laser source. *Applied Sciences, 7*(3), 227. https://doi.org/10.3390/app7030227.
200. Wang, Y. K., Shi, S. H., Fu, G. Y., & Li, C. S. (2011). Research on the key process parameters in direct laser deposition using coaxial inside-beam wire feeding. *Applied Mechanics and Materials, 43,* 401–404.
201. Brueckner, F., Riede, M., Marquardt, F., Willner, R., Seidel, A., Thieme, S., et al. (2017). Process characteristics in high-precision laser metal deposition using wire and powder. *Journal of Laser Applications, 29*(2), 022301. https://doi.org/10.2351/1.4983237.
202. Kotar, M., Fujishima, M., Levy, G., & Govekar, E. (2019). Initial transient phase and stability of annular laser beam direct wire deposition. *CIRP Annals, 68*(1), 233–236.
203. Chua, B. L., Lee, H. J., Ahn, D.-G., & Kim, J. G. (2018). Influence of process parameters on temperature and residual stress distributions of the deposited part by a Ti–6Al–4V wire feeding type direct energy deposition process. *Journal of Mechanical Science and Technology, 32*(11), 5363–5372.
204. Chua, B. L., Ahn, D.-G., & Kim, J.-G. (2019). Influences of deposition strategies on thermo-mechanical characteristics of a multilayer part deposited by a wire feeding type DED process. *Journal of Mechanical Science and Technology, 33*(12), 5615–5622.
205. Syed, W. U. H., & Li, L. (2005). Effects of wire feeding direction and location in multiple layer diode laser direct metal deposition. *Applied Surface Science, 248*(1–4), 518–524.
206. Caiazzo, F. (2018). Additive manufacturing by means of laser-aided directed metal deposition of titanium wire. *The International Journal of Advanced Manufacturing Technology, 96*(5–8), 2699–2707.
207. Brandl, E., Michailov, V., Viehweger, B., & Leyens, C. (2011). Deposition of Ti–6Al–4V using laser and wire, part II: Hardness and dimensions of single beads. *Surface & Coatings Technology, 206*(6), 1130–1141.
208. Lee, Y. S., Bandari, Y., Simunovic, S., Richardson, B. & Kirak, M. M. (2018). Correlations of interlayer time with distortion of large Ti-6Al-4 V components in laser metal deposition with wire. In *Proceedings of the 29th Annual international solid freeform fabrication symposium* (pp. 607–622).
209. Chua, B. (2019) Investigation of development of thermo-mechanical analysis method for a wire feeding type directed energy deposition process. Ph.D. Thesis, Chosun University in Korea.
210. Ding, Y., Akbari, M., & Kovacevic, R. (2017). Process planning for laser wire-feed metal additive manufacturing system. *The International Journal of Advanced Manufacturing Technology, 95*(1–4), 355–365.
211. Joe, H. E., Kang, E. G., & Jun, B. G. (2018). A review of state of the art of electron beam and ion beam machining. *Journal of Korean Society of Precision Engineering, 35*(3), 241–252.
212. Taminger, K. M. B., & Hafley, R. A. (2003). Electron beam freeform fabrication: A rapid metal deposition process. In *Proceedings of the 3rd annual automotive composites conference*. https://www.cs.odu.edu/~mln/ltrs-pdfs/NASA-2003-3aacc-kmt.pdf.
213. Lee, H. J., & Ahn, D. G. (2017). Fabrication of beads using a plasma electron beam and Stellite21 powders for additive manufacturing. *International Journal Precision Engineering and Manufacturing-Green Technology, 4*(4), 453–456.
214. Kovalchuk, D., Melnyk, V., Melnyk, I., & Tugai, B. (2016). Prospects of application of gas-discharge electron beam guns in additive manufacturing. *E + E, 51*(5–6), 36–42.
215. Urhal, P., Weightman, A., Diver, C., & Bartolo, P. (2019). Robot assisted additive manufacturing: A review. *Robotics and Computer Integrated Manufacturing, 59,* 335–345.
216. Dave, V. R., Matz, J. E., & Eagar, T. W. (1995). Electron beam solid freeform fabrication of metal parts. In *Proceeding of international solid freeform fabrication symposium* (pp. 64–71).
217. Taminger, K. M. B., & Hafley, R. A. (2006). Electron beam free-form fabrication for cost effective near-net shape manufacturing. In *Proceedings of the 3rd annual automotive composites conference*. https://ntrs.nasa.gov/citations/20080013538.
218. Taminger, K. M., & Domack, C. S. (2020). Challenges in metal additive manufacturing for large-scale aerospace applications. In *Kinsella M. (eds) Women in aerospace materials* (pp. 105–124). Springer. https://doi.org/10.1007/978-3-030-40779-7_8.
219. Baufeld, B., Widdison, R., & Dutilleul, T. (2017). Wire based electron beam additive manufacturing. In *Proceeding of 70th IIW annual assembly.* https://www.academia.edu/36404463/WIRE_BASED_ELECTRON_BEAM_ADDITIVE_MANUFACTURING.
220. Joint Stock Company, NVO Chervona Hvilya. (2016). Method and system for manufacturing of three-dimensional objects. In *International Application published under the patent cooperation treaty (PCT).* https://patentimages.storage.googleapis.com/ec/ed/f5/1bfa9c97882ed6/WO2016064369A1.pdf.
221. Wanjara, P., Brochu, M., Girard, S., & Jahazi, M. (2005). Electron beam freeforming on type 321 stainless steel using BNi-2 brazing plate. *Materials Science and Technology, 21*(5), 613–618.
222. Tarasov, S. Y., Filippov, A. V., Savchenko, N. L., Fortuna, S. V., Rubtsov, V. E., Kolubaev, E. A., et al. (2018). Effect of heat input on phase content, crystalline lattice parameter, and residual strain in wire-feed electron beam additive manufactured 304 stainless steel. *The International Journal of Advanced Manufacturing Technology, 99,* 2353–2363.
223. Denlinger, E. R., Heigel, J. C., & Michaleris, P. (2015). Residual stress and distortion modeling of electron beam direct manufacturing Ti–6Al–4V. *Proceedings of the Institution of Mechanical Engineers, Part B: Journal of Engineering Manufacture, 229*(10), 1803–1813.
224. Chen, Z., Ye, H., & Xu, H. (2018). Distortion control in a wire-fed electron-beam thin-walled Ti–6Al–4V freeform. *Journal of Materials Processing Technology, 258,* 286–295.
225. https://additivemanufacturing.com/2016/12/14/sciaky-to-deliver-large-industrial-scale-metal-3d-printer-to-airbus/.
226. Wippermann, A., Gutowski, T. G., Denkena, B., Dittrich, M.-A., & Wessarges, Y. (2019). Electrical energy and material efficiency analysis of machining, additive and hybrid manufacturing. *Journal of Cleaner Production, 251,* 119731. https://doi.org/10.1016/j.jclepro.2019.119731.
227. Cortina, M., Arrizubieta, J., Ruiz, J., Ukar, E., & Lamikiz, A. (2018). Latest developments in industrial hybrid machine tools that combine additive and subtractive operations. *Materials, 11*(12), 2583. https://doi.org/10.3390/ma11122583.
228. Merz, R., Prinz, F. B., Ramaswami, K., Terk, M., & Weiss, L. E. (1994). Shape deposition manufacturing. In *International solid freeform fabrication symposium*. http://hdl.handle.net/2152/68579.
229. Ader, C., Brosemer, M., Freyer, C., Fricke, H., Hennings, D., Klocke, F., Kühne, V., Meiners, W., Over, C., Pleteit, H., Stührmann, S., Wirth, I., Wirtz, T., & Wissenbach, K. (2004). Research on layer manufacturing techniques at Fraunhofer. In

International solid freeform fabrication symposium (pp. 26–37). http://dx.doi.org/10.26153/tsw/5705.
230. Boehm, V. (2016). Hybrid manufacturing of turbine components. *Laser Technik Journal, 13*(2), 44–47.
231. Merklein, M., Junker, D., Schaub, A., & Neubauer, F. (2016). Hybrid additive manufacturing technologies—An analysis regarding potentials and applications. *Physics Procedia, 83,* 549–559.
232. Yamazaki, T. (2016). Development of a hybrid multi-tasking machine tool: Integration of additive manufacturing technology with CNC machining. *Procedia CIRP, 42,* 81–86.
233. ELB-Schliff's New millGrind Device Melds 3D Printing & Grinding. Retrieved 17 September, 2020 from, https://3dprint.com/84336/grinding-and-am-device/.
234. Okuma Inc., https://www.okuma.com/laser. Retrieved 17 September, 2020.
235. Song, Y.-A., Park, S., Choi, D., & Jee, H. (2005). 3D welding and milling: Part I—A direct approach for freeform fabrication of metallic prototypes. *International Journal of Machine Tools and Manufacture, 45*(9), 1057–1062.
236. Xiong, X., Zhang, H., & Wang, G. (2009). Metal direct prototyping by using hybrid plasma deposition and milling. *Journal of Materials Processing Technology, 209*(1), 124–130.
237. Xinhong, X., Haiou, Z., Guilan, W., & Guoxian, W. (2010). Hybrid plasma deposition and milling for an aeroengine double helix integral impeller made of superalloy. *Robotics and Computer-Integrated Manufacturing, 26*(4), 291–295.
238. Partners Lab. Inc. Retrieved 17 September, 2020 from, http://partners-lab.com/ko/service/3d.php.
239. Hybrid™ Manufacturing Technology. Retrieved 17 September, 2020 from, http://www.hybridmanutech.com/news.html.
240. Martina, F., Colegrove, P. A., Williams, S. W., & Meyer, J. (2015). Microstructure of interpass rolled wire + arc additive manufacturing Ti–6Al–4V components. *Metallurgical and Materials Transactions A, 46*(12), 6103–6118.
241. Martina, F., Roy, M. J., Szost, B. A., Terzi, S., Colegrove, P. A., Williams, S. W., et al. (2016). Residual stress of as-deposited and rolled wire + arc additive manufacturing Ti–6Al–4V components. *Materials Science and Technology, 32*(14), 1439–1448.
242. Gu, J., Ding, J., Williams, S. W., Gu, H., Ma, P., & Zhai, Y. (2016). The effect of inter-layer cold working and post-deposition heat treatment on porosity in additively manufactured aluminum alloys. *Journal of Materials Processing Technology, 230,* 26–34.
243. Gu, J., Ding, J., Williams, S. W., Gu, H., Bai, J., Zhai, Y., et al. (2016). The strengthening effect of inter-layer cold working and post-deposition heat treatment on the additively manufactured Al–6.3Cu alloy. *Materials Science and Engineering A, 651,* 18–26.
244. Hönnige, J. R., Colegrove, P. A., Ganguly, S., Eimer, E., Kabra, S., & Williams, S. (2018). Control of residual stress and distortion in aluminium wire + arc additive manufacture with rolling. *Additive Manufacturing, 22,* 775–783.
245. Colegrove, P. A., Donoghue, J., Martina, F., Gu, J., Prangnell, P., & Hönnige, J. (2017). Application of bulk deformation methods for microstructural and material property improvement and residual stress and distortion control in additively manufactured components. *Scripta Materialia, 135,* 111–118.
246. Xie, Y., Zhang, H., & Zhou, F. (2016). Improvement in geometrical accuracy and mechanical property for arc-based additive manufacturing using metamorphic rolling mechanism. *Journal of Manufacturing Science and Engineering, 138*(11), 111002. https://doi.org/10.1115/1.4032079.
247. Tapia, G., & Elwany, A. (2014). A review on process monitoring and control in metal-based additive manufacturing. *Journal of Manufacturing Science and Engineering, 136*(6), 060801. https://doi.org/10.1115/1.4028540.
248. Reutzel, E. W., & Nassar, A. R. (2015). A survey of sensing and control systems for machine and process monitoring of directed-energy, metal-based additive manufacturing. *Rapid Prototyping Journal, 21*(2), 159–167.
249. Everton, S. K., Hirsch, M., Stravroulakis, P., Leach, R. K., & Clare, A. T. (2016). Review of in situ process monitoring and in situ metrology for metal additive manufacturing. *Materials and Design, 95,* 431–445.
250. Yan, Z., Liu, W., Tang, Z., Liu, X., Zhang, N., Li, M., et al. (2018). Review on thermal analysis in laser-based additive manufacturing. *Optics & Laser Technology, 106,* 427–441.
251. Kledwig, C., Perfahl, H., Reisacher, M., Brückner, F., Bliedtner, J., & Leyens, C. (2019). Analysis of melt pool characteristics and process parameters using a coaxial monitoring system during directed energy deposition in additive manufacturing. *Materials, 12*(2), 308. https://doi.org/10.3390/ma12020308.
252. Heralić, A., Christiansson, A.-K., Ottosson, M., & Lennartson, B. (2010). Increased stability in laser metal wire deposition through feedback from optical measurements. *Optics and Lasers in Engineering, 48*(4), 478–485.
253. Hsu, H.-W., Lo, Y.-L., & Lee, M.-H. (2019). Vision-based inspection system for cladding height measurement in direct energy deposition (DED). *Additive Manufacturing., 27,* 373–378.
254. Taminger. K., M., Domack, C. S., Zalameda, J. N., Taminger, B. L., Hafley, R. A., & Burke, E. R. (2016). In-process thermal imaging of the electron beam freeform fabrication process. In *Proceeding of SPIE 9861, thermosense: Thermal infrared applications XXXVII*, 98612. https://doi.org/10.1117/12.2222439.
255. Heralić, A., Christiansson, A.-K., & Lennartson, B. (2012). Height control of laser metal-wire deposition based on iterative learning control and 3D scanning. *Optics and Lasers in Engineering, 50*(9), 1230–1241.
256. Haley, J. C., Schoenung, J. M., & Lavernia, E. J. (2018). Observations of particle-melt pool impact events in directed energy deposition. *Additive Manufacturing, 22,* 368–374.
257. Gibson, B. T., Bandari, Y. K., Richardson, B. S., Rochli, A. C., Post, B. K., Borish, M. C., Thornton, A., Henry, W. C., Lamsey, M., & Love, L. J. (2019). Melt pool monitoring for control and data analytics in large scale metal additive manufacturing. In *Proceedings of International Solid Freeform Fabrication Symposium (SFF 2019)*. Retrieved 18 September, 2020 from, https://www.osti.gov/biblio/1561633.
258. Kim, C. Y., Kim, J. S., Lee, H., Park, M. K., Kim, S. W., Shin, S. S., et al. (2020). Effect of laser power feedback control on mechanical properties of stainless steel part built by direct energy deposition. *Journal of Welding and Joining, 38*(2), 197–202.
259. CLAMIR Inc. https://www.clamir.com/en/applications/.
260. Hassler, U., Gruber, D., Hentschel, O., Sukowski, F., Grulich, T., & Seifert, L. (2016). In-situ monitoring and defect detection for laser metal deposition by using infrared thermography. *Physics Procedia, 83,* 1244–1252.
261. https://www.optomec.com/wp-content/uploads/2018/10/LENS_Process_WEB1018.pdf. Retrieved 18 September, 2020.
262. STRATONICS Inc. Retrieved 18 September, 2020 from, http://stratonics.com/systems/software/.
263. Kenel, C., Grolimund, D., Li, X., Panepucci, E., Samson, V. A., Sanchez, D. F., et al. (2017). In situ investigation of phase transformations in Ti–6Al–4V under additive manufacturing conditions combining laser melting and high-speed micro-X-ray diffraction. *Scientific Reports, 7*(1), 16358. https://doi.org/10.1038/s41598-017-16760-0.
264. Leung, C. L. A., Marussi, S., Atwood, R. C., Towrie, M., Withers, P. J., & Lee, P. D. (2018). In situ X-ray imaging of defect and molten pool dynamics in laser additive manufacturing. *Nature Communications, 9*(1), 1355. https://doi.org/10.1038/s41467-018-03734-7.

265. Wolff, S. J., Wu, H., Parab, N., Zhao, C., Ehmann, K. F., Sun, T., et al. (2019). In-situ high-speed X-ray imaging of piezo-driven directed energy deposition additive manufacturing. *Scientific Reports, 9*(1), 962. https://doi.org/10.1038/s41598-018-36678-5n.
266. Marshall, G. J., Young, W. J., Thompson, S. M., Shamsaei, N., Daniewicz, S. R., & Shao, S. (2016). Understanding the microstructure formation of Ti–6Al–4V during direct laser deposition via in situ thermal monitoring. *JOM Journal of the Minerals Metals and Materials Society, 68*(3), 778–790.
267. Khanzadeh, M., Chowdhury, S., Tschopp, M. A., Doude, H. R., Marufuzzaman, M., & Bian, L. (2018). In-situ monitoring of melt pool images for porosity prediction in directed energy deposition processes. *IISE Transactions, 51*(5), 437–455.
268. Smurov, I., Doubenskaia, M., Grigoriev, S., & Nazarov, A. (2012). Optical monitoring in laser cladding of Ti6Al4V. *Journal of Thermal Spray Technology, 21*(6), 1357–1362.
269. Smurov, I., Doubenskaia, M., & Zaitsev, A. (2013). Comprehensive analysis of laser cladding by means of optical diagnostics and numerical simulation. *Surface & Coatings Technology, 220,* 112–121.
270. Liu, S., Farahmand, P., & Kovacevic, R. (2014). Optical monitoring of high power direct diode laser cladding. *Optics & Laser Technology, 64,* 363–376.
271. Yang, Q., Zhang, P., Cheng, L., Min, Z., Chyu, M., & To, A. C. (2016). Finite element modeling and validation of thermomechanical behavior of Ti–6Al–4V in directed energy deposition additive manufacturing. *Additive Manufacturing, 12,* 169–177.
272. Wang, Z., Denlinger, E., Michaleris, P., Stoica, A. D., Ma, D., & Beese, A. M. (2017). Residual stress mapping in Inconel 625 fabricated through additive manufacturing: Method for neutron diffraction measurements to validate thermomechanical model predictions. *Materials and Design, 113,* 169–177.
273. Ivanov, S., Zemlyakov, E., Babkin, K., Turichin, G., Karpov, I., Em, V., et al. (2019). Stress distribution in laser metal deposited multi-layer thick-walled parts of Ti–6Al–4V. *Procedia Manufacturing, 36,* 240–248.
274. Biegler, M., Marko, A., Graf, B., & Rethmeier, M. (2018). Finite element analysis of in situ distortion and bulging for an arbitrarily curved additive manufacturing directed energy deposition geometry. *Additive Manufacturing, 24,* 264–272.
275. Stender, M. E., Beghini, L. L., Sugar, J. D., Veilleux, M. G., Subia, S. R., Smith, T. R., et al. (2018). A thermal-mechanical finite element workflow for directed energy deposition additive manufacturing process modeling. *Additive Manufacturing, 21,* 556–566.
276. Heigel, J. C., Michaleris, P., & Reutzel, E. W. (2015). Thermo-mechanical model development and validation of directed energy deposition additive manufacturing of Ti–6Al–4V. *Additive Manufacturing, 5,* 9–19.
277. Li, X., Lin, X., Chiumenti, M., Cervera, M., Hu, Y., Ji, X., et al. (2019). In situ measurements and thermo-mechanical simulation of Ti–6Al–4V laser solid forming process. *International Journal of Mechanical Sciences, 153–154,* 119–130.
278. Vundru, C., Singh, R., Yan, W., & Karagadde, S. (2020). Non-dimensional process maps for residual stress in laser directed energy. *Procedia Manufacturing, 48,* 697–705.
279. Mirkoohi, E., Dobbs, J. R., & Liang, S. Y. (2020). Analytical modeling of residual stress in direct metal deposition considering scan strategy. *The International Journal of Advanced Manufacturing Technology, 106,* 4105–4121.
280. Zhang, Z., Ge, P., Yao, X. X., Li, T., & Liu, W. W. (2020). Numerical studies of residual states and scaling effects in laser-directed energy deposition additive manufacturing. *The International Journal of Advanced Manufacturing Technology, 108,* 1233–1247.
281. Ren, K., Chew, Y., Fuh, J. Y. H., Zhang, Y. F., & Bi, G. J. (2019). Thermo-mechanical analyses for optimized path planning in laser aided additive manufacturing processes. *Materials and Design, 162,* 80–93.
282. Kiran, A., Hodek, J., Vavřík, J., Urbánek, M., & Džugan, J. (2020). Numerical simulation development and computational optimization for directed energy deposition additive manufacturing process. *Materials, 13*(11), 2666. https://doi.org/10.3390/ma13112666.
283. Denlinger, E. R., & Michaleris, P. (2016). Effect of stress relaxation on distortion in additive manufacturing process modeling. *Additive Manufacturing, 12,* 51–59.
284. Li, R., & Xiong, F. (2019). Influence of interlayer dwell time on stress field of thin-walled components in WAAM via numerical simulation and experimental tests. *Rapid Prototyping Journal, 25*(8), 1433–1441.
285. Cao, J., Gharghouri, M. A., & Nash, P. (2016). Finite-element analysis and experimental validation of thermal residual stress and distortion in electron beam additive manufactured Ti–6Al–4V build plates. *Journal of Materials Processing Technology, 237,* 409–419.
286. Lu, X., Lin, X., Chiumenti, M., Cervera, M., Hu, Y., Ji, X., et al. (2019). Residual stress and distortion of rectangular and S-shaped Ti–6Al–4V parts by directed energy deposition: Modelling and experimental calibration. *Additive Manufacturing, 26,* 166–179.

Publisher's Note Springer Nature remains neutral with regard to jurisdictional claims in published maps and institutional affiliations.

Dong-Gyu Ahn received his B.S. degree from the Busan National University, Korea in 1992. He then received his M.S. and Ph.D. degrees from KAIST, Korea in 1994 and 2002, respectively. Dr. Ahn is currently a Professor at the Department of Mechanical Engineering, Chosun University, Korea. Dr. Ahn's research interests include development and application of 3D printing technology, rapid manufacturing, lightweight sandwich plate, and mold and die.